UNDERWATER SYSTEMS INC.

1776 EAST JEFFERSON STREET • ROCKVILLE, MD. 20852 • TELEPHONE: 301-770-9190

ANALYSES OF OCEANIC SUBSURFACE FEATURES USING SPACE BASED RADAR IMAGERY

Prepared By:

Underwater Systems, Inc.

Prepared For:

Mr. Vincent Pusateri
Code 07
Naval Ocean Systems Center
San Diego, California 92152

Contract N00014-82-C-0114

July 1982

UNDERWATER SYSTEMS, Inc.
1776 East Jefferson St. • Rockville, Md. 20852 • (301) 770-9190

UNCLASSIFIED

SECURITY CLASSIFICATION OF THIS PAGE (When Data Entered)

REPORT DOCUMENTATION PAGE	READ INSTRUCTIONS BEFORE COMPLETING FORM
1 REPORT NUMBER	2 GOVT ACCESSION NO. AD-A118411	3. RECIPIENT'S CATALOG NUMBER
4 TITLE (and Subtitle) Analysis of Oceanic Subsurface Features Using Space Based Radar Imagery	5. TYPE OF REPORT & PERIOD COVERED FINAL
	6. PERFORMING ORG. REPORT NUMBER
7 AUTHOR(s) Samuel Walter McCandless and Charmaine P. Mrazek	8. CONTRACT OR GRANT NUMBER(s) N00014-82-C-0114
9 PERFORMING ORGANIZATION NAME AND ADDRESS Underwater Systems, Inc. 1776 E. Jefferson St. Rockville, Maryland	10. PROGRAM ELEMENT, PROJECT, TASK AREA & WORK UNIT NUMBERS
11. CONTROLLING OFFICE NAME AND ADDRESS Office of Naval Research Department of the Navy Arlington, Virginia 22217	12. REPORT DATE July 1982
	13. NUMBER OF PAGES 200
14. MONITORING AGENCY NAME & ADDRESS (if different from Controlling Office)	15. SECURITY CLASS. (of this report) UNCLASSIFIED
	15a. DECLASSIFICATION/DOWNGRADING SCHEDULE N/A

16. DISTRIBUTION STATEMENT (of this Report)

UNLIMITED

DISTRIBUTION STATEMENT A
Approved for public release;
Distribution Unlimited

17. DISTRIBUTION STATEMENT (of the abstract entered in Block 20, if different from Report)

18. SUPPLEMENTARY NOTES

19. KEY WORDS (Continue on reverse side if necessary and identify by block number)
Synthetic Aperture Radar, Visibility of Underwater Topography, Bathymetry

20. ABSTRACT (Continue on reverse side if necessary and identify by block number)

Bathymetric features are visible on some SEASAT SAR and SIR-A images. This study surveyed as wide a data base as possible and collected available ground truth to determine the limits of this visibility. Such parameters as tidal levels, currents, wind, rain, radar incidence angle, radar aspect angle and radar processing were all considered. Some dependence of visibility on current was discovered, and conversely, independence of radar incidence angle. The results were severely limited by the lack of detailed ground truch of an appropriate nature.

DD FORM 1 JAN 73 1473 EDITION OF 1 NOV 65 IS OBSOLETE
S/N 0102-014-6601

UNCLASSIFIED
SECURITY CLASSIFICATION OF THIS PAGE (When Data Entered)

PREFACE

Synthetic Aperture Radar (SAR) images have shown striking evidence of a correlation between sea surface features and bottom morphology. Observations from space using the SEASAT SAR and the Space Shuttle Imaging Radar (SIR-A) confirm that the phenomena exists and is frequently set up by hydrologic conditions. Such observations suggest that SAR has great potential for remotely measuring surface manifestations of underwater objects and subsurface flow as well as providing inferred bathymetry. The results of this study of SEASAT SAR and SIR-A data define a range of environmental and radar parameters for which bottom topography produces surface features. However, this potential cannot be completely evaluated because of the limited number of observations currently available and the lack of data from controlled experiments where contributing variables are isolated. It is proposed to utilize the results of this study combined with the models available in three areas: (1) subsurface hydrodynamics and their effect on the surface, (2) air/sea interactions, and (3) SAR sea surface response, to develop a SIR-B (1984) controlled experiment for subsurface observations. The results of a controlled experiment would be invaluable to those interested in analyzing subsurface signatures using remotely sensed data.

SPECIAL ACKNOWLEDGEMENTS

- Dr. James Taranik, NASA, Office of Space and Terrestrial Applications, for providing access to the recently acquired SIR-A radar data.

- Bruce Needham, NOAA, Environmental Services, for providing access to the SEASAT SAR image archive and assistance in conducting a broad survey of this large data set.

- Pat De Leonibus, NOAA-NESS, for providing access to weather maps corresponding to the SEASAT overpasses and other useful weather information.

- Dr. Stephen Borchardt, Dynamics Technology Inc., for providing technical support in the fluid mechanics evaluation of the possible mechanisms of image generation.

- Dr. David Lichy, Water Resources Support Center, Army Corps of Engineers, for providing surface truth information in the Cape Hatteras area.

TABLE OF CONTENTS

LIST OF FIGURES

LIST OF TABLES

PRINCIPAL INVESTIGATORS:

Samuel W. McCandless, Jr.

Charmaine P. Mrazek

CHAPTER 1

DESCRIPTION OF STUDY APPROACH

1.1 Introduction

Qualitative analyses of many of the spaced based Synthetic Aperture Radar (SAR) images have shown a correlation between ocean subsurface and surface features. An example of such observations may be found in Figures 1-1 and 1-2. Figure 1-1 is a 100 km x 100 km SAR frame taken by the SEASAT satellite as it passed over Cook Inlet at Anchorage, Alaska. The city of Anchorage appears in the upper center of the frame; the broad and dark expanse of Cook Inlet traces a path to the lower edge. The image was taken during slack tide and shows reverse tide turbulent flow (bright areas) returning water to Cook Inlet from the two river arms embracing Anchorage. The flow sets up an effect in the Inlet southeast of Anchorage that reveals bottom morphology. The indications of bottom morphology in the image should be compared with the bathymetric chart of the same area shown in Figure 1-2. It is hypothesized that these submerged obstructions modulate the surface features to which the radar responds since over the wavelengths of interest to SAR imager designers (2 to 30 cm) the radar does not appreciably penetrate the surface. The details of this interaction between hydrodynamic flow and bottom topography and the range of physical parameters which influence what is observed in the radar images have not yet been established.

The data sets available for study include SEASAT SAR imagery collected from July 4 to October 10, 1978 and the Shuttle Imaging Radar (SIR-A) data

FIGURE 1-1. COOK INLET, REV. 289.

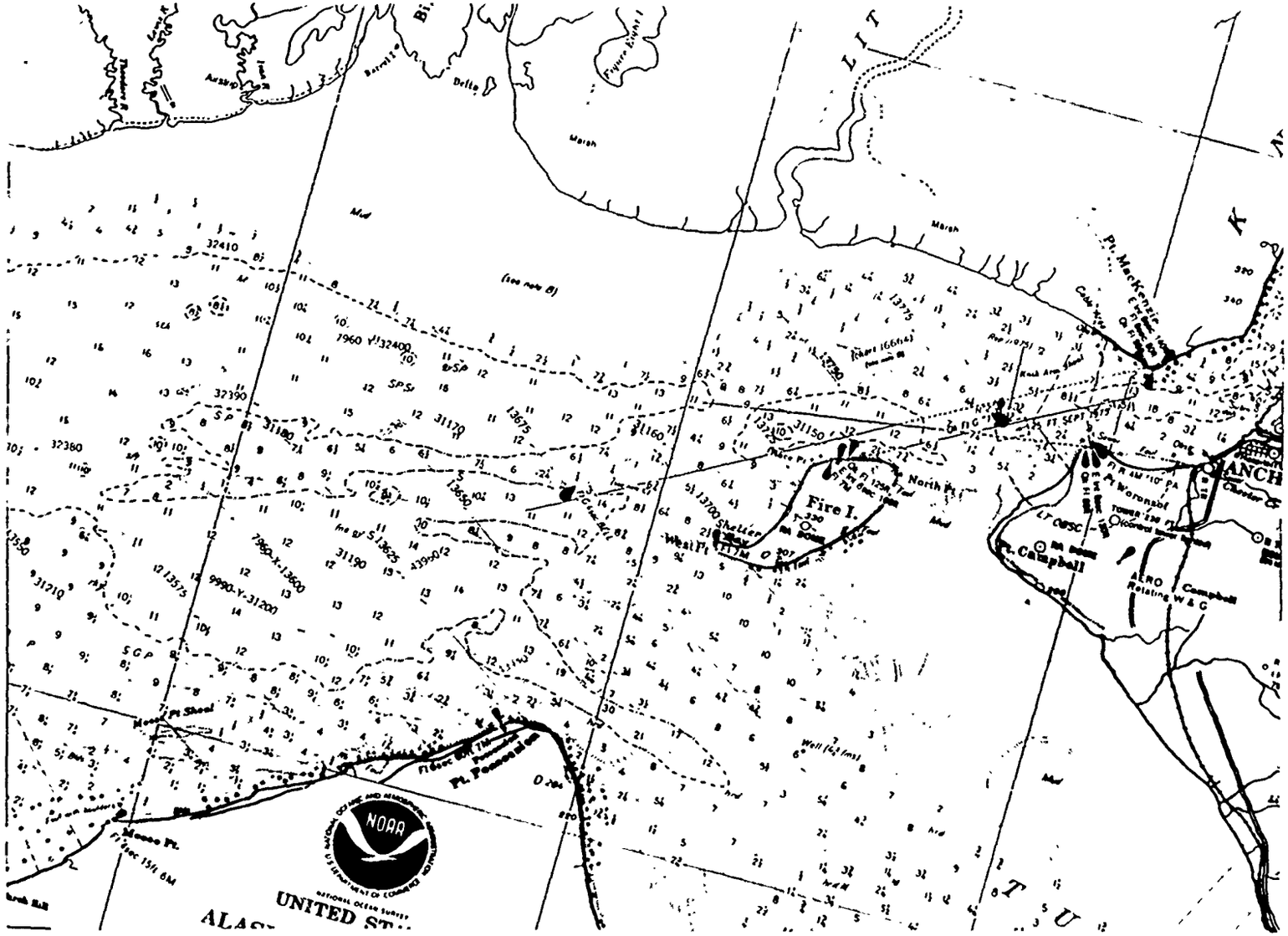

Figure 1-2. Bathymetric Map, Cook Inlet.

taken during the second space shuttle mission which occurred from November 12 to 14, 1981. Figure 1-3 illustrates the areas covered by these data sets. This existing collection of space based SAR imagery is inadequate to answer these questions by a simple visual search. Radar parameters such as polarization and wavelength are fixed in the SEASAT and SIR-A SAR data, and the range of environmental parameters observed is limited by the short lifetime of both missions. Repeat scenes are generally not available for synoptic observations. More importantly, a controlled experiment using a well instrumented ocean location(s) did not exist. Nonetheless, the present data set contains valuable observations, albeit at almost random times and locations. In several cases SEASAT and SIR-A observed the same areas (e.g. the Cape Hatteras case study in Chapter 4). This is important because it permits an evaluation of how subsurface features are observed by radars having different scene incidence angle.

Because of the limitations noted, analyses of subsurface features using available space based radar imagery are unable to exactly specify the Radar, Surface and Subsurface conditions that must exist to allow the subsurface features to transmute surface conditions or conversely to specify the conditions that block or override the appearance of subsurface features in ocean surface images. What is possible is an assessment of as large a data base as possible (i.e. all of the SEASAT and SIR-A images) to ascertain the conditions that existed when ocean subsurface signatures were or were not visible. In addition to the radar images, convenience surface truth data (e.g. wind, wave, temperature, tidal flow and currents) were acquired. The term "convenience data" is used to signify that this information was taken from existing sources of environmental data and not by site specific

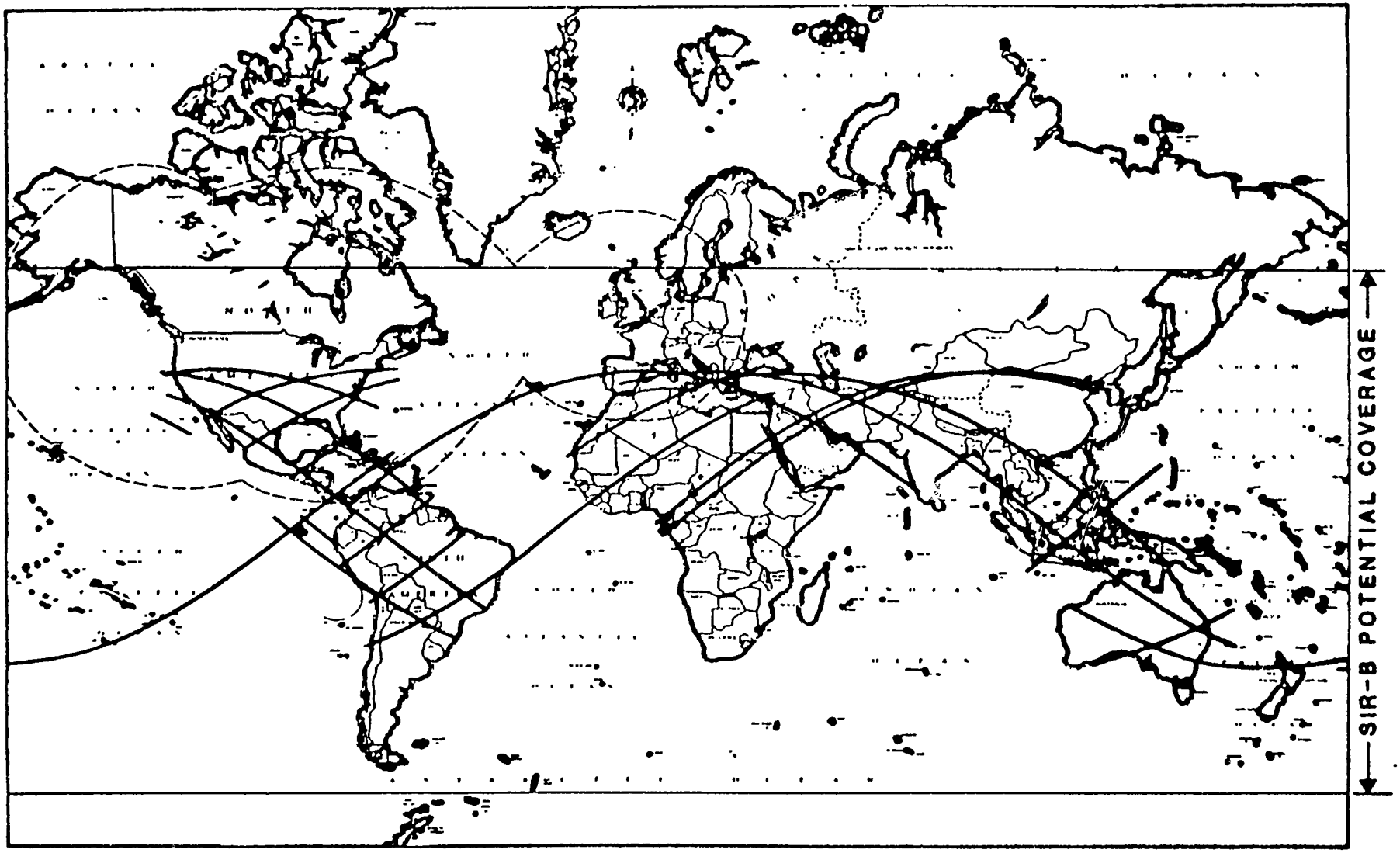

Figure 1-3. SEASAT, SIR-A and SIR-B Data Coverage.

instrumentation designed for and dedicated to a special subsurface feature experiment. This latter situation is ultimately required for a more exacting understanding about boundary conditions.

The use of all of the available data extends the base (i.e. data samples) of what is an empirical study of subsurface features. In all cases the subsurface features are known natural bottom features whose shape and orientation can be verified from available bathymetric charts.

The remaining sections in this chapter introduce some of the basic principles of radar backscatter that determine how the image is formed, describe why synthetic aperture techniques are used for space based images, and conclude with a summary of study tasks.

Chapter 2 provides a more detailed discussion of the radar and geophysical parameters that influence subsurface feature imaging. Chapter 3 tabulates the study results and offers an assessment of how the results can be applied to future radar remote sensing of subsurface phenomena. Chapter 4 treats several oceanic sites where SEASAT and SIR-A data observed subsurface signature over a variety of radar aspect and geophysical conditions in more detail. These candidates were picked from the larger data set identified in the survey to evaluate specific boundary value conditions such as current and tidal flow, wind stress, etc. Chapter 5 postulates methods that might be used to detect and trace the subsurface signature given a digital image record as input. Table 1-1 provides a reference to the subjects that are covered in this document and directs the reader to their location.

TABLE 1-1. Subject Areas in the Report

	Section
Radar Backscatter Principles	1.2.1
General Explanation of How a Radar Images Ocean Subsurface Features	1.2.2
Description of Why Aperture Synthesis Techniques Are Used for Space Based Radar Imagers	1.2.3
Study Steps and Schedule	1.3
Theoretical Analyses of Possible Mechanisms of Image Generation of Subsurface Features	2.2 and 2.3
Review of SEASAT Optical and Digital and SIR-A Optical Imagery for Possible Surface Signatures	3.2
Summary of the Results of Image Analyses of Selected Sites of Concentration Where the SAR Imaged Subsurface Features	3.3
Recommendations to Improve Our Understanding of Oceanic Subsurface Remote Sensing	3.4
Recommended SIR-B Experiment	3.4
Description of Ground Truth Limitations	4.2
SAR Image Geographical Areas of Concentration - Data and Evaluations	4.3
Individual SAR Passes - Data and Evaluations	4.4
Automatic Image Extraction Possibilities	5.2

1.2 Ocean Subsurface Signatures

1.2.1 General Radar Backscatter Principles

Figure 1-4 illustrates the fundamental interaction between a radar and any target.

The radar scattering coefficient is the fundamental measure used to quantitatively characterize the backscattered radiance of extended scenes. It depends on two factors:

- Scene parameters (wavelength scale surface roughness, larger scale features with a wide range of orientations with the illumination vector and the complex dielectric constant).
- Illumination parameters (incidence angle, wavelength and polarization).

Figure 1-5 provides a reference of what is meant by some of the defining angular relationships between the radar and the scene so the reader will know what is meant by scene incidence and grazing angle references or radar depression or nadir angle references.

A radar wave obliquely incident on a large electrically smooth conducting surface will be reflected away at an angle equal to the incidence angle. If the surface becomes slightly rough, then the energy is scattered in all directions although it will still be concentrated along the reflected angle direction, i.e. the specular direction. If the surface is quite rough, then the scattered energy will show little dependence on angle and will appear along all directions.

Surface roughness depends on the rms height (H) with respect to a wavelength (λ) and also the incidence angle (θ_i). A convenient rule of thumb is the Rayleigh criterion which states that a surface can be considered rough if the rms height exceeds one eighth wavelength divided by the cosine of the incidence angle. This means that the surface becomes smoother at

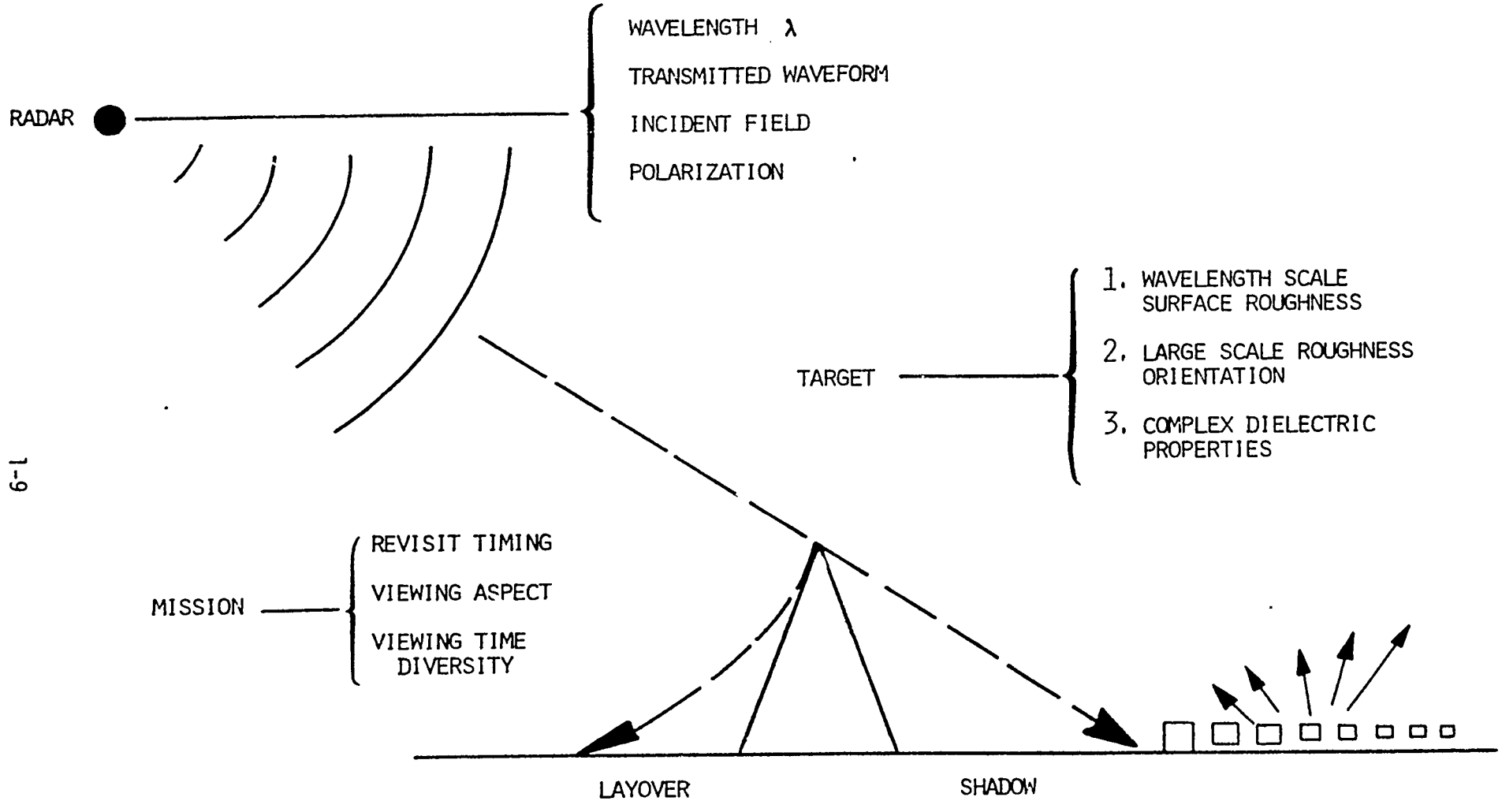

Figure 1-4. - Parametric Interaction.

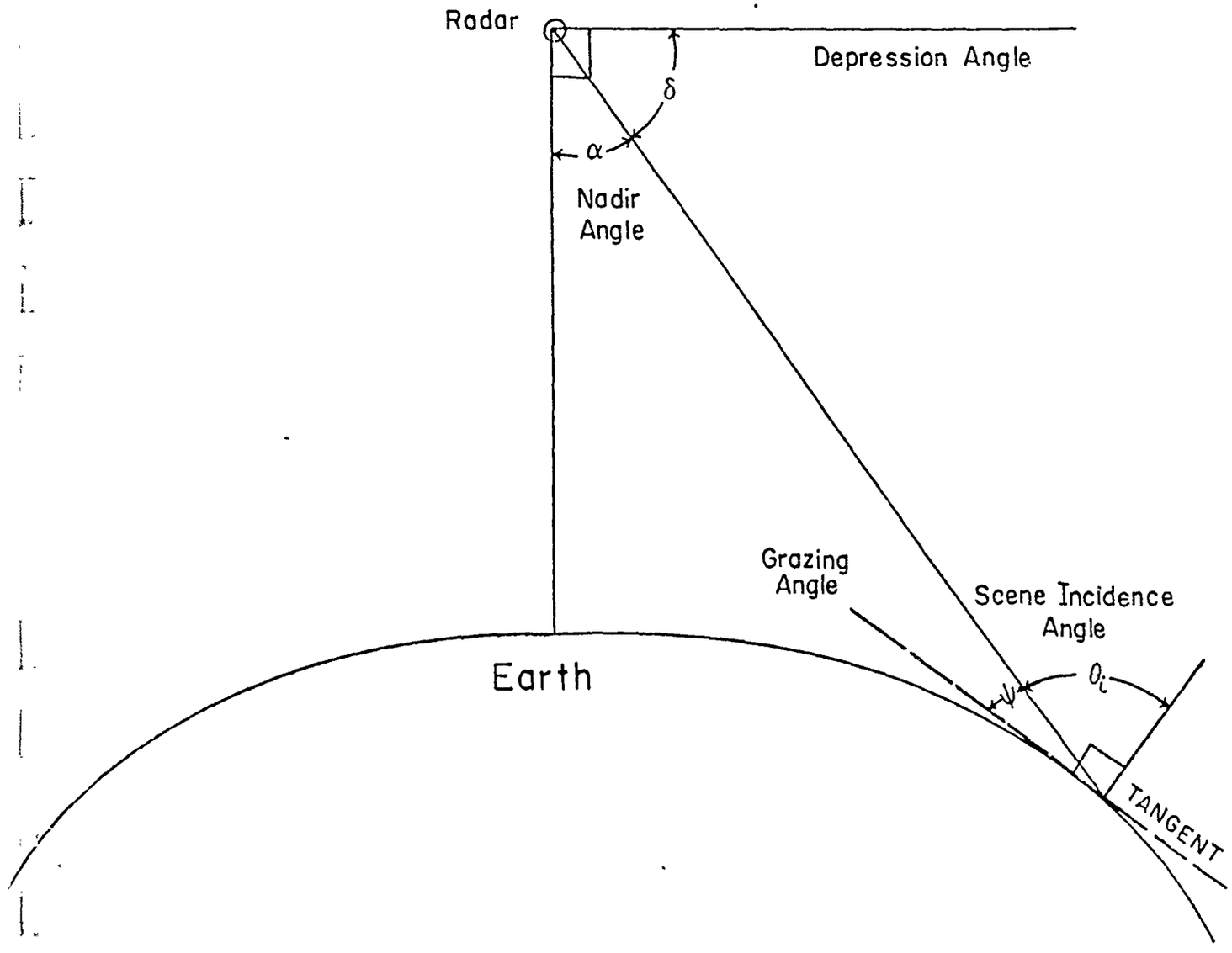

Figure 1-5. Radar/Target Scene Geometry.

near-grazing incidence and that at any angle the surface becomes rougher at higher frequencies. At normal incidence, this would mean that at an L-band frequency (e.g. 23 cm wavelength) a surface with an rms roughness greater than 8 cm would appear to be rough. It should be noted that the rms roughness is with respect to a horizontal plane and that the above criterion does not consider large scale slope or topography. Table 1-2 demonstrates how surface roughness (as observed by the radar) varies as a function of radar wavelength.

Electrically smooth surfaces will exhibit a rapid decrease in backscattered energy as the angle increases off nadir and rough surfaces will exhibit a very slow and gradual decrease in backscattered energy with increased incidence angle. Thus, a radar imaging a low relief region such as the ocean surface would depict little variation with angle if the surface were electrically rough. On the other hand, if the surface were electrically smooth then the multiangle images would show a dramatic decrease in image intensity with increasing incidence angle. This relationship is shown in Figure 1-6. Since SEASAT images have an incidence angle of approximately 20° (varies by about 3° across the 100 km image swath width) and SIR-A images have an incidence angle of approximately 50°, the use of these divergent data sets provides information about the sensitivity of subsurface feature imaging to incidence variations.

Wind stress will produce small scale surface roughness in the form of capillary waves that appear on the radar image as a bright return. Gravity waves are forms of large scale roughness and the "tilt" or slope of these waves will influence the radar return. For backscattering, the large scale

TABLE 1-2. Limiting Values of Vertical Relief (h) for Surface Roughness Categories with a Depression Angle of 45°

Roughness Category	Ka-band (λ = 0.86 cm)	X-band (λ = 3 cm)	L-band (λ = 25 cm)
Smooth	h < 0.05 cm	h < 0.17 cm	h < 1.41 cm
Intermediate	h = 0.05 - 0.28 cm	h = 0.17 - 0.96 cm	h = 1.41 - 8.04 cm
Rough	h > 0.28 cm	h > 0.96 cm	h > 8.04 cm

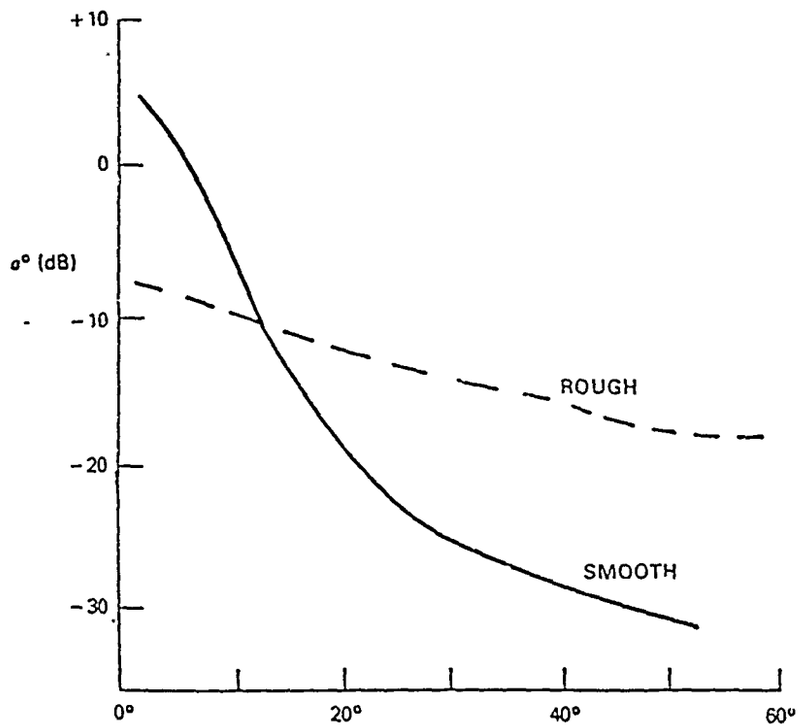

Figure 1-6. Radar Cross Section as a Function of Incidence Angle.

roughness produces a maximum in the energy along the normal to the planar angle. The reason for this is that the largest scales of roughness in natural surfaces are usually the most gently sloping and their local normal deviates little from the mean surface normal (10° to 20°).

The small scales of roughness are more sharply sloping. Optical theories no longer apply when rms heights and radii of curvature are smaller than a wavelength. A perturbation modeling approach must be employed where scattered power is not so much due to the specularly oriented facets of the surface as it is to their spacing and volume. The result is power scattered into directions other than that of the specular return. The oceanic surface exhibits both small scale irregularities and large scale undulations. Dielectric properties will be fairly constant except in regions where fresh water mixing or entrained substance loading (e.g. sediment) will vary the dielectric properties slightly.

This idea, that the surface may be usefully decomposed into large structures and small structures (which dominate the surface roughness), forms the essential ingredient in the so-called "two-scale models" of SAR response as outlined in Ruck et al. (1970). The modeling techniques predict radar response at various wavelengths, polarizations and viewing angles.

In reality, surfaces are not as simplistic in form as described above. Composite surfaces are the most common type of roughness surface at microwave frequencies and oceanic surfaces are good examples of composite surfaces. The large scale (compared to radar wavelength) features scatter specularly in a facet-like manner. The return from many facets could be almost completely incoherent. The small scale roughness variations on top of them further redistribute the scattered energy and might fill in where specular scattered

power is at a minimum. This contribution is sometimes referred to as the "diffuse component" by radar experimentalists. Both types of roughness scatter only incoherently since the coherent component is suppressed by the large scale random roughness. Both types of roughness are for the most part statistically independent in nature. Hence, the composite rough surface model consists of the average scattered power from a very rough surface added to the average scattered power from a slightly rough surface.

Radar design deals with the relationship between scene parameters and illumination parameters. It seeks to find the best illumination parameters of wavelength, incidence angle and polarization for remote sensing of a specific thematic objective such as subsurface features.

1.2.2 Radar Imaging of Subsurface Phenomena

The ocean surface exhibits both small scale irregularities corresponding to capillary waves and white caps, and large scale undulations corresponding to gravity waves and swells. Some aspects of the wave structure of the ocean are related to the wind acting on the surface at that instant, while other aspects are related to winds that blew days ago and thousands of miles away.

There are still other considerations which might ultimately be required in a complete analysis of SAR-sea surface interactions. In the SAR system it has been previously mentioned that a uniform motion is assumed between the radar and the scene it is imaging. Thus, in addition to nonuniform satellite motion, it may be necessary to consider the fact that the sea surface is constantly changing with time. These changes occur within the resolution cell as well as over a region covered by many resolution cells. Consequently, an analysis might be performed to investigate the effects on the return radar

signal due to nonuniformity of sea surface features within the SAR resolution cell, and also the effects on the SAR image due to changes occurring during the radar signal integration time (about 2 seconds). Basically, one would proceed by decomposing the motion of the sea surface along three orthogonal directions; along-track, cross-track and radial relative to the radar beam. For the SAR, the along-track component may cause image defocusing, the cross-track component has negligible effect, and the radial component causes a Doppler frequency shift in the radar return signal so that the processed image becomes shifted in the along-track direction. In performing a more detailed analysis, it would be necessary to take into account the ocean wave speed and the direction, the radar depression angle and the signal integration time.

Since the penetration depth of electromagnetic waves at the radar frequencies of interest is on the order of millimeters to centimeters, the radar is not seeing the bottom directly. Because the radar wave only penetrates a few centimeters, it can only be directly modulated by matter within those few centimeters. This means that some other physical mechanism must be transferring the information on bottom topography to the surface layer of the ocean and modifying that layer in some fashion to which the radar is sensitive. The nature of this transfer mechanism is not well understood, but several mechanisms have been hypothesized.

One way that the bottom influences the surface in a manner that can affect SAR image intensity is through its impact on surface gravity waves. The effect of bottom topography on waves can be seen on any beach. As a wave moves from deep water to water shallower than one half the wavelength of the waves in deep water, the speed and length of the waves decrease as shown in Figure 1-7. The height of the waves first slowly decreases to about a tenth

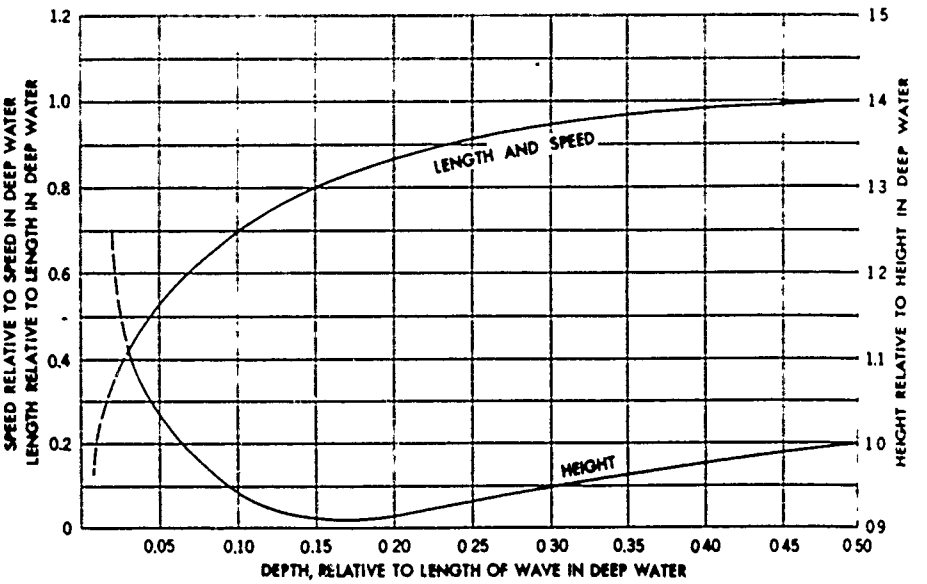

Figure 1-7. Alteration of the Characteristics of Waves As They Cross a Shoal.

From Bowditch, 1977.

of the original height at a water depth of about 15% of the deep water wavelength and then dramatically increases in even shallower water. This is the cause of the large surf on a beach, when the waves appear to roll gently further out at sea.

The relationship of the history of the relative length, speed and height of waves as they approach shallow water is not as simple as indicated in Figure 1-7. The values of these parameters at a particular location may depend on the bathymetry of the water the waves have passed through as well as the depth at that particular location. As the waves move from deep to shallow water, they lose energy due to the resistance of the bottom as well as to breaking of the crest at the surface. Also, the water depth at different points along the wave front may change at different rates and this would lead to refraction of the waves. As a result, the waves can change in direction and can be focused or defocused. The wave energy tends to be refracted towards shallow water.

One problem with the standard wave analysis developed above is that the waves which feel the bottom are of the same order of magnitude as the water depth, whereas radar sensors respond to much shorter period waves. If water depths are on the order of 30 m (100 ft), a wavelength of approximately 60 m or more is required before the wave is affected by the bottom. Radar returns are most strongly affected by water wavelengths of the same order of magnitude as the radar wavelength, which are typically a few centimeters to tens of centimeters. However, a 1978 paper by J. W. Wright of the Naval Research Laboratory explores two mechanisms by which longer period waves modulate short gravity and capillary waves. One is tilting of the small scatterers by the larger waves; the scattering cross-section of the small

waves depends strongly on the local angle of incidence. Also, Wright concludes that two-scale hydrodynamic interactions (principally straining) between the long and short waves can result in large modulations of the small-wave amplitude.

Other possible mechanisms for the detectability of bottom contours at the surface exist. One proposed by G. P. De Loor is tidal currents moving over a dune pattern which modulate the capillary and short gravity waves at the surface. In his October 1981 paper, De Loor (one of the first to note subsurface signatures in radar imagery) outlines several interesting features of SLAR imagery. He gives examples of the visibility of salinity boundaries, current edges and bathymetry, and provides limits on some important parameters. The underwater dunes in the North Sea near Rotterdam Harbor were seen when the tidal current was at least 0.5 to 1 m/sec and the sea state was between 1 and 4. His experience indicated that at high wind speeds, the bathymetry disappears as the sea becomes too choppy.

Other researchers have made some effort to correlate SAR image intensity to bathymetry. The Environmental Research Institute of Michigan (ERIM) has done the most detailed numerical comparison to date. They plotted SEASAT SAR image intensity and water depth along three orbital tracks near Nantucket Island and have performed an analysis of SEASAT SAR images taken over the English Channel. Both of these sites have very obvious signatures resulting from predominant combinations of hydrologic events.

The Radar design and Ocean Surface and indirectly the Subsurface geophysical parameters all influence the resultant image. We know, empirically, that subsurface characteristics transmute the surface characteristics and are reproduced in image form. What this study attempts to

determine is the bounding conditions of the three areas of influence shown in Figure 1-8. Answers to the following types of questions are important to a complete understanding of the conditions that govern the appearance or disappearance of the subsurface signature:

1. How strong must the wind be to create enough surface stress and capillary wave roughness to mask subsurface features?
2. What is the hydrologic (strength, orientation) interaction with subsurface conditions required to produce surface modulation?
3. What are the radar parameters best suited for subsurface signature extractions?
4. Are there several kinds of surface modulation associated with radar observation of subsurface phenomena?
5. Can the complex interactions between the Radar, Air/Sea and Subsurface regimes be determined via well controlled testing combined with modeling techniques?

These are some of the important questions that must be answered before routine use of radar techniques to observe subsurface phenomena can take place. The successful solution of what is currently a poorly understood imaging mechanism will depend on:

1. Observation - Perform as complete an analysis as possible of existing data sets.
2. Prediction - Using the results of Step 1, formulate a mathematical description(s) model of SAR subsurface interactions.
3. Verification - Exercise the model for a specific instance to predict SAR returns from given radar, bathymetric and environmental

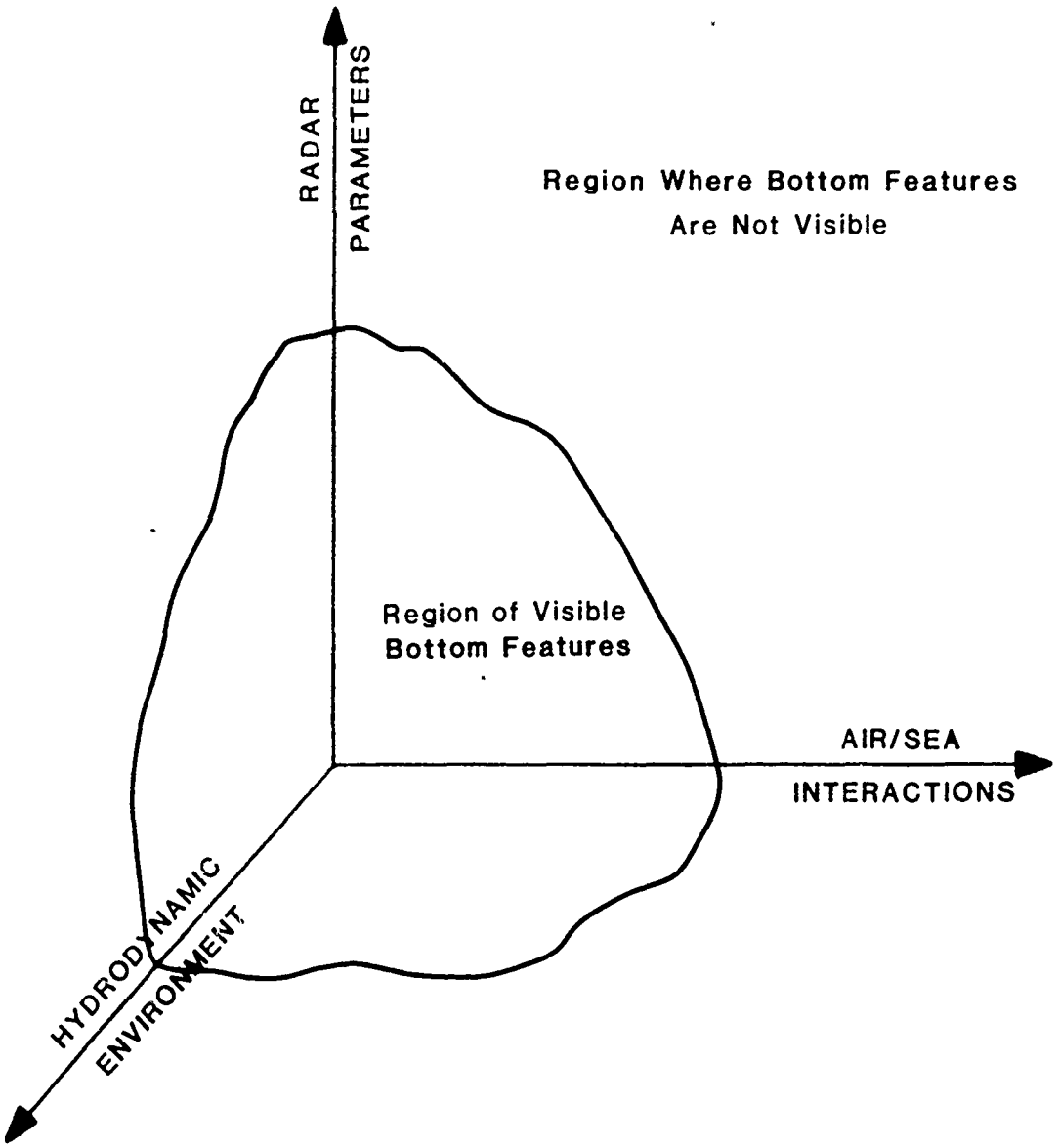

Figure 1-8. Partition of the Radar Parameter - Air/Sea Interaction - Hydrodynamic Environment Space Into Regions Where Bottom Topographic Features Are and Are Not Visible.

conditions. This step (3) and Step 2 are expected to be iterative until comparisons between prediction and observation are deemed satisfactory.

4. System Specification - Use the best model to define the range of radar and environmental parameters for which radar bathymetric observations are expected. This study product can be used to articulately plan new experiments of a confirming or mapping and charting nature.
5. Validation - After the algorithm described in Step 4 is completed, test validations may be performed using controlled experiments specifically designed to test the hypotheses developed in Steps 1 through 4.

This study considers only Step 1. Chapter 2 describes some possible mechanisms of image generation. Chapter 4 reveals some geophysical hypotheses as a result of the analysis of the SEASAT and SIR-A data sets, but these results stem from incomplete understanding of the mechanisms involved and use of data for which no controlled experiments were conducted to investigate subsurface signatures.

1.2.3 Why SAR Techniques Are Used in Space

An important distinction in a Synthetic Aperture is that this technique is used to improve along-track (azimuth) resolution; a SAR and a conventional real aperture system achieve range resolution the same way. A conventional radar's along-track resolution is governed by the diffraction limit of the real aperture and is:

$$\text{Azimuth Resolution} = \frac{\lambda R}{D_{AZ}}$$

where

λ is the radar wavelength

R is the range to target

D_{AZ} is the aperture dimension in azimuth

So the reasoning behind aperture synthesis techniques is founded on along-track resolution improvement where a resolution of $\frac{D_{AZ}}{2}$ becomes possible if all of the synthetic aperture is used. Aperture synthesis requires the movement of a real aperture along a navigation path as shown in Figure 1-9. Basic steps in a typical space based image production include:

- Format raw radar (I,Q) data
- Define the range reference function
- Perform range compression achieving a range resolution of $\frac{\tau c}{2}$ where τ is the effective compressed pulse width and c is is the speed of light
- Corner turning - reorder data in azimuth alignment direction
- Define azimuth reference functions
- Perform azimuth compression achieving an azimuth resolution of $\frac{M D_{AZ}}{2}$ where M is the number of looks in the azimuth processing step
- Geometric and radiometric corrections and display adjustments
- Form image

Some current and certainly more future systems will perform range and azimuth compressions simultaneously.

Perturbations to the path or relative aperture/target movement or geometric variation are not shown above and will generally make the construction of an image from collected doppler phase histories more

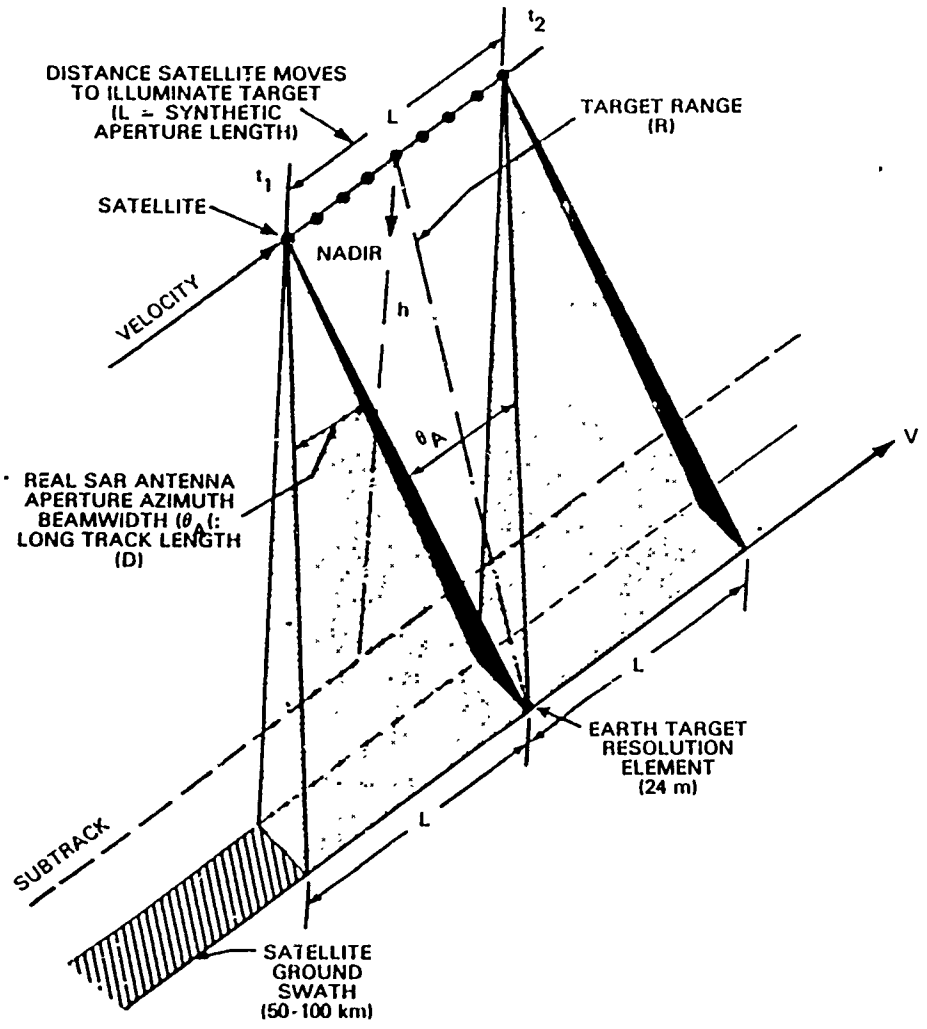

$\theta_A = \frac{2\lambda}{D}$ EFFECTIVE REAL SAR ANTENNA APERTURE 2-WAY 3-dB AZIMUTH BEAMWIDTH IN RADIANS

$\therefore L = \theta_A R = \frac{2\lambda R}{D}$

SYNTHETIC APERTURE AZIMUTH ANGULAR RESOLUTION $= \frac{\lambda}{L}$ (RADIANS)

SAR LINEAR AZMIUTH RESOLUTION (A_Z)

$$\frac{R\lambda}{\frac{2\lambda R}{D}} = \boxed{\frac{D}{2}}$$

Figure 1-9. SEASAT SAR Azimuth Resolution.

difficult. Perturbation effects and methods for correcting these effects is important to a study of the Synthetic Aperture Radar and include:

- Earth rotation effects:
  - Range walk
  - Squinting
- Orbit eccentricity
- Spacecraft attitude noise
- Cartographic distortion
- Topographic distortion (layover)
- Shadowing
- Speckle
- Radiometric resolution

Like any other remote sensor, the choice of radar, signal processing and mission parameters are dependent on user need and requirements. The design for a ocean mission will be very different from the design for a geologic, geographic or agricultural mission.

Application arts must also consider post-image correlation enhancement or information extraction techniques. These techniques can be as basic as visual recognition mnemonics or as complex as computer-aided pattern recognition or dimensional transformations. Subsurface signature recognition could benefit greatly from automated pattern recognition image data extraction techniques (as discussed in Chapter 5).

1.3 Study Steps and Schedule

Sections 1.1 and 1.2 presented the objectives and geophysical mechanisms that formed the basis for the study. This section outlines the steps that Underwater Systems, Inc. (USI) used in the conduct of the study.

The USI study team met with Mr. Vincent Pusateri, the Navy Technical Study Coordinator from the Naval Ocean Systems Center, San Diego, California on January 21, 1982. The USI project team consists of Samuel W. McCandless, Principal Investigator; Charmaine P. Mrazek, Scientist; and Eric L. Sander, Senior Scientist, who provided advisory consultation on surface mechanisms. USI presented two phenomena that could serve as specific study subjects within the context of the "Variable Signal Processing of Synthetic Aperture Radar for Target Detection and Classification" study. The candidate phenomena were: (1) analysis of the conditions for the appearance of ocean bottom topographic features in SAR images and (2) analysis of surface ship induced wake dynamics using a SAR.

Candidate 1 was selected by the Navy as the subject for detailed study analysis and a summary project plan was prepared and submitted to the Navy in early February 1982.

The expected result of the study analysis is a boundary value understanding of the combination(s) of conditions for which bottom topographic signatures appear. These conditions include:

1. Radar perspective (aspect and incidence) and subsequent signal processing choice (optical or digital).
2. Underwater hydrologic conditions such as tides, currents and wave actions.
3. Air/sea conditions such as surface wind stress, temperature, etc.

Conversely, the study would attempt to bound conditions under which we expect bottom features to be absent from the SAR images.

The SAR images to be analyzed during the study include:

1. The approximately 10,000 100 km x 100 km images collected by the SEASAT SAR.
2. The approximately 2700 60 km x 60 km images collected by the Space Shuttle Imaging Radar (SIR-A).

Table 1-3 outlines the steps accomplished during the study and indicates the general time period in which they occurred.

TABLE 1-3. Study Steps and Schedule

DATA ANALYSIS	THEORETICAL ANALYSIS
February:	
Survey SEASAT-A and SIR-A data to identify frames having subsurface signatures. • Interim Report No. 1, Feb. 15	Review literature on: • Generation of the radar backscatter by capillary and short gravity waves • Modulation of the backscatter by long waves, currents and bottom generated turbulence • Modulation of waves, current and turbulence by the bottom topography • Impact of backscatter modulation on SAR image and how it is influenced by variable processing techniques
March:	
Obtain corollary surface truth information from available records: • Tides, currents, shear • Surface winds, temperature, pressure • Thermocline, bathymetry • Other	
April:	
• Interim Report No. 2, April 1	
Meet with the Navy to select the most promising image candidates.	
Select the most promising image candidates for phenomenological analysis. Obtain computer compatible tape (CCT) records of selected images (4).	Perform relevant and study focused extensions of available enhancement and image analysis techniques.

DATA ANALYSIS	THEORETICAL ANALYSIS
May:	
Perform detailed analyses of CCT images. Map out regions of radar, air/sea interaction and hydrodynamic parameter values which provide or do not provide bottom topographic features on the images. • Interim Report No. 3, May 5	Postulate mechanisms that may influence the physics of the bottom topographic signature visibility.
June:	
Correlate data analysis results to theoretical results. Perform additional data analysis guided by theoretical results.	Suggest possible modification of theory based on data results. Postulate optimum SAR parameter values.
July:	
Complete the final report. Coordinate presentation to cognizant Navy personnel.	

CHAPTER 2

POSSIBLE MECHANISMS OF IMAGE GENERATION

2.1 Introduction

Obviously, a comprehensive mathematical description of all the physical phenomena which influence the sea surface radar backscatter is beyond the scope of the present, formative study. Accordingly, simple available models of subsurface hydrodynamics, their affect on surface waves and radar/sea-surface response will be used.

Currently, mathematical equations exist which relate sea-surface roughness to surface wind stress and SAR radar parameters. Hydrodynamic equations can be readily developed relating bottom topography and current flow to sea-surface elevation and subsurface currents. The remaining ingredient needed to complete this picture is a description of the affect on surface waves. In the presence of surface wave forcing by wind, this model should predict modulations in the surface wave spectrum by variable subsurface currents and in shallow water by direct bottom effects. This link between the subsurface hydrodynamics and the surface wave spectral modulations is probably the most difficult element of this analysis.

In developing a description of the observations of bathymetry information in SAR images, it is convenient to divide the analysis into the three parts that were depicted in Figure 1-8. In causal order, the three regions are:

1. Subsurface hydrodynamic interactions with bottom topography,
2. Spatial modulation of surface waves and elevation by the subsurface flows, and
3. SAR response to the modulated surface features.

The modeling for regions 1 and 2 is treated in order in the following sections. SAR backscatter response was discussed in Section 1.2.

2.2 Subsurface Hydrodynamics

The central hydrodynamic questions to be addressed in explaining the observation of bathymetric features in SAR images are: (1) how is topographic information communicated to the surface, (2) which is the physical mechanism whereby the ambient surface waves may be affected, and (3) how may this process be described in the context of the spectral transport formalism? This section addresses the first two questions while the third question is treated in the following section.

There are a number of hypotheses one may advance to answer the first two questions. Two in particular will be explained below.

SAR-bathymetry interactions are most commonly observed in shallow coastal waters. Perhaps the most interesting features of such environments in the present context are the relatively shallow water depths and the likely presence of appreciable currents (associated, for example, with tidal flows). Conceptually, the simplest hypothesis for a surface manifestation of bottom topography involves tidal flow over a rough bottom. Two surface signatures would be expected in this picture; a change in elevation of the free surface and a spatial modulation of the surface current above the bottom feature. A simple example is illustrated in Figure 2-1 (not drawn to any particular scale).

For the simple geometry illustrated in Figure 2-1 and for small tidal Froude numbers;

$$F = u_o/\sqrt{gD}$$

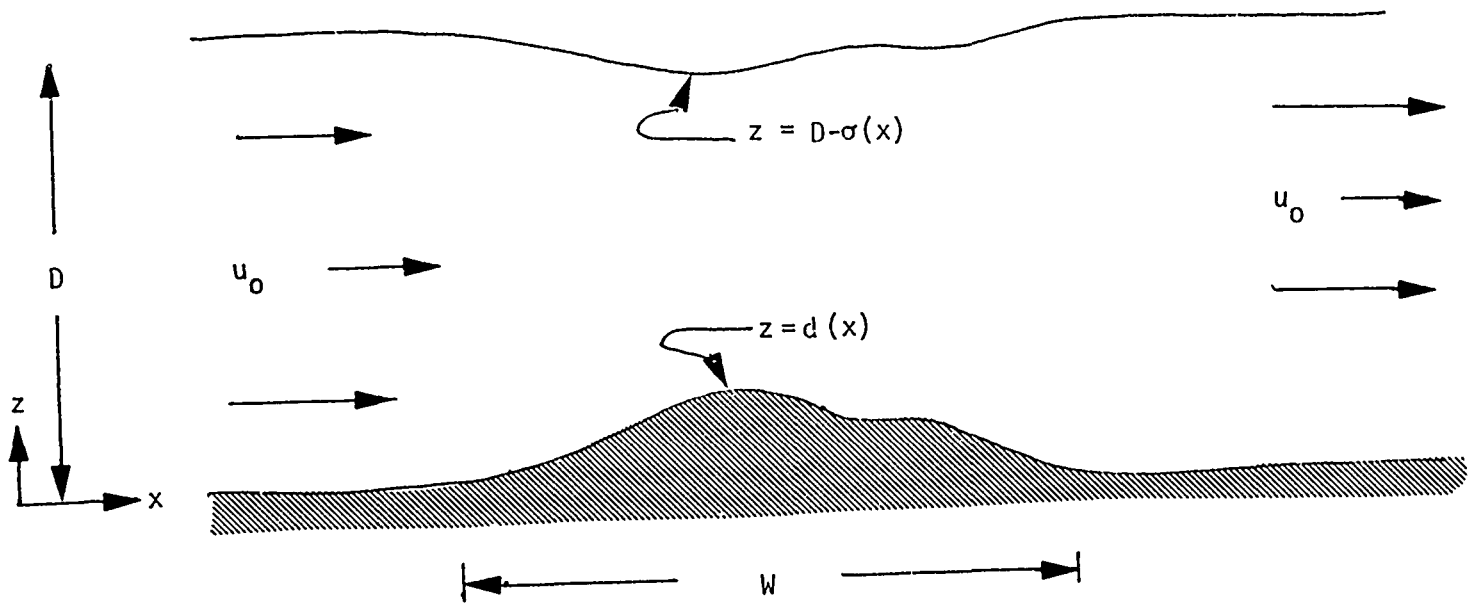

Figure 2-1. Free Surface Perturbations Induced By Tidal Flow Over Bottom Topography.

it is easy to compute the surface currents u(x) and the depression of the free surface $\sigma(x)$ for broad features in shallow water ($H^2/W^2 << 1$):

$$u(x) \simeq u_o(1-d(x)/D)^{-1}$$

$$\sigma(x) \simeq F^2 d(x)$$

$$<< d(x)$$

For the case of this simple tidal flow-bottom interaction hypothesis, perturbations in the surface wave patterns would occur primarily through the bathymetric modulation of the surface currents u(x). The interaction of surface waves with variable surface currents is a subject of some importance and one which has received serious attention in the literature (e.g. Phillips, 1977; Lewis, Lake and Ko, 1974). Of particular interest in the present context is the experimental work of Hughes and Grant (1978) and the theoretical study by Hughes (1978). Hughes and Grant experimentally observed the modulation of the surface wind wave spectrum by surface currents which were induced by artificially generated internal waves on a strong, shallow thermocline. In the companion article, Hughes analyzed the phenomenon with some success using a simple version of the spectral transport formalism. A similar analysis is envisioned for the future study of bathymetric modulation of surface waves and SAR returns. For the tidal flow modulation described above, surface wave-surface current interactions would be the relevant dynamical process.

It is worth pointing out that there was a potentially important surface wave spectral regime where Hughes' analysis of the Hughes and Grant experiment encountered some difficulties. Whereas the theory seemed to be in reasonable agreement with the observations in the spectral regime where the largest effect was observed, there was also a secondary spectral region

associated with shorter waves where a large effect was observed which was not well described by the theory. Although the authors felt that the observations may not have been as reliable in this regime, the possibility that the simplest theory may fail to predict a secondary but sizeable spectral response for the shorter waves must be given consideration in the present context since radar returns are affected to a considerable extent by the very short wind waves which may substantially dominate the local surface roughness.

It is not difficult to imagine the likely source of such a theoretical failure if it exists. The problem lies in the implicit assumption of relatively small surface wave slopes and concomitant weak nonlinear interactions among the spectral components. Such an assumption is not likely to be accurate for the shortest waves in a surface wave spectrum since even rather modest surface slopes and wave-induced orbital velocities can represent large perturbations to the environment seen by the shortest waves (e.g. long wave orbital velocities can be comparable to short wave phase speeds and small values of long wave slopes lead to surface displacements comparable to the wavelengths of the short waves). This observation, together with the importance of the short waves to radar returns, is the basis for the interest in long wave-short wave interactions within the ocean remote sensing community (Valenezuela and Wright, 1979; Phillips, 1981). It is felt that this may represent an important two-stage process whereby, for example, surface current variations may effectively modulate relatively long surface waves which in turn modulate the shorter wind waves. There exists a number of theoretical models of these long-short interactions (e.g. Liu and Benney, 1980; Phillips, 1981; Valenzuela and Wright) and it will undoubtedly prove necessary to include this effect in the future analysis of SAR-bathymetry interactions.

Besides the flow of tidal currents over bottom topography, there are other mechanisms whereby bathymetry might affect surface waves (Shemdin et al., 1980). Another simple process viable in shallow water arises from direct bottom effects on long gravity waves or swell. A surface gravity wave traveling in water involves water particle motion that extends downward to a depth of about one-half wavelength. As shown in Figure 2-2, in deep water, a particle traces a circular orbit whose radius decreases with increasing water depth. In shallow water, these orbits are elliptical. The eccentricity (flatness) of the ellipse increases as the water depth decreases. The transition from deep to shallow water is the depth at which any significant particle motion occurs, which is a depth equal to approximately one-half of the gravity wavelength. This is the physical description of the bottom depth influence on waves.

Mathematically, the situation is described by hydrodynamic equations whose solution is a velocity potential function:

$$\phi = \frac{H}{2} g \frac{\cosh k(D+z)}{\omega \cosh(kD)} \sin (kx - \omega t)$$

where

H is the wave height

g is the gravitational constant

k is the wave number = $\frac{2\pi}{\lambda}$ where λ is the wavelength

D is the water depth

z is the vertical coordinate

x is the horizontal coordinate

ω is the wave angular frequency = $\frac{2\pi}{T}$ where T is the wave period

t is the time

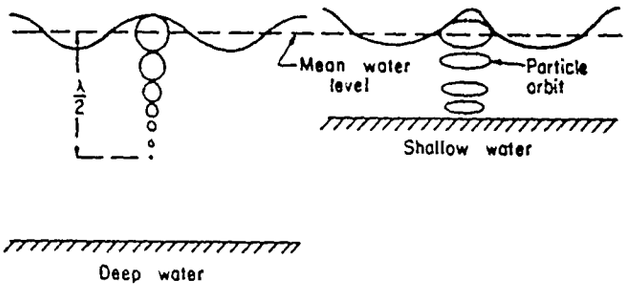

Figure 2-2. Wave Surface Profile and Particle Orbit Geometries.

This is shown in Figure 2-3. The general solution gives a period (T) of $\sqrt{gk \tanh (kD)}$ and a phase velocity (C) of $\sqrt{\frac{g\lambda}{2\pi} \tanh (\frac{2\pi D}{\lambda})}$ which are both functions of water depth. In deep water ($D/\lambda > 1/2$) $\tanh (\frac{2\pi D}{\lambda}) \simeq 1$, and so the water depth drops out leaving $\omega = \sqrt{\frac{2\pi g}{\lambda}}$ and $C = \sqrt{\frac{g\lambda}{2\pi}}$. These are the commonly used equations for deep water waves. The shallow wave approximation, valid when $D/\lambda < 1/2\pi$, or $\tanh (\frac{2\pi D}{\lambda}) \simeq \frac{2\pi D}{\lambda}$, is $C = \sqrt{gD} = \lambda/T$. Wavelength and velocity become dependent solely on water depth. Therefore, in identifying waves which will be directly affected by the bottom, the criterion is $\lambda \geq 2\pi D$.

The simplest of these direct bottom effects is the modulation of the propagation speed of the surface waves by topographic variations in water depth. This phenomenon would also produce an associated modulation of the long wave slopes and orbital velocities above the bottom features. Such effects might be directly visible in the SAR images as modulations of effective tilt angles or, more likely, by a secondary modulation of the local surface roughness via the long-short interaction discussed above. In this case as well it appears necessary to include the long-short interactions.

There are still other bottom/surface interactions which may be operative, although they are considered somewhat less promising than those outlined above. Among these are the direct generation of surface waves or the generation of internal lee waves by tidal flows (the latter mechanism is possible only in the presence of significant density stratifications in the Grant and Hughes experiment).

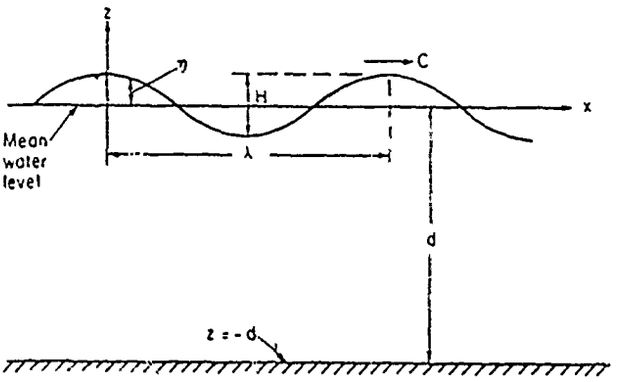

Figure 2-3. Definition Diagram for a Two-Dimensional Monochromatic Gravity Wave.

2.3 Surface Wave Modulations

A complete mathematical framework for describing the hydrodynamics requires an ability to predict modulations in ambient surface waves by the mechanisms discussed in Section 2.2. This description can be provided for future work by the spectral transport formalism, which will be briefly introduced below. A more detailed discussion of the formalism may be found in Hasselmann et al. (unpublished). Also, the review article by Barnett and Kenyon (1975) offers a lucid summary of previous applications.

Ocean surface waves are intrinsically stochastic and are most easily described in terms of average quantities. The simplest statistical characterization of a zero-mean random field is in terms of its mean square and associated power spectral density (PSD). To a first approximation, ocean waves are stationary and homogeneous, so that mean quantities are in practice computed by space or time averaging. It is evident, of course, that stationarity and homogeneity are only idealizations and it is expected that these average quantities have only local significance. Thus, surface wave PSD is expected to depend gradually on spatial location and time.

In the spectral transport formalism, this globally variable but locally stationary and homogeneous character of the random surface waves is described in a local PSD. $F(\underset{\sim}{k}, \underset{\sim}{x}, t)$, which varies rapidly in the local wave vector $\underset{\sim}{k}$ (which is in general also allowed to depend slowly on $\underset{\sim}{x}$ and t) and depends only slowly on spatial location $\underset{\sim}{x}$ and time t. In terms of F, the local surface elevation (η) has a mean square value given in terms of the PSD:

$$\langle \eta^2(\underset{\sim}{x},t) \rangle = dk\, F(\underset{\sim}{k},\underset{\sim}{x},t).$$

The implicit assumption in this picture is that the dynamic processes determining the wave field evolution dictate a distinct separation of scales; a regime of small lateral distances and time intervals over which the wave field may be regarded as stationary and homogeneous, and a regime of much larger horizontal separations and time intervals over which these properties fail to hold. Rigorous justification of this assumption is seldom possible so that the description must be regarded as phenomenological; to be judged by the success or failure of its predictions.

The dynamic evolution of the spectral density $F(\underset{\sim}{k},\underset{\sim}{x},t)$ is described in this language by an energy balance or spectral transport equation:

$$\frac{\partial F}{\partial t} + \frac{dx_i}{dt}\frac{\partial F}{\partial x_i} + \frac{dk_i}{dt}\frac{\partial F}{\partial k_i} = S; \qquad (1)$$

repeated indices indicate a summation over all index values. In this equation, the source S represents the net transfer of energy to (or from) the spectrum at wave vector $\underset{\sim}{k}$ by all dynamic processes effective at that scale. The three terms on the left side of Eq. (1) represent respectively: (1) the rate of change of energy at a fixed $\underset{\sim}{x}$ and $\underset{\sim}{k}$, (2) advection of energy by surface wave propagation from nearby spatial locations, and (3) transfer of energy in the spectral domain by the spatial modulation of the local wave vector due to environmental inhomogeneities.

Surface wave energy is expected to propagate along paths defined by the local surface wave group velocity so that:

$$\frac{dx_i}{dt} = \frac{\partial \sigma}{\partial k_i}(\underset{\sim}{k},\underset{\sim}{x}) \qquad (2)$$

where $\sigma(\underset{\sim}{k},\underset{\sim}{x})$ is the frequency of the surface wave given as a function of $\underset{\sim}{k}$ and $\underset{\sim}{x}$ by the local dispersion relation. Similarly, variations in the propagation medium lead to modulation in the local wave vector of a wave packet, a phenomenon described by:

$$\frac{dk_i}{dk} = -\frac{\partial \sigma}{\partial x_i}(\underset{\sim}{k},\underset{\sim}{x}) \tag{3}$$

These three equations describe the evolution of the wave field once the source function S is known and initial conditions for F, $\underset{\sim}{x}$ and $\underset{\sim}{k}$ are given.

A complete description of the source function S is well beyond the scope of the present discussion. It is sufficient to note that there exist well-studied phenomenological models for most of the important source mechanisms (e.g. energy input by wind, nonlinear resonant interactions and wave-current interactions) which can be employed directly in the proposed SAR-bathymetry analysis. The only serious exception to this statement is the mechanism of long-short interactions discussed in Section 2.2. Even in this case, the major concern is not the existence of adequate models (e.g. Liu and Benney), but merely that such models have not been widely applied and empirically tested. The reader interested in more detailed descriptions of the source function should consult the articles by Hasselmann et al. and Barnett and Kenyon.

CHAPTER 3

OVERVIEW OF STUDY CONCLUSIONS AND RECOMMENDATIONS

3.1 Introduction

This chapter begins with a review of the available SEASAT and SIR-A data sources including a tabulation of each of the orbits considered in the study and our survey findings as a result of analyzing this large set of data. The results of the SEASAT and SIR-A survey are followed by the selection of a subset of the identified candidates for special study.

The results of the analyses of both the survey and special study subsurface images are then summarized in Section 3.3. The last section considers ways to improve our understanding of radar remote sensing of subsurface features and to design experiments that support this objective.

3.2 Available SEASAT and SIR-A Data Sources

On June 26, 1978, SEASAT was launched into a 108° orbit at an altitude of 800 km. In addition to an L-band SAR (the first to be placed in space), SEASAT carried an altimeter, a scatterometer and a microwave radiometer. On October 10, 1978, SEASAT failed as a result of a massive short circuit in its electrical power system. During its 100-day lifetime, the SEASAT SAR collected almost 42 hours of data equivalent to about 100 million square kilometers areal coverage of the earth. Nearly all of the SEASAT data was optically processed and selected 100 km x 100 km scenes were also digitally processed at the Jet Propulsion Laboratory (JPL) and by other digital processors capable of processing SEASAT SAR data as listed in Table 3-1.

TABLE 3-1. Digital Processors for Space SAR Image Correlation

Country	Acronym	Representation
Canada	CCRS	Canada Centre for Remote Sensing
Canada	CRC	Communications Research Centre
Canada - B.C.	MDA	MacDonald Dettwiler and Assoc., Ltd.
Germany	DFVLR	Deutsche Forschungs-V Versuch Sanstalt fur Luft-V. Raumfahrt E.V.
Japan	MELCO	Mitsubishi Electronics Company
Japan	NEC	Nippon Electric Company
Norway	NDRE	Norwegian Defense Research Establishment
UK	RAE	Royal Aircraft Establishment
USA	JPL	Jet Propulsion Laboratory
USA	NRL	Naval Research Laboratory

On November 12, 1981, the second space shuttle (STS-2) was launched into a circular orbit at 39° inclination and 268 km altitude. The major payload was the OSTA-1 experiment pallet which included the Shuttle Imaging Radar-A (SIR-A) in addition to various other remote sensing instruments. The shuttle was forced to abbreviate its mission and landed at Edwards AFB at 1:23 p.m. EST on November 14, 1981. However, during this short two-day mission, SIR-A optically recorded nearly 8 hours of data equivalent to 10 million square kilometers areal coverage of the earth. The SIR-A sensor was derived from SEASAT and used the same type of antenna panels, transmitter, modulator and receiver. The illumination geometries were different. The SIR-A angle of incidence was 47° compared to 20° for SEASAT.

SEASAT and SIR-A used L-band, HH-polarized SAR designs. The SEASAT SAR data was both digitally and optically processed over a 100 km swath; the Instantaneous Field of View (IFOV) of the digitally processed data was 25 m, four looks. SIR-A echoes were optically processed only; the swath width was 50 m and the IFOV was 37 m. Table 3-2 compares the system parameters and processor performance for SEASAT SAR and SIR-A.

During the months of February and March 1982, the study effort focused on a comprehensive SAR image data survey including data acquisition and associated ground truth acquisition. A unique characteristic of our study was that every orbit of space based SAR data collected to date was reviewed. All potential candidates were then carefully evaluated in image form by two evaluators. This provided the broadest possible base for the empirical deductions that serve as the study objective. The use of both the SEASAT SAR and the Shuttle Imaging Radar SIR-A provide multiple views of the same geographic areas using different radar performance parameters.

TABLE 3-2. SEASAT SAR and SIR-A System and Processor Characteristics

SAR System Parameters	SEASAR SAR	SIR-A
SAR Orbit	Polar (108°)	Shuttle (38°)
Norminal Altitude	794 km	268 km
Nominal Speed	6844 m/sec	7450 m/sec
Transmit Frequency	1275 MHz	1272 MHz
Pulse Repetition Frequency	1463, 1537, 1645 Hz	1464 to 1770 Hz
Pulse Duration	33.8 μsec	33.8 μsec
Pulse Bandwidth	19 MHz	6 MHz
A/D Sample Rate	45.53 MHz	N/A
Optical Record Bandwidth	N/A	6 MHz
Antenna Dimensions	2 x 10.5 m	2.16 x 9.35 m
Antenna Look Angle	20°	47°
Attitude Accuracy	±0.5°	±1°

Processor Performance Requirements		
Type	Digital	Optical
Image Frame Size	100 km x 100 km	Continuous strip, 54.6 km wide
Image Resolution	25 m	37 m
Number of Looks	4	7

Within this set there are three types of data available: the SIR-A optically processed data, the SEASAT SAR optically processed data and the SEASAT SAR digitally processed data. This provides an added dimension of processing variability. The digitally processed SEASAT data was surveyed and all potential candidates were obtained in print form. Four very good candidates (Nantucket Shoals; English Channel; Cook Inlet, Alaska; and Santa Barbara, California) were obtained on computer compatible tape for extensive classification analysis using computerized techniques. The objective of this effort was to find ways of automatically extracting and mapping bathymetric contours. Complete sets of both the SIR-A and SEASAT optical data have been examined and any possible bathymetry noted for future analysis. Table 3-3 provides a tabulation of each of the data sets (full orbits of optically processed data and 100 km x 100 km frames of digitally processed data) that were reviewed.

Confirmation and definition of conditions for visibility rest on ground truth. Bathymetric maps or nautical charts showing subsurface topography were acquired for all candidate areas. A portion of these have been compared in detail (map to photograph at the same scale) to locate underwater features. Several natural effects are visible on SAR images; underwater features, internal waves, storms and rainfall areas, current boundaries and areas of fresh water or sediment-laden water. A few characterization rules were developed for the data survey. When a spherically shaped bright or dark line exists and is followed by a few more lines with decreasing spacing, internal waves are present. These have been observed extensively in the Sea of Cortez (Gulf of California) and also in the Alaskan Bay. A bright or dark perimeter outline is likely to be subsurface feature. A bright or dark solid area may

TABLE 3-3A. Summary of Image Evaluation Results, SEASAT SAR Digitally Processed Data

Location	Rev	Date	Time (GMT)	Map #	Comments
Point Loma	107 ascending	7/4/78	12:11	18765 18772 18773	Offshore traces do not correlate with map
Straits of Georgia	230 descending	7/13/78	02:54	18424 18425 18427 18429 18430 18431 19432	Bottom topography visible south of Point Roberts
Straits of Georgia	236 ascending	7/13/78	12:36	Already Listed	Bottom topography clearly evident south of Point Roberts
Blake Escarpment	242 descending	7/13/78	23:06	Atlantic Basin east of Savannah Georgia	Definite evidence of Blake Escarpment
Cook Inlet, Anchorage, Alaska	289 descending	7/17/78	05:47	16660	Bathymetry visible
St. Nicolas Island, southern California coast	308 ascending	7/18/78	13:16	18720 18755	Very interesting ocean pattern of offshore shelf areas
Dominican Republic Pair	335 ascending	7/20/78	10:31	No Map	Faint offshore outline possibly not bottom topography
Cuba	371 descending	7/22/78	23:06	11013 11420	Some coastal traces on southern coast
Cape Hatteras	378 ascending	7/23/78	10:39	11555 12204 12205	Diamond Shoals clearly visible, more visible than 974

TABLE 3-3A. Summary of Image Evaluation Results, SEASAT SAR Digitally Processed Data (Continued)

Location	Rev	Date	Time (GMT)	Map #	Comments
Mississippi Delta	393 ascending	7/24/78	11:48	11363 11364 11371	River channels clearly visible in Gulf area
Les Cayas, Haiti	450 ascending	7/28/78	11:21	No Map	Some evidence of coastal structure near major fault line
Straits of Georgia	474 descending	7/30/78	04:07	Already Listed	Bottom topography faint but clearly evident
Strait of Juan de Fuca	474 descending	7/30/78	04:07	18460 18465 18468	Bottom topography faint
Straits of Georgia	480 ascending	7/30/78	13:49	18400 18421	Bottom topography clearly evident south of Point Roberts
Yakutat, Alaska	552 ascending	8/04/78	14:38	No Map	No bathymetry
Unimak Island, Alaska	605 descending	9/8/78	07:48	16520 16535	Interesting offshore features off north and south coasts
Jamaica	608 ascending	8/8/78	12:20	411 26120	Possible bottom topography
Miami	608 ascending	8/8/78	12:22	11451 11463 11465 11468	Definite topography traces off coast of Miami
Georgia coast	651 ascending	9/11/78	12:31	11507 or 11508 11510	Offshore traces of shoal and shallow regions
Great Glenn Fault	719 ascending	9/16/78	06:42	No Map	Interesting embayment, linear hydrographic features

TABLE 3-3A. Summary of Image Evaluation Results, SEASAT SAR Digitally Processed Data (Continued)

Location	Rev	Date	Time (GMT)	Map #	Comments
Straits of Georgia	724 ascending	9/16/78	15:02	Already Listed	Very clear subsurface features south of Point Roberts
Isle De La Gonave	737 ascending	9/17/78	12:42	No Map	Slight signatures that cannot be map confirmed
Port Au Prince, Haiti	737 ascending	9/17/78	12:42	No Map	Some slight signatures north of Haiti
St. Nicholas, Haiti	737 ascending	9/17/78	12:42	No Map	Possible line west of Haiti
Gulf of Honduras	759 descending	8/19/78	02:15	No Map	Possible signatures in Amatique Bay
Pacific coast Guatemala, El Salvador	759 descending	8/19/78	02:16	No Map	Some lines present that are very similar to confirmed signatures in other areas
Columbia River, Oregon	761 descending	8/19/78	05:27	18504 18520 18521	Large internal waves, sediment patterns. Columbia bar clearly evident
English Channel	762 ascending	8/19/78	06:45	No Map	Definite bathymetry
West of Faeroe Islands	762 ascending	8/19/78	06:48	No Map	Internal waves
Middle Atlantic, Ormonde Seamount	785 descending	8/20/78	21:43	No Map	Seamount visible
Bejaia, Algeria	791 ascending	8/21/78	07:17	No Map	Definite sediment, possible bathymetry
Jamaica	809 ascending	8/22/78	13:22	Already Listed	Definite sediment, faint evidence of bathymetry

TABLE 3-3A. Summary of Image Evaluation Results, SEASAT SAR Digitally Processed Data (Continued)

Location	Rev	Date	Time (GMT)	Map #	Comments
Florida Keys	809 ascending	8/22/78	13:24	11452 11462	Subsurface areas between Keys and Everglades visible
Cypress Swamp, Florida	809 ascending	8/22/78	13:25	11430	Nothing
Mississippi Delta	839 ascending	8/27/78	14:02	11361	Submerged river channels clearly visible in Gulf
Duck, North Carolina	845 descending	8/25/78	02:18	12204 12205	Probable bathymetry
Hamilton, Buffalo	874 descending	8/27/78	02:56	14800 14806 14822	Definite patterns of unknown origin
Nantucket Shoals	880 ascending	8/27/78	12:34	13233 13237	Definite bathymetry
East of Delaware A, B, C	931 descending	8/31/78	02:39	No Map	Internal waves
Cape Hatteras	974 descending	9/03/78	02:53	Already Listed	Possible bathymetry
Controller Bay, Alaska	1126 ascending	9/13/78	17:46	16723	Bathymetry visible
Shetland Islands	1149 ascending	9/15/78	08:22	No Map	Bathymetry visible
Sea of Cortez, Isla Angel De La Guarda	1183 ascending	9/17/78	17:20	No Map	Internal waves, possible bathymetry
Puerto Rico	1253 ascending	9/22/78	14:49	25640	Very faint bathymetry

TABLE 3-3A. Summary of Image Evaluation Results, SEASAT SAR Digitally Processed Data (Continued)

Location	Rev	Date	Time (GMT)	Map #	Comments
Bermuda	1267 ascending	9/23/78	14:24	No Map	Definite bathymetry
Strait of Juan de Fuca, Pacific coast	1269 ascending	9/23/78	17:50	Already Listed	Definite sediment, bathymetry
Hudson Canyon	1318 descending	9/27/78	04:33	NJ 18-3 123263	Complex pattern of unknown origin
Rockaway Seamount	1446 descending	6/10/78	03:32	Woods Hole Map	Surface patterns trace seamount area, 800 m depth
Boston Harbor	1447 descending	10/6/78	05:10	13270 13275	Some faint tracings in immediate harbor area
Chesapeake Bay	1468 ascending	10/7/78	15:59	12222 12224 12226 12235 12238	Some definite traces of shallow regions and shoals

TABLE 3-3B. Summary of Image Evaluation Results,
SEASAT SAR Optically Processed Data

ID/Rev	Time	Location	Comments
001 107 A	12:10	California coast	Interesting wake trace, no ship near San Diego
003A 163 B	10:01 10:21	Andros Island	Florida and Andros Island, TOTO bathmetry
011C-193	12:20:22	Southern tip of Baja	Mud flat areas, suspected contours
16B-221	11:34:00 11:34:10-20	North of Alaska	Possible underwater features
16C-221	11:19:50 11:20:40	Gulf of Mexico	Shallow seamounts can be seen in the Gulf
18A-230		Vancouver, Washington	Storms over Pacific, bottom features evident near Vancouver
18B-230	02:54:40	Vancouver Fir	Interacting lines in river, possible bottom contours
021B 236 A	12:32	Vancouver, BC	Straits of Juan de Fuca, bottom contour patterns
025 263 A	9:51	New York	Slight traces
026 273 D	2:61	Seattle	Some traces
031 289 D	5:48	Alaska	Cook Inlet, strong signature of 10-fathom line
037 322 D	12:48	Columbia River	Bar traces
038 323 A	14:33	Kodiak, Alaskan coast	Bottom and sediment traces
039 335 A	10:35	North Carolina coast	Traces
040 337 A	14:04	Cook Inlet	Bottom traces not as visible as Rev. 289
046A 351 B C	13:24	San Diego Los Angeles	Los Angeles harbor - Offshore wave line

TABLE 3-3B. Summary of Image Evaluation Results,
SEASAT SAR Optically Processed Data (Continued)

ID/Rev	Time	Location	Comments
51A-378	10:41:30	Cape Hatteras	Outer banks, Diamond Shoals clear. Other contours near Diamond Shoals evident.
51B-378	10:36:30 10:36:40	Bahamas	Subsurface atoll submerged (seamount) portion of island
056 393 A	11:40	Louisiana	Mississippi Delta signatures below surface
060A 407 B C	11:13	Andros Island Florida	Florida and Andros Island, TOTO bathymetry. South coast of Florida coastal traces.
062 416 D	2:54	Los Angeles	Offshore wave breaking area
63B-422	12:26:35	Gulf of Mexico	Contour lines matching maps in many locations
69A-443	00:19:40	Costa Rica	Possible features off coast
69B-443	00:15:00 00:15:30 00:16:30	Gulf of Mexico Florida Keys Coast of Cuba	Definite subsurface features near Florida Keys. Shelf visible.
69C-443		Northern Ice Packs	Possible offshore signatures near Mackenzie Delta
69D-443	06:47:50	Labrador - Nova Scotia	River mouth submerged features evident
73B-465	12:34:10	Gulf of Mexico	Large internal waves, subsurface strong outlines
077 474 D		Vancouver, Straits of Georgia	Traces very faint
79A-480		Vancouver Fir	Subsurface signatures
080 488 D	3:39	San Francisco	Bay traces
082 493 A	11:29	Bahamas	Bottom traces

TABLE 3-3B. Summary of Image Evaluation Results, SEASAT SAR Optically Processed Data (Continued)

ID/Rev	Time	Location	Comments
87A-508	12:37:30 12:39:00 12:41	Honduras, Nicaragua	Definite coastal subsurface traces
087A 508 B	12:41	Louisiana	Mississippi delta offshore signatures of submerged features
088 509	14:25	Point Reyes	San Andreas fault line clearly visible. Deep offshore traces near Cape Mendocino.
091 517 D	4:14	Seattle	Slight traces
093 522 A	12:07	Cuba	Faint offshore traces
098 536 A	11:40	Cape Fear	Coastal traces
106 552 A	14:31	San Franciso	Bay traces
107 556 D	21:37	Faeroe Island	Some traces Azores
108A:558 descending		Charleston	Mud flats and shallow shoaling
108B:558 descending	01:07:00 01:08:00 01:09:00 01:10:00 01:06:00 01:10:20 01:08:30 01:07:30	Tampa Bay Gulf of Mexico	String of underwater shoals, islands
111B-565	12:15:40-50 12:14:50 12:15:00	Off Florida Keys South of Cuba	Submerged features Subsurface signatures
118 590 A	6:17	Mediterranean	Slight traces
121 599 D		Azores	No traces
125 608 A	12:22	Florida	Coastal traces
127 617 D	4:02	Coast of California	Santa Barbara Channel trace

TABLE 3-3B. Summary of Image Evaluation Results, SEASAT SAR Optically Processed Data (Continued)

ID/Rev	Time	Location	Comments
1302A-1183	17:19:40	Sea of Cortez	Bottom topography
	17:25:40	Vancouver Strait	Bottom topography
131 633 A	6:29	French coast	Slight traces
135 642 A	21:50	Azores	No traces
138A:651 ascending	12:28:40	Cuba, Florida	Good underwater features
	12:29:25		
	12:30:10	Andros Island	Good subsurface feature, can detect Autec Range outlines.
	12:30:50		
	12:31:00-10		
	12:31:50	Gulf Coast	Offshore features
	12:30:20-40	Georgia Coast	
147 687 D	1:24	Bahamas	TOTO traces, Andros Island
150 694 D	12:37	Bahamas	TOTO - Andros Island traces
155A:719 ascending		North Scottish Coast	Ice between Iceland and Greenland
		North of Iceland	
		North of Sicily	
		South of Marseilles	
		English Channel	Subsurface signatures faint to non existent
155C:719		Same as 155A:719	
165A:757		Island	Faint structure off island
165B:757	22:44:40-50	North of Faeroe Island	Possible subsurface structure
167 761 D	5:27	Seattle	Faint traces
168 762 A	6:41	Mediterranean	Slight traces
	6:47	English Channel	Bottom traces
176 785 D	21:37	English Channel	Interesting lack of expected traces
177A 780 B	2:46	Louisiana	Mississippi delta and subsurface signatures

TABLE 3-3B. Summary of Image Evaluation Results,
SEASAT SAR Optically Processed Data (Continued)

ID/Rev	Time	Location	Comments
179 791 A	7:19	English Channel	Bottom traces
182A-795		Gulf of Mexico tip of Honduras	Definite subsurface lines
186 809 A	13:25	Florida/Jamaica	Some traces Florida coast
188 811 A	16:56	Alaskan coast	Interesting traces Kodiak Island and coast
193:834	7:32:20 7:31:30 7:28 to 7:29:30 7:27:00	North of Iceland South Coast of Iceland Islands between Scotland and Ireland	Structure in the Channel
	7:32:20 7:32:25	Coast of Iceland	Continuation of a Fault Line off coast of Iceland
196 838 A	2:47	Louisiana	Mississippi Delta, visible traces
200:852	13:29:40 13:31:30	Bahamas	Signatures north of island. Long signatures as subsurface island ridge descends.
	12:32:10	Coast of Georgia	Subsurface signatures
210-888	2:28:40	Cape Hatteras	Diamond Shoals outline
	2:26:55	Long Island	Offshore shoaling signatures
216 909 A	13:14	Chesapeake Bay	Bridge tunnel signatures
226:931	02:41:30 :40 02:41:00 02:39:20	South Atlantic South of Cape Hatteras Cape Hatteras Long Island Sound	Diamond Shoals signatures. Some turbulent boundaries bottom features.
240 974 D	2:51	Massachusetts coast	Slight subsurface traces
286 1126 A	17:46	Alaskan coast	Sedimentation and possible bottom traces at coast

TABLE 3-3B. Summary of Image Evaluation Results, SEASAT SAR Optically Processed Data (Continued)

ID/Rev	Time	Location	Comments
290A 1140	17:06		Baja internal waves
B	17:10	Vancouver	Vancouver - probable tidal/current signatures
298A 1177 B	7:44	Vancouver	Some slight indications
300:1181	14:02:30	Maine	Slight signatures off coast
302C-1183	17:19:40	Sea of Cortez	Bottom topography
	17:25:40	Vancouver Strait	Bottom topography
314A-1210	14:41:30	Atlantic Ocean	Ship and extensive wake
	14:41:35		
317A 1212 B	18:08	Gulf of Alaska	Underwater signatures
327 1232 D	4:10	Cape Hatteras	Diamond Shoals visible
329A 1235 B	9:06	Gulf of Alaska	Coastal sedimentation Some bathymetry
339A 1253A B	14:54	Chesapeake	Subsurface traces - Delmarva Peninsula - bridge and tunnel contours visible
342A 1255 B	18:18	Gulf of Alaska	Coastal river sedimentation and underwater contours
350A 1269 B C	17:46	California - Alaska	Long pass, much shoreline - No obvious signatures
358A-1282	15:36:10	Port Royal Sound, Broad River	Subsurface signatures
	15:34:30	Bahamas Islands	Subsurface features
	15:34:50	Barrier Reefs Island	Outcropping chain
	15:34:00		Island (subsurface) chain
358B-1282	15:33:50	Bermuda area	
	15:34:25		Dark subsurface triangle shape

TABLE 3-3B. Summary of Image Evaluation Results, SEASAT SAR Optically Processed Data (Continued)

ID/Rev	Time	Location	Comments
364 1292 D	9:01	Canada coast	Some coastal traces
365A 1296 B	15:09	Chesapeake	Subsurface traces - Delmarva Peninsula. Bridge and tunnel contours.
368A 1298 B	18:32	Gulf of Alaska	Coastal river sedimentation and underwater contours
371A 1308 B	8:20	Vancouver Island	Slight signatures
376 1312 A	17:57	Sea of Cortez	Internal waves
379 1318 D		New England, Quebec	Good coverage St. Lawrence - traces of channel dredging
386 1334 D	7:26	Los Angeles	Offshore wave action breaking
400 1359 D	1:17	Hebrides	Slight traces
410 1378	9:15	Canada coast	Some coastal traces
429 141A	16:13	Bahamas	TOTO Andros Island traces
433 1420 D	7:52	Los Angeles	Offshore wave action breaking
435A-1425	15:46:30	Chesapeake Bay	Subsurface contours
	15:46:40-50		Bottom contours
	15:46:00		Probable storm center
448B-1447	05:16:20	Caribbean	Very stormy
	05:18:10		Possible underwater islands
	05:16:50		Possible underwater islands
	05:16:50	Off Florida, just off coast of Honduras	Continental shelf
	5:15:15	North of Cuba	Island subsurface extension

TABLE 3-3B. Summary of Image Evaluation Results, SEASAT SART Optically Processed Data (Continued)

ID/Rev	Time	Location	Comments
467 1483 A		Caribbean - Cuba	No traces in expected areas
471A-1490	05:16:50 05:17:00	Southwest coast of Greenland	Good contours
	05:19:00 05:19:15	North coast of Labrador	Good contours
471B-1490	05:25:15 05:25:40	South of Cape Cod	Lines: probably current boundaries
	05:25:30	Cape Hatteras	Diamond Shoals clearly evident
471C-1490	05:30:50	North of Honduras	Seamounts visible
	05:31:10	Cuba to Florida	Some contours and sediment visible on south coast of Cuba
	05:31:20		Interesting rip tide through bar island, cyclonic storm patterns
	05:28:00 05:28:20 05:28:30	North of Cuba	Possible seamounts

TABLE 3-3C. Summary of Image Evaluation Results, SIR-A Optically Processed Data

ID No.	Location	Comments
2B	Mediterranean, Sardinia, Italy, Cephalonia	Ships, very very slight wakes in the Mediterranean. Near shore bottom signatures.
4	Lebanon, Syria, Iraq, Beirut, Damascus	Pipelines, railroads, river deltas
	Greece, Turkey, Cyprus, Rhodes	Ocean and island details, ships, no wakes
6A	Iraq, Saudi Arabia	None
6C	Persian Gulf, Iran	Port areas, evidence of oil
7	ABO Zabi Oman	Many ships, no wakes
	Indian ocean	Oil refinery networking, offshore bottom signatures
16-17	Spain, Tortuga	First evidence of clearly defined wake signatures
16-17	Spain, Portugal to Caribbean, Venezuela	Ships, no wakes
		Caribbean seamount indications
		Atlantic Ocean features, many squall and small storm zone areas
16-17	Lesser Antilles to Venezuela	Cultural detail on the coast of Venezuela
		Cyclonic storm out to sea
		Ship and wake (not prominent but present)
		Good display of ocean wave features
21	Mexico, Mississippi Delta, Cape Hatteras, Atlantic Ocean .	Cape Hatteras bottom signatures. Good subsurface patterns in Gulf and near Mississippi Delta

TABLE 3-3C. Summary of Image Evaluation Results, SIR-A Optically Processed Data (Continued)

ID No.	Location	Comments
22	New York, Pennsylvania, Ohio, Across U.S. to Baja	Excellent cross country sampling of farms, cities, geology, hydrology and open areas
		Large flood plane around Mississippi, offshore Gulf bottom signatures
24A	Upper California to Cape Hatteras	Large farming regions
		Mississippi flood plane areas, Missouri, Ohio River basins
		Good image of Diamond Shoals region, Cape Hatteras. Bottom topography off of Diamond Shoals.
24B	California to Florida	Island shelf regions visible
	Caribbean, Bahamas	Faint traces of bottom topography
	Trinidad	Ocean waves, storm visible
24BB	Java, Kalimantan, Celebes Sea,	Storm, hint of subsurface features east of Java, probable sedimentation northeast of Borneo
	Philippines	Philippine Sea, dark circular signatures near seamount regions
24C	Panama, Columbia, Brazil	Very complex watershed areas
		Amazon Basin, contrasting water flow patterns (some exposed and some faint traces through vegetation contours) and uniform jungle interlaced with river traces
24C	Sonora, Mexico Vera Cruz	Good mountains, Mexican agriculture, railroads, open areas, ocean perfectly specular, no wakes

TABLE 3-3C. Summary of Image Evaluation Results, SIR-A Optically Processed Data (Continued)

ID No.	Location	Comments
24C	Yucatan, Gulf of Mexico	Topography, hydrology, vegetation. Possible bottom signatures in the Gulf.
24C	Honduras	
28	Africa, Chad, Nigeria, Egypt, E. African Rift, Saudi Arabia, Iran, Afghanistan, Gobi Desert, Tsingtau	Spectacular geology and cultural journey over this wide expanse. Oil emplacement in Persian Gulf. Large Supply areas in Afghanistan. Desert regions in northern China.
29-30	Africa	Railroad, powerline patterns, circular irrigation patterns Sahara expanse - similar to northern China geology Company pattern cities in many locations (compounds) Nile River areas - Delta regions bottom contours very evident.
34	Brazil	Extensive river and vegetation coverage, good inland hydrography
35-36	Spain, Iran, India, Indonesia, Australia	Heavy farming and agricultural development, industrial region
37A		
	Al Jabuyl, SA	Good geology, roads clearly visible
	Indian Ocean	Ships, no wake
37A	Persian Gulf, Saudi Arabia	Very detailed look at Persian Gulf installation.
	Aveiro, Portugal	Ships, no wakes.
	Mediterranean	Greek islands, Corinth Canal
	Greek Islands, Italy, Spain	Ships and wakes off coast of Spain. Unusual as wakes do not ordinarily appear in SIR-A data.

TABLE 3-3C. Summary of Image Evaluation Results, SIR-A Optically Processed Data (Continued)

ID No.	Location	Comments
37	Ocean, South Pacific to Central America and the Gulf of Mexico	Ships, no wakes. Agriculture farms in Panama. Canal Zone very evident. Portions of Puerto Rico and Haiti visible. Very unusual geological patterns in Galapagos Island area. Bottom signatures.
37A	Pacific Ocean	Ship - first evidence of Kelvin Wake signature

be one of two things: in the open ocean, this is probably a storm center or area of rainfall; near a coastline or in an enclosed area (bay or river), a solid area of different reflectance is either an area of different salinity or a volume of sediment or sand-laden water. Current boundaries have also been observed as bright or dark lines, and many are very predominant in the Gulf of Mexico and the Atlantic Ocean near the Gulf Stream.

Image negatives were acquired to produce same-size overlays between the map and photograph for several scenes. This allowed very detailed comparison of these areas.

Weather maps corresponding to all of our digital prints and information on tides and currents in these areas were obtained. Data sources included the following specific information sets:

- Tidal information came from the tidal predictions for 1978 published as Tide Tables 1978, High and Low Water Predictions, by the U.S. Department of Commerce, National Oceanic and Atmospheric Administration, National Ocean Survey.
- Tidal current information was also taken from the 1978 prediction tables. These were Tidal Current Tables 1978, by the U.S. Department of Commerce, National Oceanic and Atmospheric Administration, National Ocean Survey.
- Bathymetry information was obtained from various charts published by either the National Oceanic and Atmospheric Administration or the Defense Mapping Agency.
- Weather information was derived from official U.S. weather maps for the period which give the weather at 6-hour intervals and are archived at the World Weather Building, Camp Springs, Maryland.

As a result of the broad survey summarized in Table 3-3, a number of areas were selected as being worthy of more detailed analysis. About half of these have actually been comprehensively analyzed to date and the results are discussed in the next section.

3.3 Sites of Concentration

The possible sites of concentration are listed in Table 3-4. A detailed, comprehensive analysis of an area includes correlation of each image with tidal, current and other synoptic environmental data such as wind and wave histories. Each image which has a confirmed bathymetric signature is also compared 1:1 on a map scale basis with the most recent bathymetric map covering the image area. These images were selected to cover a range of representative conditions associated with several radars (satellite SAR's - SEASAT and SIR-A; aircraft radar), different radar aspect and incidence angles; many air/sea interface states ranging from low to high range wind and wave states; a similar sampling of diverse tidal/current conditions, and a wide variability in subsurface bathymetric shape, orientation and depth.

Radar Aspect/Feature Orientation	0° to 180°
Radar Incidence Angle	20° to 50°
Wind Speed and Aspect Angle	0 to 15 kt, 0° to 180°
Wave State $H^{1/3}$	$\leq$ 2 m
Tide and Current Speed and Aspect Angle	$\leq$ 6 kt, 0° to 180°
Bathymetric Orientation, Depth	0° to 180°
Many patterns from single seamount or shoal projections to multiple braided or interconnected shapes	Shallow to 100's of m
Bathymetric SAR Signature	Faint to Very Strong

TABLE 3-4. Sites of Concentration

Area	Signature
Straits of Georgia, BC	Moderate
Anchorage, AL	Good
St. Nicolas Island, CA	Moderate
Nicaro Mountains, Cuba	Moderate
Diamond Shoals, NC	Moderate
Mississippi Delta	Faint
Port a Piment, Haiti	Moderate
Miami, FL	Moderate
Straits of Georgia, BC	Good
Columbia River, OR	Moderate
English Channel	Very Good
Everglades, FL	Moderate
Nantucket Island	Very Good
Diamond Shoals, NC	Faint
Controller Bay, AL	Good
Shetland Islands	Good
Bermuda	Very Good
Straits of Juan de Fuca, BC	Faint
Misteriosa Bank	Very Good
Chesapeake Bay	Moderate
Tongue of the Ocean (TOTO)	Very Good
Rockaway Seamount	Moderate

Many of the sites were viewed several times by SEASAT and/or SIR-A. At least one digitally processed frame is available for each site to provide a high quality image and facilitate future automatic signature extraction.

This study of the sites of concentration set out to define the limits of the hydrologic, air-sea and radar parameters for the visibility of underwater morphology. Several questions were asked. How deep can the bathymetry be and still be visible? Is there a dependence on current flow - tidal or otherwise? Do high winds obscure the effect? Does rain dampen the waves which are involved? Is there a dependence on radar incidence or aspect angle? Does the image processing affect bathymetry visibility? We have only partially answered some of these questions. In some cases, the data was too limited; SEASAT operated during the summer months in low to moderate latitudes, so there are very few examples of high wind conditions in the data set. In all cases there is a separation of variables problem. When any one of six parameters can make bathymetry disappear and three are in the suspected negative range, which is responsible?

The questions listed above will now be addressed. Besides an absolute limit on water depth, there appears to be a conditional limit. The absolute limit would be the deepest place that it is possible to observe bathymetry with radar. The deepest confirmed observations in our data set were off Port a Piment, Haiti (20 fathoms or 120 ft), Hurd Deep in the English Channel (50 fathoms or 300 ft), south of the Florida Keys (500 ft) and the Straits of Juan de Fuca and the Straits of Georgia (100 fathoms or 600 ft). Seamount observations, such as the Rockaway Seamount, provide speculation as to what is causing an unusual and obvious surface pattern over the seamount. Direct correlation deserves further study.

The Haiti and Florida observations are of much higher reliability than the English Channel and British Columbia (Straits of Georgia, Straits of Juan de Fuca) observations. The latter were only observed on one revolution each and may be due to causes other than bathymetry. Nevertheless, there is reliable evidence to 500-ft depths. This gives a lower limit on depth of bathymetry visibility but not an upper limit; images of other areas could reveal yet deeper bathymetry.

The conditional limit on depth of visible features depends on the conditions at the time of image or the conditions in the area. At the Diamond Shoals off Cape Hatteras, the edges of the shoal are about 20 ft deep and they appear in some images but not in others with what looks like a current dependence. The higher the current, the better the visibility on the outer Diamond Shoals. In one image of the Shetland Islands, a 12 fathom bank is visible while the 16 fathom bank next to it is not. There is only one pass over the Shetland Islands in this data set and no current information is available for it. Several passes over this area with both strong and weak currents could give a better limit on depth visibility versus current magnitude.

Both the speed and direction of underwater currents seem to affect the visibility of underwater features. In their North Sea work, McLeish et al. (1981) saw a directional dependence: when a linear feature was perpendicular to a rotary tidal current, it was visible; when the current turned and ran parallel to the bank, it disappeared. In our Florida image, the 500 ft contour is parallel to the Gulf Stream flow and is visible. It is possible that some kind of current shear affect is happening in the Florida image that does not happen in the North Sea image. This conflict of observations requires more investigation.

A plot of bathymetry visibility versus tidal current at Cape Hatteras gave a positive correlation; the stronger the current, the better the visibility. A similar plot for the Straits of Georgia gave inconclusive results, although the image with the strongest current had the best visibility. There is also evidence of place that either a current, wave or swell action is necessary for bathymetry visibility. The two coasts of Florida are an excellent example; the southern Atlantic coast has both more wave action than the Gulf coast and the Gulf Stream moving northward close in to shore and shows a distinct 500 ft line from Key West to Lake Worth. The Gulf Coast has much weaker wave action than the Atlantic and lacks the Gulf Stream current and shows no bathymetry. Again though, we have two variables (current and wave action) which cannot be separated. On the north coast of Cuba, there is a dark line at the 10 m (30 ft) break north of the Nicara Mountains where the chart indicates breakers. Since this outline does not appear elsewhere on the coast (only where breakers are indicated), this seems to be a wave action and not current dependent mechanism. The sum total is that currents, waves or swell are necessary for viewing underwater features with radar.

The effects of wind and rain are still undetermined. As mentioned before, there were very few instances of winds over Beaufort Force 4 (13 to 18 mph) in the entire SEASAT data set, so the predictions that a high wind would totally obscure bathymetry could not be checked. The Shetland Islands image had definite bathymetry with a wind Force 3 to 4 (8 to 18 mph). A graph of wind versus visibility at Cape Hatteras gave a negative correlation; higher winds yielded lower visibility. This graph had a large scatter in values, however, making it of low reliability. Also, the one extreme determining

point at wind Force 4 also had possible rain and the lowest currents of any Cape Hatteras image.

Rain is still a complete unknown. The prediction was that rain would dampen the ocean waves which are responsible for the Bragg scattering which creates the radar return. With weather stations hundreds of miles apart and records only every 6 hours, it is usually impossible to be certain whether or not there was rain during an image.

The radar parameters which were expected to affect visibility were incidence angle, aspect angle and processing. The SEASAT radar viewed the earth with an incidence angle of 20° from the vertical, while SIR-A used an angle of 47°. The Diamond Shoals are just as visible in the SIR-A image as the SEASAT passes, so over that range at least visibility is independent of incidence angle. There is an aspect angle dependence in viewing ocean waves. When the radar look direction is either upwind or downwind, the waves are more visible than when it is crosswind. At the Straits of Georgia the ascending passes give somewhat better visibility than the descending passes. This is the only evidence in this data set for an aspect angle dependence.

Lastly, the processing of the images is important. Both in the Straits of Georgia and at Cape Hatteras, there is one image which was processed so that no detail shows in the ocean. If these were reprocessed to bring out ocean detail, some bathymetry might become evident.

e detailed limits on the radar, air/sea, tidal/current flow and subsurface characteristics for the radar observations of the sites have been determined and are plotted in Chapter 4. What is clear from our analyses is that neither SEASAT nor SIR-A experiments were designed to evaluate the radar's ability to view subsurface features. Hence, there were no controlled

surface measurements or attempts to isolate one or more of the variables that contribute to subsurface imaging.

There are several parameters which affect the ability to detect bottom morphology, such as current magnitude, current direction, water depth, etc. In a controlled experiment of N variables, N-1 would be held constant while the Nth is varied and the effects observed. This would be done for each variable and a mathematical relationship could be set up for each such that:

$$V = A_N X_N + C_N$$

where

V is the visibility of bathymetry, in percent

A_N is the multiplier determined from experimental data

X_N is the Nth variable

C_N is the offset determined from data

For example, if the current velocity was measured from 0 to 7 kt and the visibility went from 50% to 100% the equation would be V = 7.14 (current velocity) + 50%, so that A_N is measured from data as 7.14 and C_N as 50%.

SEASAT was not designed to measure bottom morphology; hence there were no controls for this particular effect. Therefore, several parameters varied from scene to scene. The equation required to determine the effect of these parameters would have to be of the form:

$$V = A_1X_1 + A_2X_2 + A_3X_3 + \ldots A_{N-1}X_{N-1} + A_NX_N + C$$

or possibly:

$$V = A_1X_1 + A_2X_2 + A_3X_3 + \ldots A_{N-1}X_{N-1} + A_NX_N + C$$

There is now no simple way to isolate and measure A_N or C. Guided by physical reasoning and an intuition developed by many observations, values for

A_N may be guessed at and tried against the data. By rejecting or confirming each trial, a better understanding of the effect of each parameter on bathymetry visibility may be obtained. Control of these parameters requires the design and execution of a well instrumented experiment such as the one prescribed in the following section.

3.4 Recommendations to Improve Our Understanding of Oceanic Subsurface Remote Sensing

A future experiment using the August 1984 space shuttle SAR (SIR-B) can be designed using the knowledge gained during the current study. Experiment regions and instrumentation networks can be prescribed using the study results. The new space shuttle SAR (SIR-B) has important incidence angle and aspect angle (squint) adjustment variability which can be used to test many bathymetric signature conditions. Automatic extraction techniques are possible because of the primary digital recording mode used.

SIR-B is a National Aeronautics and Space Administration (NASA) experiment and planning is currently in process for this mission. Initial proposals spelling out experiment objectives, sites, required observation timing, etc. are due to NASA in February 1983. Detailed mission and experiment plans including sea surface and undersea instrumentation need to be finalized by the Fall of 1983, some nine months prior to the SIR-B overflights. Selection of experiment sites and identification and scheduling of ship, current meter, wind and wave measuring devices and other resources should begin as soon as possible to be consistent with these dates.

SIR-B represents the first step toward an eventual radar research instrument which exploits the full information content in backscattered

microwave energy. It is a very significant first step since the ability to control the illumination geometry is very important in a wide variety of potential research applications. SIR-B's digital data record will permit valuable signature extraction experiments to be conducted in the assessment of radar image utility for operational applications.

SIR-B will also permit a number of technological experiments to be conducted which will assess the performance of both the sensor itself and the capabilities and limitations inherent in digitally processed SAR images.

The second Shuttle Imaging Radar (SIR-B) mission is the next step in the evolutionary sequence of NASA spaceborne Synthetic Aperture Radar (SAR) which began in 1978 with the SEASAT SAR and continued in 1981 with SIR-A as shown in Table 3-5. SIR-B will be the largest instrument of the third Office of Space and Terrestrial Applications (OSTA-3) experiment pallet on the seventeenth flight of the space shuttle (STS-17) scheduled for launch in August 1984. Like SEASAT and SIR-A, SIR-B will be an L-band, HH-polarized SAR. However, SIR-B will for the first time provide the ability to control the angle of incidence from 15° to 60° by mechanically tilting the antenna. SIR-B will provide 25 hours of digital data acquisition using the NASA Tracking and Data Acquisition Satellite System (TDRS) in addition to 8 hours of optically recorded data. In the case of digital data acquisition, radar echoes will be digitally sampled at 3 to 6 bits each, transmitted to the ground via the Shuttle-TDRS Ku-band communications link, and subsequently digitally processed into image format at JPL. Approximately 30 million square kilometers of the earth's surface will be imaged in swaths ranging from 30 to 60 km wide and with a range IFOV of 55 m at a 15° angle of incidence to 17 m at a 60° angle

TABLE 3-5. SAR Ocean Subsurface Data Availability

	SEASAT SAR 1978	Shuttle SIR-A 1981	Shuttle SIR-B 1984
Wavelength	23.5 cm	Same	Same
Incidence Angle	20°	47°	15° to 65° Variable
Data Record	Digital	Film	Digital
Capacity (Scenes)	10,000	2,400	9,000

of incidence. The azimuth IFOV will be 25 m with four look image processing. The peak transmit power will be 1 kW and the antenna will be a 2.16 m (range) x 10.7 m (azimuth) planar array of microstrip patch elements having a one-way gain of 32.9 dB. In order to make efficient use of the available space in the orbiter payload bay, during launch and landing the antenna will be folded into a stack of three sections. Table 3-6 compares the SEASAT SAR, SIR-A and SIR-B radars.

The SIR-B instrument will be mounted on the OSTA-3 pallet which will also carry the Large Format Camera (LFC), the Feature Identification and Location Experiment (FILE), the Measurement of Air Pollution System (MAPS) and possibly other remote sensors. OTSA-3 will be launched from the Kennedy Space Center into a 57° inclination circular orbit with 225 km altitude. Using its optical recorder, SIR-B will be able to provide imagery of any selected areas of the earth between 60° south latitude and 60° north latitude. With the digital shuttle-to-TDRS link, the areas of coverage are restricted to those where the shuttle Ku-band antenna is in view of the TDRS satellite.

The exciting possibilities of observations of bottom topography brought forth in the SEASAT imagery can be exploited with SIR-B. In particular, sites where the evidence is already available from SEASAT and/or SIR-A can be surveyed with SIR-B, but this time with extensive surface truth instrumentation in place.

Beyond SIR-B, additional shuttle based and independent platform imaging radar experiments are being planned by NASA which will add the additional parameters of controllable wavelength and polarization to space based radar remote sensing research. Both SIR-B and these advanced radars will be

increasingly put to use in combination with satellite imagery from optical sensors such as the Landsat-D Thematic Mapper and solid-state linear array pushbroom scanners beyond Landsat-D.

TABLE 3-6. SEASAT SAR, SIR-A and SIR-B System and Processor Characteristics

SAR System Parameters	SEASAT SAR	SIR-A	SIR-B
SAR Orbit	Polar (108°)	Shuttle (38°)	Shuttle (58°)
Nominal Altitude	794 km	268 km	220 km
Nominal Speed	6844 m/sec	7450 m/sec	7800 m/sec
Transmit Frequency	1275 MHz	1275 MHz	1285 MHz
Pulse Repetition Frequency	1463, 1537, 1645 Hz	1464 to 1770 Hz	1480 to 1800 Hz
Pulse Duration	33.8 μsec	33.8 μsec	33.8 μsec
Pulse Bandwidth	19 MHz	6 MHz	12 MHz
A/D Sample Rate	45.53 MHz	N/A	30 MHz
Optical Record Bandwidth	N/A	6 MHz	6 MHz
Antenna Dimensions	2 x 10.5 m	2.16 x 9.35 m	2.16 x 10.7 m
Antenna Look Angle	20°	47°	15° to 65°
Attitude Accuracy	±0.5°	±1°	±1°

Processor Performance Requirements

Type	Digital	Optical	Digital Optical
Image Frame Size	100 km x 100 km	Continuous strip 54.6 km wide	60 km x 60 km Continuous strip
Image Resolution	25 m	37 m	50 m to 17 m Variable
Number of Looks	4	7	4

CHAPTER 4

SAR DATA, GROUND TRUTH AND EVALUATIONS

4.1 Introduction

The SAR and surface truth data is presented and evaluated in this chapter. It is divided into two sets: areas of concentration and individual passes. In the data survey, the areas with the most promising bathymetry were selected and a comprehensive data search was done on these areas. This included searching the lists to find every single SEASAT pass over the area, whether optically or digitally processed; evaluating possible bathymetry on each with the aid of bathymetric maps; and then obtaining all possible ground truth for each image. For the less promising areas, the digital images were evaluated for bathymetry and as much ground truth was gathered as possible. For any one pass, in either set, the data presented includes an evaluation of the bathymetry, the weather as obtained from 6-hour weather maps, information on tidal level and information on current flow. Occasionally, some piece of this data is missing. For example, current information for the English Channel is not reported. Readers interested in an extensive treatment of this area are referred to work in progress by Shuchman. The areas of concentration are presented first, in alphabetical order by geographical region. The other images are presented in alphabetical order by geographical area in the next section.

The ground truth which was gathered has some definite limitations, which are described in the following paragraphs and which should be carefully noted. It should also be noted that unless rain is specifically mentioned in the weather data, it is assumed that it did not exist.

4.2 Limitations of Available Ground Truth

Surface currents are predicted in the tables published by the National Oceanic and Atmospheric Administration (NOAA), but current direction may change as much as 180° with depth and depth currents are of great importance in viewing bathymetry.

Tidal currrents are predicted; wind driven currents are not considered. At Cape Hatteras, an average of 0.5 kt wind current exists, but wind data are usually insufficient to predict this. Currents such as the Gulf Stream are not accounted for, but they do affect places like Florida and Cape Hatteras.

Even the tidal currents measured/predicted are at too coarse a scale geographically; i.e. the closest predictions to Diamond Shoals are at Hatteras Inlet, and these two areas may be very different. Hatteras Inlet is a channel from the bay to the ocean while Diamond Shoals is removed from the Bay and protrudes into the ocean, so bay to ocean flow should not affect the Shoals as much as the Inlet. Also, since Hatteras Inlet is back from the point, it is not as affected by winds or the Gulf Stream. Little change between the Hatteras and Ocracoke Inlets indicates some continuity of physical effects, but how much extends to a point such as Diamond Shoals is unknown. Measurements on Diamond Shoals itself are actually needed.

Wind measurements are every 6 hours and often the closest station is a hundred miles or more away from the SAR image. According to private conversations with Pat De Leonibus of NOAA-NESS, the length of time for which winds can be assumed constant is only about an hour. Within 2 hours, radical changes may occur. If the 6-hour interval measurements before and after the image are fairly close; it can be assumed that the wind remained

at the measured level during the interval, and where possible, this has been checked in our data. However, if the wind changed significantly in the 6-hour interval, no reliable data is known.

Rain measurements require even more frequent repetition. As anyone who has been caught in a sudden downpour knows, rain can come, go and be gone in 5 or 10 minutes. Since rain is considered to be a primary damping mechanism for the short gravity waves which radar responds to, this is a critical factor which is essentailly unmeasured in our data. At times, it can be inferred from the appearance of the ocean surface (large blacked out areas), but a positive identification does not exist.

Sea state is another critical parameter in radar observation of the ocean surface and bathymetric effects. This consists of two factors at any one site; the immediate waves and the swell coming in from some distance. The measurements of both these quantitites (direction, period and height for both sea and swell) are sparse both in space and time. The closest buoy may be hundreds of miles from an imaged area, and sea and swell measurements are often missing from even the 6-hour interval weather reports.

4.3 Areas of Concentration

4.3.1 Summary of Sea of Cortez Images

The Sea of Cortez (Gulf of California) is a puzzling and fascinating area. There are marks which appeared very characteristic of bathymetry, but turned out not to follow any contours. The marks which do follow contours at all do so very poorly and may or may not be related to bathymetry. These lines in the Gulf of California may be of a totally different origin than any explored or tentatively explained elsewhere and should be noted for future work.

Sea of Cortez (Gulf of California)

No definite bathymetry was found in the Gulf of California.

Rev. 150, ascending pass, 7/07/78, 12:16 GMT

There are large internal waves and possible bathymetric contours in the Pacific, but nothing in the Gulf.

Rev. 193, ascending pass, 7/10/78, 12:23 GMT

There are large internal waves in the Gulf and a good portion of it is covered, but no bathymetry is visible.

Rev. 387, descending pass, 7/24/78, 02:19 GMT

Large internal waves, no bathymetry is visible.

Rev. 473, descending pass, 7/30/78, 02:33 GMT

No bathymetry is visible

Rev. 545, descending pass, 8/04/78, 03:18 GMT

No bathymetry is visible

Rev. 631, descending pass, 8/10/78, 03:32 GMT

No bathymetry is visible

Rev. 1140, ascending pass, 9/14/78, 17:06 GMT

This is the first of two digitally processed images. It contains many internal waves and some sedimentation areas, but no bathymetry.

Rev. 1183, ascending pass, 9/17/78, 17:20 GMT

This is the second digitally processed image. There is a very well outlined pattern north of Isla Angel de la Guarda which appears in a few different passes, but does not correspond to any bathymetric contours. It does not correlate with the internal waves present, does not have the characteristic appearance of storm or wind lines, and the V shapes present (one large V and one triangle in this image) are not typical of current boundaries. The origin of these lines is a very interesting puzzle.

Rev. 1226, ascending pass, 9/20/78, 17:32 GMT

Between Isla San Pedro Martir and the volcanic island to the south directly east of Santa Rosalia, there is a distinct line which very roughly follows the 800 m contour. The alignment is only approximate so this may or may not be a bathymetric expression.

The V shape pattern north of Isla Angel de la Guarda seen on Rev. 1183 is again present, and again does not follow the bathymetric contours.

Rev. 1312, ascending pass, 9/26/78, 17:57 GMT

No bathymetry is visible.

Rev. 1355, ascending pass, 9/29/78, 18:10 GMT

There is one line just south of the Colorado River, but it does not follow a contour line.

Rev. 1398, ascending pass, 10/02/78, 18:23 GMT

The line south of the Colorado River is here in the same position and the V pattern north of Isla Angel de la Guarda is present also, but no bathymetry is visible.

Rev. 1441, ascending pass, 10/05/78, 18:36 GMT

All of the Gulf is visible on this pass and the line south of the Colorado River which does not follow the bathymetry is again present. Another line south of the Colorado and east of the first one may very roughly follow an 80 m contour.

Rev. 1484, ascending pass, 10/08/78, 18:48 GMT

The V pattern north of Isla Angel de la Guarda is present but no bathymetry is present.

4.3.2 Summary of English Channel Images

No current information was obtained for the English Channel. Since there are undoubtedly strong and variable currents in areas such as the Dover Strait, this is a critical deficiency. Bathymetry was evident on all but one of the passes which covered the shoal areas north of Belgium, near Dunkirk, but with varying clarity. Rev. 719 is the only pass with any rain indicated anywhere in sight on the weather map. However, the ocean did not have the mottled appearance characteristic of rain - it had the very smooth appearance which indicates no rain. Despite the weather report 40 minutes earlier at London, there was probably no rain over Dover Strait. The maximum wind for any of these passes was 7 mph (Force 2), which is a low wind, giving great visibility in many areas. Thus it does not seem that wind or rain were the cause of any variability in the clarity of bathymetry. The current information must be obtained before any real conclusion can be drawn.

English Channel
Rev. 547

8/04/78

06:11 GMT
07:11 On the Continent

Bathymetry Visibility Evaluation

This is the western part of the channel. No bathymetry is visible and very few marks of any kind show in the water.

Weather

06:00 GMT
50°N, 6°30'W
Overcast
Air temp. - 14°C
Dew point - 13°C
Barometer - 1016.9 mb
Wind, Force 2 - 4 to 7 mph
from the SW

51°30'N, 0°30'W
Slightly overcast
Air temp. - 13°C
Dew point - 11°C
Barometer - 1014.9 mb
Wind, Force 1 - 1 to 3 mph
from the SW

Falmouth - 50°09'N, 5°03'W

High tide	05:13	16.0 ft
Low tide	11:47	3.3 ft

Roscoff - 48°43'N, 3°58'W

High tide	06:07	25.3 ft
Low tide	12:29	5.3 ft

Cherbourg - 49°39'N, 1°38'W

Low tide	03:36	4.9 ft
High tide	09:11	19.0 ft

Time Meridian, 15°E

Ventnor (Isle of Wight) - 50°36'N, 1°12'W

Low tide	04:12	1.0 ft
High tide	11:16	9.4 ft

Dover - 51°07'N, 1°19'E

High tide (3rd)	23:08	20.3 ft
Low tide	06:25	4.3 ft

English Channel
Rev. 590

8/07/78

06:19 GMT
07:19 On the Continent

Bathymetry Visibility Evaluation

No bathymetry is visible

Weather

06:00 GMT
50°N, 1°30'W
Partly cloudy
Air temp. - 13°C
Dew point - 12°C
Barometer - 1011.5 mb
Wind, Force 1 - 1 to 3 mph
from the W

51°30'N, 0°30'W
Partly cloudy
Air temp. - 13°C
Dew point - 12°C
Barometer - 1007.9 mb
Wind, Force 1 - 1 to 3 mph
from the W

Falmouth - 50°09'N, 5°03'W

Low tide	01:17	3.3 ft
High tide	06:56	16.3 ft

Roscoff - 48°43'N, 3°58'W

Low tide	01:51	4.5 ft
High tide	07:44	25.8 ft

Cherbourg - 49°39'N, 1°38'W

Low tide	05:14	4.3 ft
High tide	10:48	19.4 ft

Time Meridian, 15°E

Ventnor (Isle of Wight) - 50°36'N, 1°12'W

Low tide	05:51	0.76 ft
High tide	12:51	9.6 ft

Dover - 51°07'N, 1°19'E

High tide	00:42	21.0 ft
Low tide	08:07	3.6 ft

English Channel 8/10/78 06:26 GMT
Rev. 633 07:26 On the Continent

Bathymetry Visibility Evaluation

South of St. Alban's Head (English coast), the 10 fathom line shows spectacularly. Between St. Alban's Head and Barfleur (French coast), a pattern shows which looks like bathymetry, but nothing shows on the small scale map presently available.

Weather

06:00 GMT

50°N, 6°30'W
Partly cloudy
Air temp. - 11°C
Dew point - 11°C
Barometer - 1022.6 mb
No wind

51°30'N, 0°30'W
Overcast, fog
Air temp. - 13°C
Dew point - 12°C
Barometer - 1020.5 mb
Wind, Force 1 - 1 to 3 mph from the NNE

Falmouth - 50°09'N, 5°03'W

Low tide	03:05	4.0 ft
High tide	08:48	15.6 ft

Roscoff - 48°43'N, 3°58'W

Low tide	03:39	6.0 ft
High tide	09:31	24.5 ft

Cherbourg - 49°39'N, 1°38'W

Low tide	06:57	5.4 ft
High tide	12:32	18.2 ft

Time Meridian, 15°E

Ventnor (Isle of Wight) - 50°36'N, 1°12'W

High tide	02:13	9.0 ft
Low tide	07:32	1.3 ft

Dover - 51°07'N, 1°19'E

High tide	02:25	19.7 ft
Low tide	09:48	4.6 ft

English Channel 8/16/78 06:40 GMT
Rev. 719 07:40 On the Continent

Bathymetry Visibility Evaluation

Absolutely nothing shows north of Gris Nez and Calais where there is distinct bathymetry on Rev. 762 and a few other passes.

Weather

06:00 GMT
51°30'N, 0°30'W
Partly cloudy, rain in sight, but not at station
Air temp. - 13°C
Dew point - 12°C
Barometer - 1011.7 mb
Wind, Force 1 - 1 to 3 mph from the SW

Falmouth - 50°09'N, 5°03'W

High tide	02:49	15.6 ft
Low tide	09:33	3.3 ft

Roscoff - 48°43'N, 3°58'W

High tide	03:36	25.0 ft
Low tide	10:05	5.5 ft

Cherbourg - 49°39'N, 1°38'W

High tide	06:40	18.7 ft
Low tide	13:28	5.1 ft

Time Meridian, 15°E

Ventnor (Isle of Wight) - 50°36'N, 1°12'W

Low tide	01:47	0.8 ft
High tide	08:55	9.4 ft

Dover - 51°07'N, 1°19'E

Low tide	03:47	4.3 ft
High tide	08:56	20.3 ft

English Channel | 8/19/78 | 06:46
Rev. 762 | | 07:46 GMT (at Zeebrugge)

Bathymetry Visibility Evaluation

This image has the most outstanding and distinct bathymetry of any of the English Channel. Many of the sandbanks north of Calais and Dunkirk are outlined well, although a few just offshore east of Dunkirk are not visible. On the optically processed image which extends farther north than the digital print, the bathymetry is just as obvious off the coast of England near Yarmouth.

Environmental data (meterological and oceanographic)
Noord Hinder Vessel - 51°39'N, 02°33'E
Met - Konin Klijk Netherlands Met Institute
Ocean - Hydrographers of the Navy, British Admiralty

Weather

06:00 GMT
Wind speed - 4 kt
Direction - 146°
Water temp. - 16.4°C
Air temp. - 17°C
Period of Waves - 1 sec
Dew point - 13°C
No rainfall
Wave height - 0.5 m

Dover - 51°07'N, 1°19'E

Low tide	06:40	2.0 ft
High tide	11:27	23.3 ft

Calais - 50°58'N, 1°51'E

High tide	00:23	23.5 ft
Low tide	07:45	1.7 ft

Zeebrugge - 51°20'N, 3°12'E

High tide	01:50	16.6 ft
Low tide	08:15	2.1 ft

Time Meridian, 15°E

English Channel 8/20/78 21:40 GMT
Rev. 785 22:40 On the Continent

Bathymetry Visibility Evaluation

The bathymetry shows around Guernsey Island, Casquets and the Roches Douvers. The outline of Hurd Deep at 50 fathoms is partially evident.

Weather

18:00 GMT
50°N, 6°30'W
Partly cloudy
Air temp. - 17°C
Dew point - 14°C
Barometer - 1022.2 mb
Wind, Force 1 - 1 to 3 mph
from the SW

51°30'N, 0°30'W
Partly cloudy
Air temp. - 23°C
Dew point - 14°C
Barometer - 1017.7 mb
Wind, Force 2 - 4 to 7 mph
from the W

Falmouth - 50°09'N, 5°03'W

High tide	18:36	17.9 ft
Low tide (21st)	01:15	2.0 ft

Roscoff - 48°43'N, 3°58'W

High tide	19:20	29.3 ft
Low tide (21st)	01:45	1.9 ft

Cherbourg - 49°39'N, 1° 38'W

High tide	22:24	22.1 ft
Low tide (21st)	05:08	2.3 ft

Time Meridian, 15°E

Ventnor (Isle of Wight) - 50°36'N, 1°12'W

Low tide	17:41	0.4 ft
High tide (21st)	00:15	10.3 ft

Dover - 51°07'N, 1°19'E

Low tide	19:57	1.0 ft
High tide (21st)	00:37	22.6 ft

English Channel 8/21/78 07:21 GMT
Rev. 791 08:21 On the Continent

Bathymetry Visibility Evaluation

Nothing shows, even around Guernsey and Jersey islands where there is bathymetry visible on other images. There are what look like storm markings scattered over the whole channel.

Weather

06:00 GMT

50°N, 6°30'W
Clear
Air temp. - 14°C
Dew point - 14°C
Barometer - 1023.1 mb
Wind, Force 2 - 4 to 7 mph
from the SW

51°30'N, 0°30'W
Partly cloudy
Air temp. - 15°C
Dew point - 13°C
Barometer - 1021.8 mb
Wind, Force 1 - 1 to 3 mph
from the W

Falmouth - 50°09'N, 5°03'W

High tide	06:54	17.9 ft
Low tide	13:39	1.7 ft

Roscoff - 48°43'N, 3°58'W

High tide	07:41	28.3 ft
Low tide	14:06	2.5 ft

Cherbourg - 49°39'N, 1°38'W

Low tide	05:08	2.3 ft
High tide	10:46	21.3 ft

Time Meridian, 15°E

Ventnor (Isle of Wight) - 50°36'N, 1°12'W

Low tide	06:00	0.1 ft
High tide	12:48	10.5 ft

Dover - 51°07'N, 1°19'E

High tide	00:37	22.6 ft
Low tide	08:12	1.6 ft

English Channel
Rev. 834

8/24/78

07:26 GMT
08:26 On the Continent

Bathymetry Visibility Evaluation

East of the Cherbourg peninsula (coast of France), the very shallowest water next to the beach appears as a perfectly black area with a discontinuous bright line on the ocean side which may be breakers. Otherwise, no bathymetry is visible on this image.

Weather

06:00 GMT

50°N, 6°30'W
Clear
Air temp. - 13°C
Dew point - 11°C
Barometer - 1029.2 mb
Wind, Force 2 - 4 to 7 mph
from the NE

51°30'N, 0°30'W
Overcast
Air temp. - 14°C
Dew point - 11°C
Barometer - 1029.0 mb
Wind, Force 1 - 1 to 3 mph
from the N

Falmouth - 50°09'N, 5°03'W

Low tide	03:22	3.6 ft
High tide	09:02	16.3 ft

Roscoff - 48°43'N, 3°58'W

Low tide	03:53	5.8 ft
High tide	09:46	24.7 ft

Cherbourg - 49°39'N, 1°38'W

Low tide	07:10	5.4 ft
High tide	12:46	18.4 ft

Time Meridian, 15°E

Ventnor (Isle of Wight) - 50°36'N, 1°12'W

High tide	02:35	9.2 ft
Low tide	07:56	1.1 ft

Dover - 51°07', 1°19'

High tide	02:46	20.0 ft
Low tide	10:08	3.9 ft

English Channel
Rev. 1430

10/05/78

00:35 GMT
01:35 at Zeebrugge

Bathymetry Visibility Evaluation

This image is slightly west of Rev. 762, but overlaps in coverage. The same bathymetry north of Calais is visible. This image is more distinct to the east than Rev. 1473, less distinct to the west and overall less distinct, ranking third after Rev. 762 and 1473. The small v just north of Calais is clear, while the south half of the large V further out is very low contrast but still visible. Around the bend to the west and south of Dover Strait (French coast), nothing shows. The 1 fathom banks just south of Dover are only partly visible.

Weather

0000 GMT
52°N, 0°30'W
Clear
Air temp. - 7°C
Dew point - 6°C
Barometer - 1027.7 mb
Wind, Force 1 - 1 to 3 mph
from the W

53°N, 5°E
Partly cloudy
Air temp. - 12°C
Dew point - 6°C
Barometer - 1021.6 mb
Wind, Force 2 - 4 to 7 mph
from the NW

Dover - 51°07'N, 1°19'E

High tide	00:23	21.7 ft
Low tide	07:57	3.0 ft

Calais - 50°58'N, 1°51'E

Low tide (4th)	20:48	2.3 ft
High tide	01:43	22.6 ft

Zeebrugge - 51°20'N, 3°12'E

Low tide (4th)	21:17	1.7 ft
High tide	03:00	16.2 ft

Time Meridian, 15°E

English Channel | 10/08/78 | 00:47 GMT
Rev. 1473 | | 01:47 at Zeebrugge

Bathymetry Visibility Evaluation

Swath 2 covers the same area as digital image Rev. 762. The same bathymetry is visible, but it is much less distinct, consisting of faint, fuzzy lines instead of clear, high contrast lines. On Swath 4, the 1 and 1.5 fathom banks show south of Dover and the south half of the large V just north of Calais is visible on Swath 3. The bathymetry becomes clear further east of Dunkirk. This is the second most distinct image, following Rev. 762.

Weather

0000 GMT

52°N, 0°30'W
Clear
Air temp. - 11'(C
Dew point - 10°C
Barometer - 1015.8 mb
Wind, Force 1 - 1 to 3 mph
from the SE

53°N, 5°E
Clear, light fog
Air temp. - 8°C
Dew point - 8°C
Barometer - 1018.7 mb
Wind, Force 1 - 1 to 3 mph
from the SE

Dover - 51°07'N, 1°19'E

Low tide (7th)	21:35	3.9 ft
High tide	02:24	20.3 ft

Calais - 50°58'N, 1°51'E

Low tide (7th)	22:40	3.6 ft
High tide	03:44	21.2 ft

Zeebrugge - 51°20'N, 3°12'E

Low tide (7th)	23:11	2.7 ft
High tide	04:56	14.9 ft

Time Meridian, 15°E

4.3.3 Summary of Florida Images

There are four SEASAT passes over Florida which were surveyed but which are not described in detail in the following section: Revs. 651, 759, 802 and 845. They are all in the northern part of Florida where no bathymetry was observed on any other passes, and there was none to be seen on these four passes either.

The other Florida images give certain bounds on our parameters. Since we seem to see a 500-ft contour on Revs. 400 and 608, it says that bathymetry at least that deep can be seen. The Gulf Stream current comes by here, moving rapidly because of the compression in extent due to Cuba to the south and the Florida panhandle to the north. This current is probably the cause of the bathymetry being visible. This indicates another factor. In some work in the North Sea, McLeish et al. (1981) found that underwater features were visible if the rotary tidal current was perpendicular to them, but invisible if the current was parallel to the feature. South and east of Florida, the Gulf Stream moves parallel to the 50- and 500-ft contours and yet reveals them. This indicates that a current need not always be perpendicular to a feature to reveal it.

No limits can be put on wind or rain effects with the Florida images. In the areas where bathymetry is at all visible, it is present in all images. Rev. 852 has many lines which may be due to the storm or may still be bathymetry, so the presence of rain here tells us little.

Rev. 809 is shown in Figure 4-1 with a sketch (Figure 4-2) indicating the underwater contours.

FIGURE 4-1. FLORIDA, REV. 809.

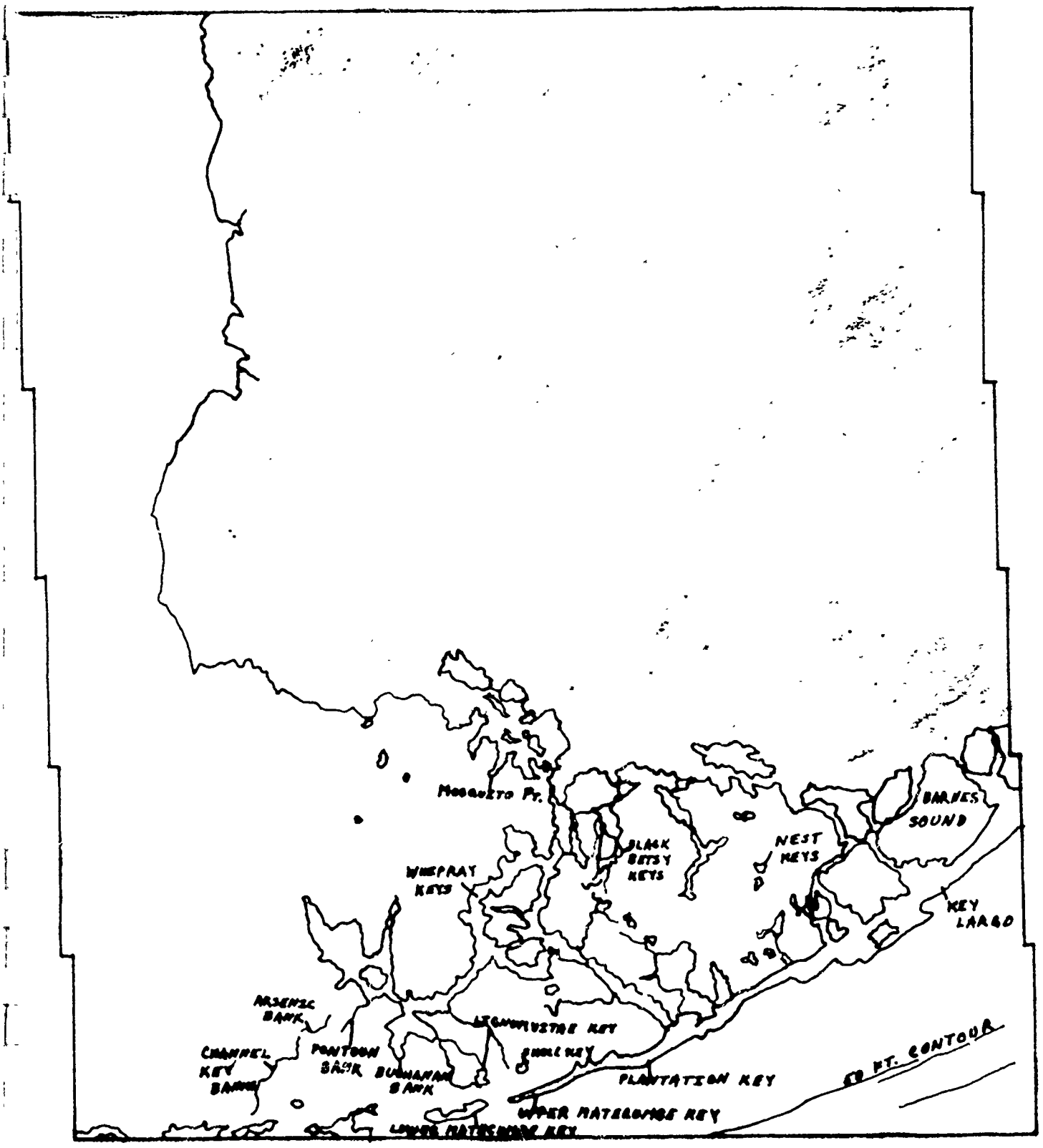

Figure 4-2. Bathymetric Sketch, Florida Keys.

Florida	7/25/78	00:08 GMT
Rev. 400	7/24/78	19:08 Local Time

Bathymetry Visibility Evaluation

From Lake Worth, all the way down the coast and around to the tip of the Florida Keys, a line follows the 50-ft contour. North of Lake Worth, the line continues but moves out to sea and no longer strictly follows any contour. This is most likely the edge of the Gulf Stream. Gulf Stream flow may also be producing the 50-ft contour line. South of the Keys, other lines parallel the 50-ft line, the next deepest and most distinct following the 500-ft line. These are undoubtedly of Gulf Stream origin.

Within the Florida Bay (between the Florida mainland and the outside line of the Keys)., the above water islands show as bright areas, while the underwater shoals are dark areas. Areas as deep as 6 to 10 ft produce these dark spots, with deeper places being fainter than shallower ones.

Two different physical mechanisms may be present in this image. The very shallow effect is seen within the Florida Keys and the current flow effect is seen off the coast.

Weather

0000 GMT
Partly cloudy
Air temp. - 29°C
Dew point - 23°C
Barometer - 1021.2 mb
Wind, Force 2 - 4 to 7 mph
from the E

Bahama, Station 27°N, 77°15'W
Partly cloudy
Air temp. - 28°C
Dew point - 24°C
Barometer - 1021.9 mb
Wind, Force 1 - 1 to 3 mph
from the E

Tides

Ft. Pierce Inlet - 27°28'N, 80°17'W

Low tide	17:22	-0.4 ft
High tide	23:40	2.7 ft

Ft. Lauderdale - 26°07'N, 80°06'W

Low tide	18:12	-0.4 ft
High tide (25th)	00:22	2.4 ft

Miami Harbor - 25°46'N, 80°08'W

Low tide	17:40	-0.4 ft
High tide	23:54	2.6 ft

Molasses Reef - 25°01'N, 80°23'W

Low tide	17:51	-0.4 ft
High tide (25th)	00:10	2.3 ft

American Shoal Light - 24°31'N, 81°31'W

Low tide	16:44	-0.4 ft
High tide	22:42	2.3 ft

Currents

Ft. Pierce Inlet - 27°28'N, 80°18'W

Slack	Maximum		
14:08	16:50	3.5 kt ebb	070°
20:31	23:19	3.3 kt flood	250°

1.75 kt ebb current at time of image

Miami Harbor - 25°46'N, 80°08'W

Slack	Maximum		
13:18	16:25	2.5 kt ebb	125°
19:41	22:54	2.2 kt flood	290°

0.63 kt ebb current at time of image

Key West - 24°33'N, 81°49'W

Slack	Maximum		
13:21	16:32	1.8 kt ebb	195°
20:18	22:54	1.0 kt flood	020°

0.8 kt ebb current at time of image

Florida 8/05/78 01:07 GMT
Rev. 558 8/04/78 20:07 Local Time
Descending pass

Bathymetry Visibility Evaluation

This is the more northerly part of Florida, from Tampa Bay across to St. Augustine. No bathymetry is visible anywhere.

Weather

0000 GMT
Tampa - 28°N, 82°40'W
Partly cloudy
Air temp. - 28°C
Dew point - 23°C
Barometer - 1015.7 mb
Wind, Force 1 - 1 to 3 mph
from the N

0000 GMT
Atlantic Beach - 30°30'N, 82°W
Clear
Air temp. - 27°C
Dew point - 22°C
Barometer - 1017.3 mb
Wind, Force 2 - 4 to 7 mph
from the SE

Tides

Atlantic Beach - 30°20'N, 81°24'W

Low tide	13:57	-0.1 ft
High tide	20:24	5.5 ft

Sebastian Inlet - 27°52'N, 80°27'W

Low tide	13:47	-0.2 ft
High tide	20:13	2.2 ft

Clearwater - 27°57'N, 82°48'W

High tide (5th)	00:54	2.7 ft
Low tide	18:49	0.2 ft

Apalachee Bay (Aucilla River Entrance) - 30°05'N, 84°00'W

High tide	14:16	3.9 ft
Low tide (5th)	00:01	0.3 ft

Currents

Nassau Sound - 30°31'N, 81°27'W

Slack	Maximum		
16:07	18:56	1.7 kt flood	310°
22:05	00:49 (5th)	1.7 kt ebb	135°

0.85 kt flood current at time of image

Ft. Pierce Inlet - 27°28'N, 80°18'W

Slack	Maximum		
~~17:17~~	~~20:01~~	2.7 kt flood	250°
23:15	01:54 (5th)	3.2 kt ebb	070°

2.7 kt flood current at time of image

Tampa Bay - 27°37'N, 82°49'W

Slack	Maximum		
~~13:45~~	~~17:41~~	2.7 kt ebb	285°
21:50	00:45 (5th)	1.5 kt flood	100°

1.6 kt ebb current at time of image

Apalachee Bay (St. Mark's River) - 30°03'N, 84°11'W

Slack	Maximum		
~~13:55~~	~~16:56~~	1.1 kt ebb	170°
20:20	00:00 (5th)	0.9 kt flood	340°

0.2 kt ebb current at time of image

Florida | 8/05/78 | 12:16 GMT
Rev. 565 | | 07:16 Local Time
Ascending pass

Bathymetry Visibility Evaluation

This pass catches the northern part of the Gulf coast of Florida near Apalachee Bay. Again, no bathymetry is visible.

Weather

1200 GMT

Apalachee Bay, 30°N, 84°30'W
Clear
Air temp. - 24°C
Dew point - 23°C
Barometer - 1018.2 mb
Wind, Force 1 - 1 to 3 mph from the W

Tampa, 28°N, 82°50'W
Clear
Air temp. - 23°C
Dew point - 23°C
Barometer - 1017.8 mb
Wind, Force 1 - 1 to 3 mph from the W

Tides

Apalachee Bay (Aucilla River Entrance) - 30°05'N, 84°00'W

High tide	03:17	3.4 ft
Low tide	08:56	1.4 ft

Clearwater - 27°57'N, 82°48'W

Low tide	06:44	1.1 ft
High tide	12:25	3.1 ft

Key West - 24°33'N, 81°48'W

Low tide	03:59	0.2 ft
High tide	10:17	1.6 ft

Currents

Apalachee Bay (St. Mark's River) - 30°03'N, 84°11'W

Slack	Maximum		
04:14	05:19	0.3 kt ebb	285°
06:51	10:58	0.7 kt flood	100°

0.07 kt flood current at time of image

Tampa Bay (Entrance) - 27°37'N, 82°46'W

Slack	Maximum		
04:04	06:04	0.7 kt ebb	285°
08:21	11:43	1.2 kt flood	100°

0.5 kt ebb current at time of image

Key West - 24°33'N, 81°49'W

Slack	Maximum		
05:21	07:44	1.0 kt flood	020°
10:28	13:51	2.1 kt ebb	195°

1.0 kt flood current at time of image

Miami, Florida 8/8/78 12:22 GMT
Rev. 608 07:22 Local Time
Ascending pass

Bathymetry Visibility Evaluation

This image is very similar to Rev. 400 in visibility: a 50- or 60-ft contour is visible around the entire tip of Florida up to Lake Worth, a 500-ft line appears south of the Keys and the underwater Keys appear as dark areas. The underwater Keys are a little less distinct than on Rev. 809.

Weather

1200 GMT
Partly cloudy
Air temp. - 27°C
Dew point - 25°C
Barometer - 1019.3 mb
Wind, Force 1 - 1 to 3 mph from the S

Tides

Ft. Lauderdale - 26°07'N, 80°06'W

Low tide	05:06	0.0 ft
High tide	11:12	2.2 ft

Miami Harbor (Entrance) - 25°46'N, 80°08'W

Low tide	04:34	0.0 ft
High tide	10:44	2.4 ft

Cape Florida (West Side), Key Biscayne - 25°40'N, 80°10'W

Low tide	05:36	0.0 ft
High tide	11:33	1.6 ft

Fowey Rocks - 25°35'N, 80°06'W

Low tide	04:36	0.0 ft
High tide	10:47	2.3 ft

Currents

Ft. Lauderdale (New River) - 26°07'N, 80°07'W

Slack	Maximum		
23:34 (7th)	02:37	0.5 kt ebb	130°
06:07	08:33	0.8 kt flood	0 5°

0.6 kt flood current at time of image

Bakers Haulover Cut - 25°54'N, 80°07'W

Slack	Maximum		
00:04	03:02	2.8 kt ebb	090°
06:37	08:58	2.9 kt flood	270°

1.3 kt flood current at time of image

Miami Harbor (Entrance) - 25°46'N, 80°08'W

Slack	Maximum		
00:14	03:17	2.3 kt ebb	125°
06:47	09:13	1.9 kt flood	290°

1.7 kt flood current at time of image

Fowey Rocks Light - 1.5 miles SW of 25°35'N, 80°07'W
Currents too weak and variable to be predicted.

Everglades, Florida 8/22/78 13:24 GMT
Rev. 809 8:24 Local Time
Ascending pass

Bathymetry Visibility Evaluation

The 50-ft contour line shows, but the 500-ft line would be off this frame. Inside Florida Bay, the Channel Key Banks, Arsenic Bank and Pontoon Bank are outstanding.

Weather

1200 GMT, Miami station
Partly cloudy
Light rain
Air temp. - 25°C
Dew point - 24°C
Barometer - 1016.3
Winds, Force 1 - 1 to 3 mph from the E

Tides

Garden Cove, Key Largo - 25°10'N, 80°22'W
Low tide 05:43 0.0 ft
High tide 11:20 2.1 ft

Molasses Reef - 25°1'N, 80°23'W
Low tide 04:45 0.0 ft
High tide 11:00 2.1 ft

Lignumvitae Key - 24°54'N, 80°42'W
From here east within Florida Bay, the periodic tide has a mean range less than 1/2 foot.

Arsenic Bank - 24°53'N, 80°52'W
High tide 06:10 0.6 ft
Low tide 13:56 0.1 ft

Marathon, Vaca Key (North Side) - 24°43'N, 81°06'W
High tide 05:25 0.8 ft
Low tide 10:41 0.1 ft

Currents

Ceaser Creek, Biscayne Bay (North of Image) - 25°23'N, 80°14'W

Slack	Maximum		
00:03	03:28	1.9 kt ebb	125°
07:07	09:30	1.2 kt flood	315°

1.0 kt flood current at time of image

Long Key (East of Drawbridge) - 24°50'N, 80°46'W

Slack	Maximum		
01:48	05:02	1.3 kt ebb	200°
07:51	11:05	1.1 kt flood	000°

0.3 kt flood current at time of image

Long Key Viaduct - 24°48'N, 80°52'W

Slack	Maximum		
01:58	05:12	1.3 kt ebb	170°
08:01	11:15	0.9 kt flood	350°

0.2 kt flood current at time of image

Florida 8/25/78 13:30 GMT
Rev. 852 08:30 Local Time
Ascending pass

Bathymetry Visibility Evaluation

This pass is north of Revs. 400 and 608 and only overlaps them in a small area around Lake Worth. There is a huge storm to the south and east of Florída which is mottling and darkening the whole ocean surface. There are many storm lines just north of Lake Worth which roughly parallel the bathymetry and current lines. It is impossible to tell if we are seeing bathymetry effects, storm effects or both.

Weather

1200 GMT	0000 GMT, 26°N, 80°10'W
Coastal station, 26°N, 80°10'W	Partly cloudy
Partly cloudy	Continuous rain
Air temp. - 23°C	Air temp. - 27°C
Dew point - 22°C	Dew point - 21°C
Barometer - 1017.5 mb	Barometer - 1016.2 mb
Wind, Force 1 - 1 to 3 mph from the N	Wind, Force 1 - 1 to 3 mph from the S

Both times show the station to be behind a tropical storm front.

Tides

St. Augustine Inlet - 29°53'N, 81°17'W

Low tide	07:24	0.4 ft
High tide	13:38	4.6 ft

Jupiter Inlet - 26°57'N, 80°05'W

High tide	01:56	1.9 ft
Low tide	08:34	0.1 ft

Currents

Mandarin Point - 30°09'N, 81°41'W

Slack	Maximum	
06:22	09:29	0.6 kt ebb current 15°

0.54 kt ebb current at time of image

Lake Worth Inlet - 26°46'N, 80°02'W

Slack	Maximum	
02:36	05:48	3.4 kt ebb 95°
09:20	12:39	2.1 kt flood 275°

1.4 kt ebb current at time of image

4.3.4 Summary of Straits of Georgia Images

One of the first parameters of importance on these frames is the processing. Rev. 230 was processed so that almost no detail shows in the water. If it were reprocessed with a different dynamic range or grey scale, many details including bathymetry might become visible.

Graphs were done of some of the parameters given in Table 4-1. The first, Figure 4-3, is the bathymetry visibility versus the tidal current. The second, Figure 4-4, is the visibility versus the component of the current in the direction of the radar range or look direction. While it is true that the highest current corresponds to the highest visibility (Rev. 724), the rest of the points on these graphs show little relationship between current and visibility of bathymetry. Revs. 480 and 230 were both descending passes; while Revs. 236, 474 and 724 were ascending passes. This may indicate some dependence on radar look direction.

Since these are fairly shallow banks (1 to 2 fathoms), it might seem reasonable that they would show more at lower tidal levels. This was graphed also, in Figure 4-5, giving inconclusive results.

The conclusion is that some unknown variables are affecting the visibility of the bathymetry here.

Rev. 724 is shown in Figure 4-6, and an enlarged version of the bathymetric chart provided in Figure 4-7. The map includes Point Roberts and the Roberts and Sturgeon Banks, which are just above center and centered left to right in the picture. The edges of both the Roberts and Sturgeon Banks are visible on the image and the breakwaters off of English Bluff.

TABLE 4-1. Straits of Georgia Image Parameters

Rev.	Visibility of Bathymetry	Pass Direction	Tidal* Level (ft)	Current (kt)	Dot Product of Current with Radar Look Direction (kt)
230	None	Descending	10.0	2.6	0.67
236	Medium to high	Ascending	5.5	0.3	0.289
474	Low	Ascending	10.5	0.3	0.289
480	Low	Descending	4.0	2.6	0.67
724	High	Ascending	6.0	5.0	4.8

*Feet above mean low water level.

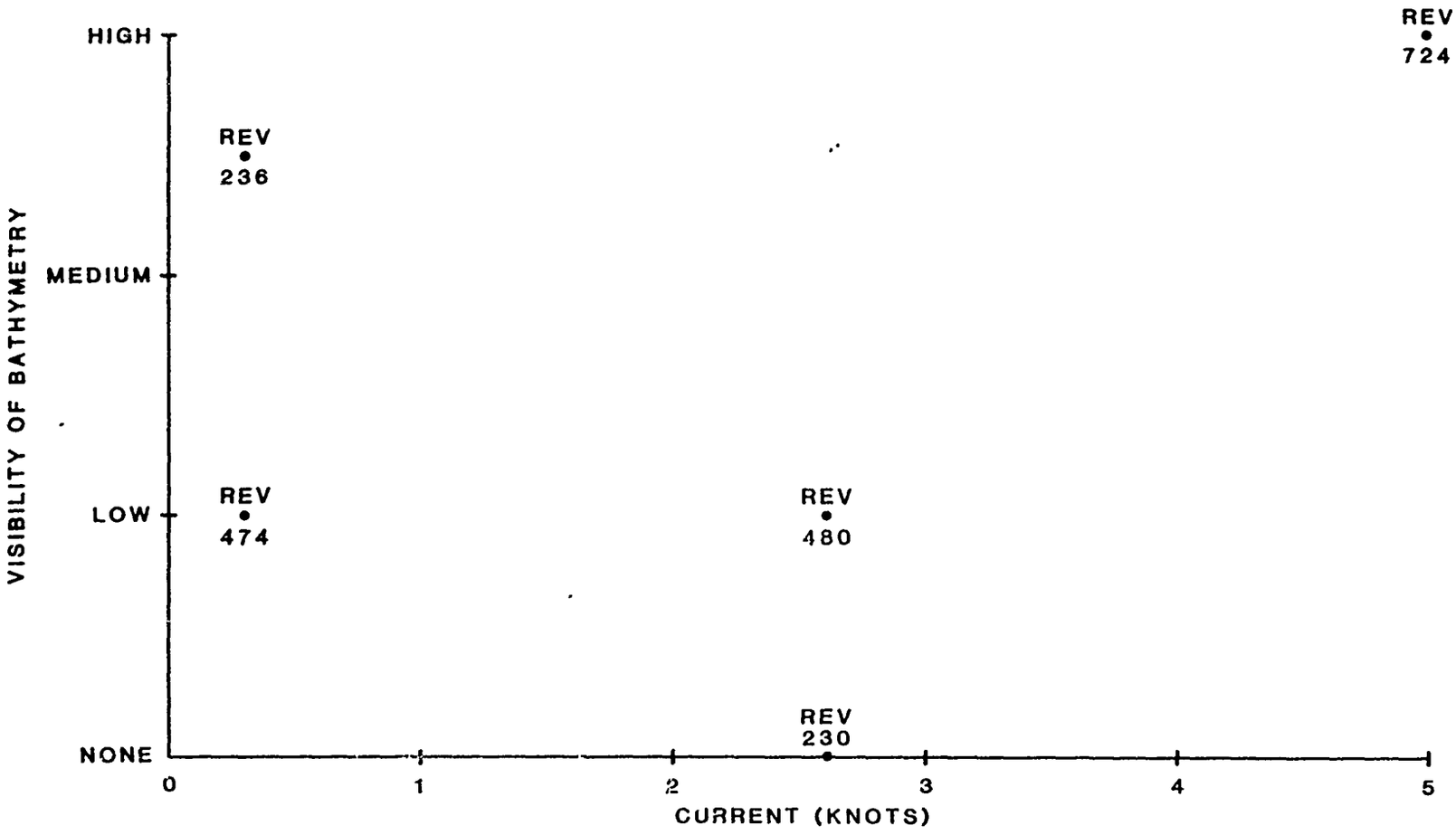

Figure 4-3. Visibility of Bathymetry in the Straits of Georgia vs Tidal Current.

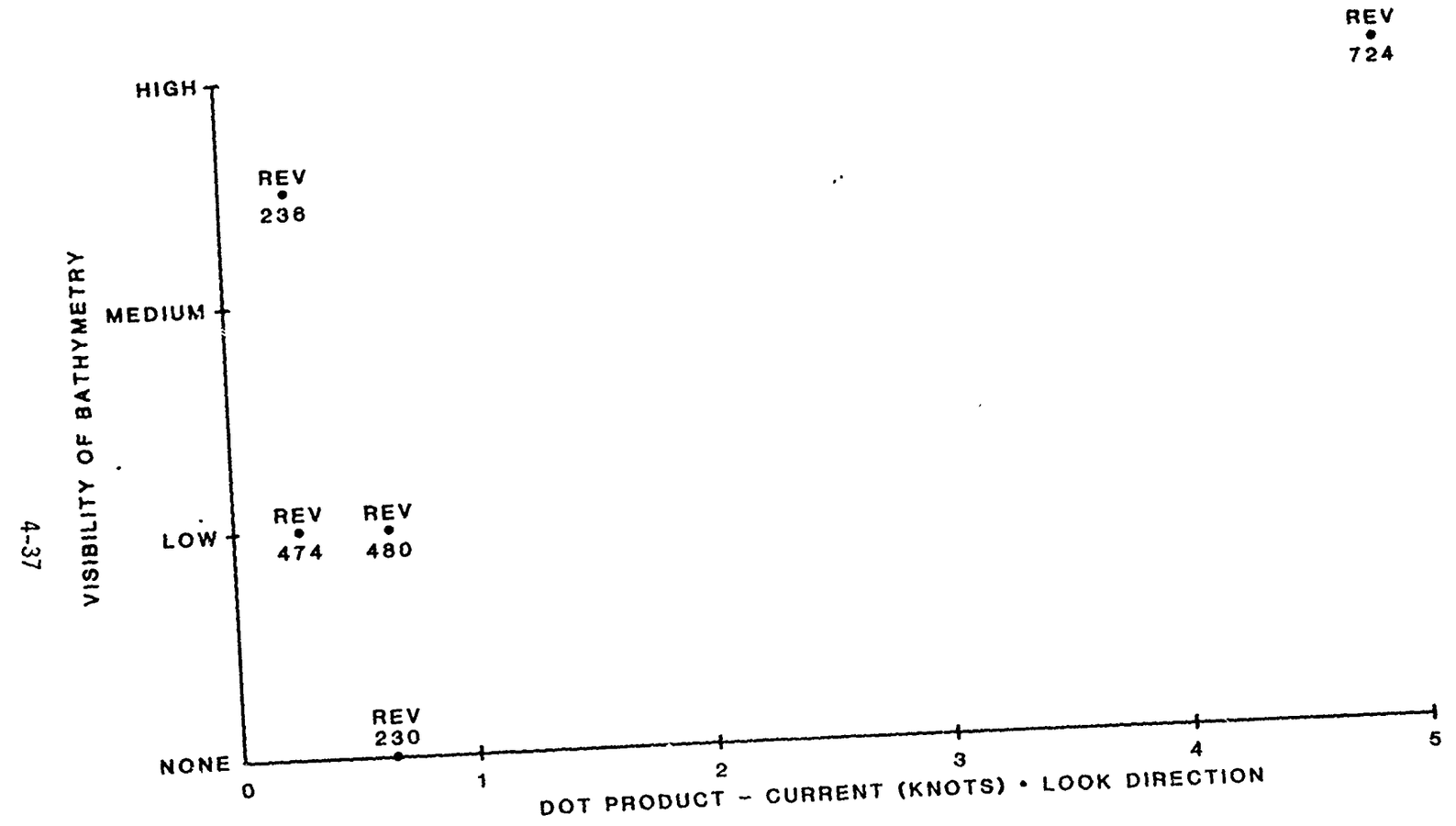

Figure 4-4. Visibility of Bathymetry in the Straits of Georgia vs Component of Tidal Current in Look Direction of Radar.

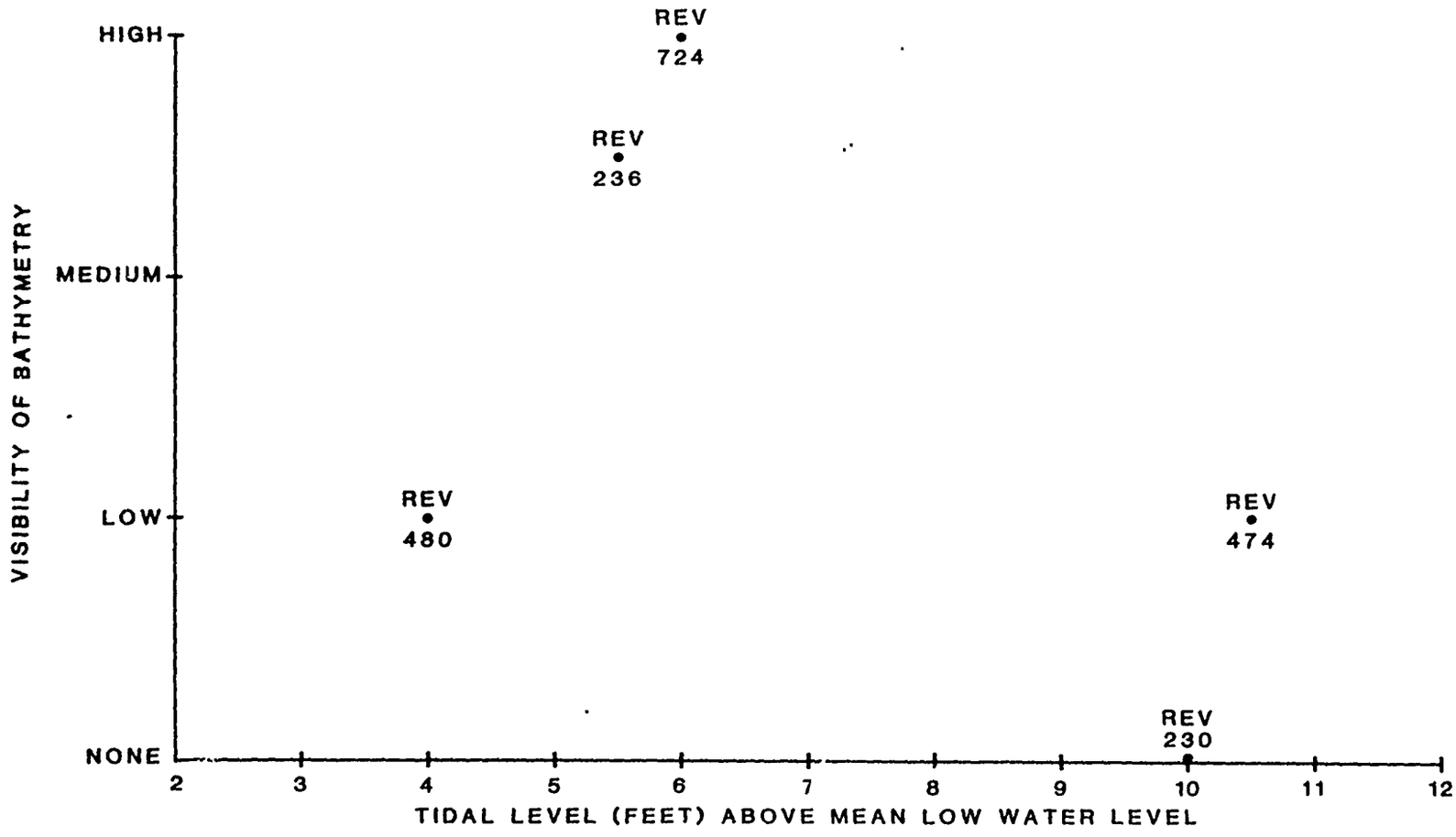

Figure 4-5. Visibility of Bathymetry in the Straits of Georgia vs Tidal Level

FIGURE 4-6. STRAITS OF GEORGIA, REV. 724.

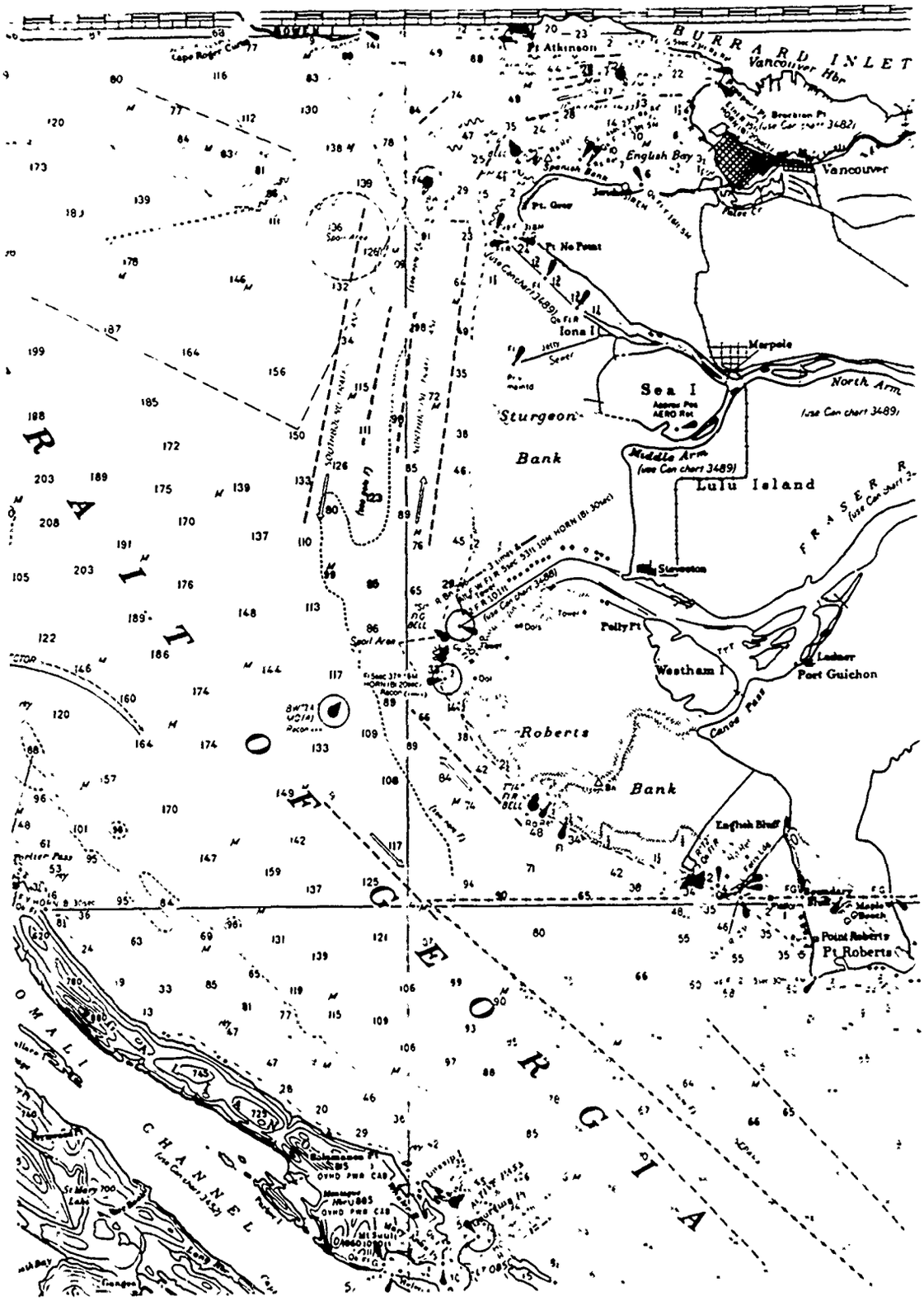

Figure 4-7. Bathymetric Map, Straits of Georgia.

Straits of Georgia

Rev. 230	7/13/78	02:54 GMT
48.48° descending pass	7/12/78	18:54 Local Time

Bathymetry Visibility Evaluation

The Roberts and Sturgeon banks have only the faintest of lines - they are not really visible at all. There are very few markings of any kind in the ocean on this image. Part of the 100 fathom contour north of Patos Island may be showing.

Weather

0000Z
Air temp. - 22°C
Dew point - 12°C
Slightly overcast
Barometer - 1017.1 mb
Wind, Force 2 - 4 to 7 mph
from the SSE

0600Z
Air temp. - 14°C
Dew point - 11°C
Clear
Barometer - 1016.5 mb
Wind, Force 1 SW

Tides

Low tide 15:20 5.8 ft
High tide 22:03 13.7 ft
Tidal level approximately 10 ft at the time of image

Currents

1 hr after flood maximum, approximately 3 kt maximum
4 kt ebb maximum follows

Straits of Georgia
Rev. 236 7/13/78 12:36 GMT
257.98°N ascending pass 04:36 Local Time

Bathymetry Visibility Evaluation

The edge of Roberts Bank is very clear, while the edge of Sturgeon Bank is faint.

Weather

1200Z

Air temp. - 11°C
Dew point - 11°C
Fog
Barometer - 1016.3 mb
Wind, Force 1 - 1 to 3 mph, from the W

Tides

High tide - 22:03, 13.7 ft
Low tide - 05:10, 5.4 ft
Tidal level, 5.5 ft at time of image

Currents

Minutes after flood minimum
3 hrs later, flood maximum, approximately 2.8 kt
4 hrs earlier, ebb maximum, 4 to 5 kt

Straits of Georgia

Rev. 474	7/30/78	04:07 GMT
48.47°N descending pass	7/29/78	20:07 Local Time

Bathymetry Visibility Evaluation

The Fraser River channel is visible between the Roberts and Sturgeon banks, which may be due to the difference in sedimentation or salinity between the river water and strait water. No other bathymetry is visible.

Weather

0600Z

Air temp. - 12°C
Dew point - 10°C
Quarter overcast
Barometer - 1021.1 mb
Wind, Force 1 - 1 to 3 mph from the NE

July 29

Tides

Low water 19:18 9.9 ft
High water (30th) 00:25 12.1 ft
Tidal level, 10.5 ft at time of image

Currents

1-1/2 hrs before flood maximum, approximately 1.5 kt maximum
4-1/2 hrs after ebb maximum, approximately 2.5 kt maximum

Straits of Georgia
Rev. 480 7/30/78 13:49 GMT
257.99°N ascending pass 05:49 Local Time

Bathymetry Visibility Evaluation

The Fraser River channel is again evident between the Roberts and Sturgeon banks. There are dark areas around these banks that do not correspond in outline with any bathymetric contours and are likely due to sedimentation run off from the rivers.

Weather

1200 GMT

1/3 overcast, continuous shallow fog
Air temp. - 15°C
Dew point - 13°C
Barometer - 1019.9 mb
Wind, Force 0, less than 1 mph from the ESE

Tides

High tide 00:25 12.1 ft
Low tide 08:13 2.9 ft
Tidal level, 4 ft at time of image

Currents

Approximately 2 hrs after ebb maximum, approximately 4 kt maximum
Approximately 5 hrs before flood maximum, approximately 4 kt maximum

Straits of Georgia
Rev. 724 9/16/78 15:02 GMT
257.63°N ascending pass 07:02 Local Time

Bathymetry Visibility Evaluation

Salmon Bank south of San Juan Island shows and there are marks in the approximate location of Middle Bank. North of Blakely Island in Rosario Strait, the 20 fathom line is outstanding and continues to the 7 fathom shoal just south of the east corner of the island. West of Point Roberts, the 10 fathom line shows well. The edge of both the Roberts and Sturgeon banks are highly visible and the 100 fathom line west of Sturgeon Bank is also faintly detectable.

Weather

1200 GMT

Clear
Air temp. - 7°C
Dew point - 6°C
Barometer - 1026.3 mb
Wind, Force 0

1800 GMT

Overcast
Light showers
Air temp. - 10°C
Dew point - 9°C
Barometer - 1024.7
Wind, Force 1 - 1 to 3 mph
from the ENE

Tides

High tide 04:15 12.6 ft
Low tide 10:33 3.0 ft
Tidal level, 6 ft at time of image

Currents

Minutes after ebb maximum, 5 to 6 kt
6 hrs later, flood maximum 5 to 6 kt

4.3.5 Summary of Cape Hatteras Images

Since there are nine SEASAT passes and one SIR-A pass here that actually view the same spot (Diamond Shoals), some attempt at a quantitative evaluation of parameters is possible. In Table 4-2, a subjective evaluation of the visibility of the Diamond Shoals is given along with the wind force and the currents estimated for both the Ocracoke and Hatteras Inlets at the time of the image. There are variables which have not been included in this analysis which the reader should bear in mind. One is that the Gulf Stream moves out and around the point of Cape Hatteras at some distance but may nevertheless affect the area. The second is that wind-driven currents are important here. The average wind driven current at the Diamond Shoals Lightship Station, (35°05'N, 75°20'W) is 0.5 kt for a 10 mph wind. Tables exist for determining both the direction and average magnitude of this current at any time but they require an instantaneous wind measurement. Since our wind measurements were as much as three hours away from the image time, no reliable estimate of the wind driven current can be made.

Figures 4-8, 4-9 and 4-10 are graphs of the parameters given in Table 4-2. Their reliability is not high since nine points is a very small sample of parameters that may have a large random fluctuation. Nonetheless, a correlation seems to exist between both wind speed and current magnitude and bathymetry visibility. As the current increases at either the Hatteras or Ocracoke Inlets, the bathymetry becomes more visible. As the wind speed increases, the visibility decreases. One of the definitive points on all three graphs, Rev. 1447, had both the lowest currents of any SAR pass, rain and the highest winds. It is unknown whether the same rain and wind conditions with a good stiff current would give good or poor visibility.

TABLE 4-2. Cape Hatteras Image Parameters

Rev.	Visibility of Diamond Shoals	Wind Force (Beaufort Scale)	Ocracoke Inlet Current (kt)	Hatteras Inlet Current (kt)
378	Good	?	2.0	2.1
400	Moderate	2	1.2	1.6
888	Very Good	1	1.8	1.6
931	Low	2	0.9	0.7
974	Moderate	2	0.7	1.0
1232	Moderate	2	1.5	1.8
1404	Moderate to Good	2	1.8	1.7
1447	None	4	0.4	0.5
1490	Good	1	1.6	2.0

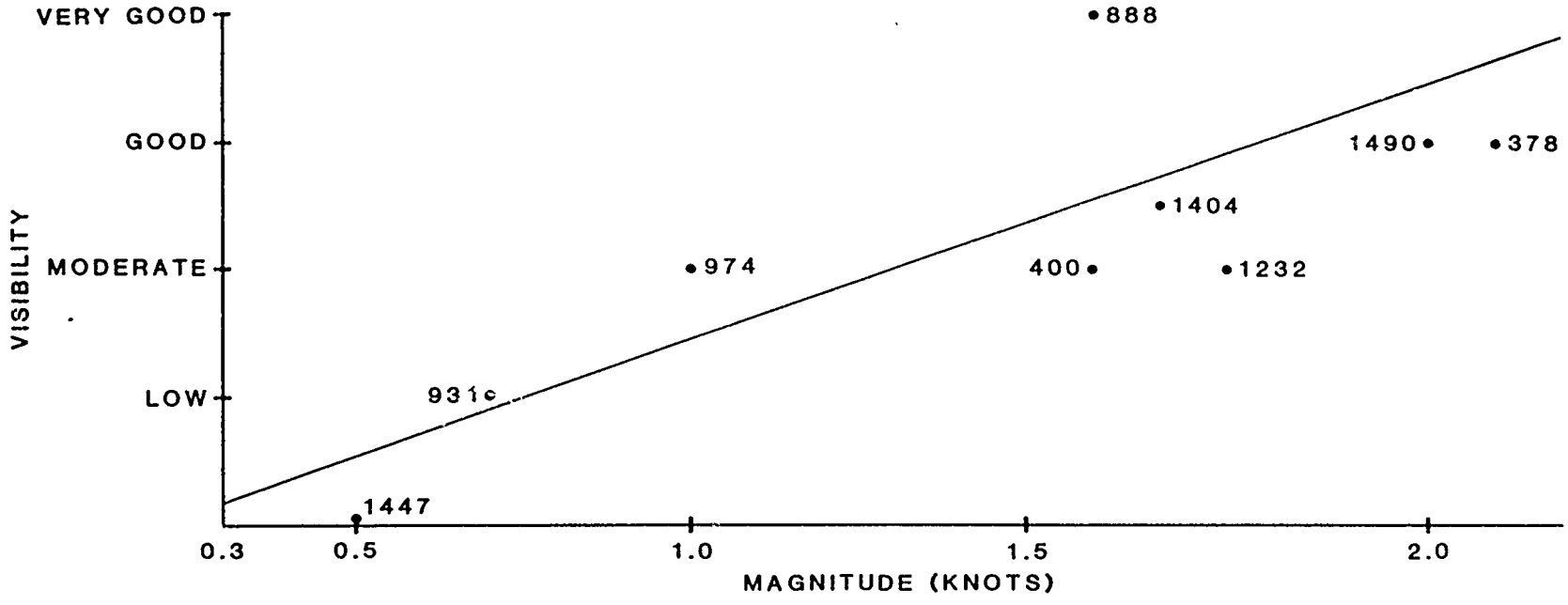

Figure 4-8. Visibility of Diamond Shoals vs Magnitude of Current at Hatteras Inlet.

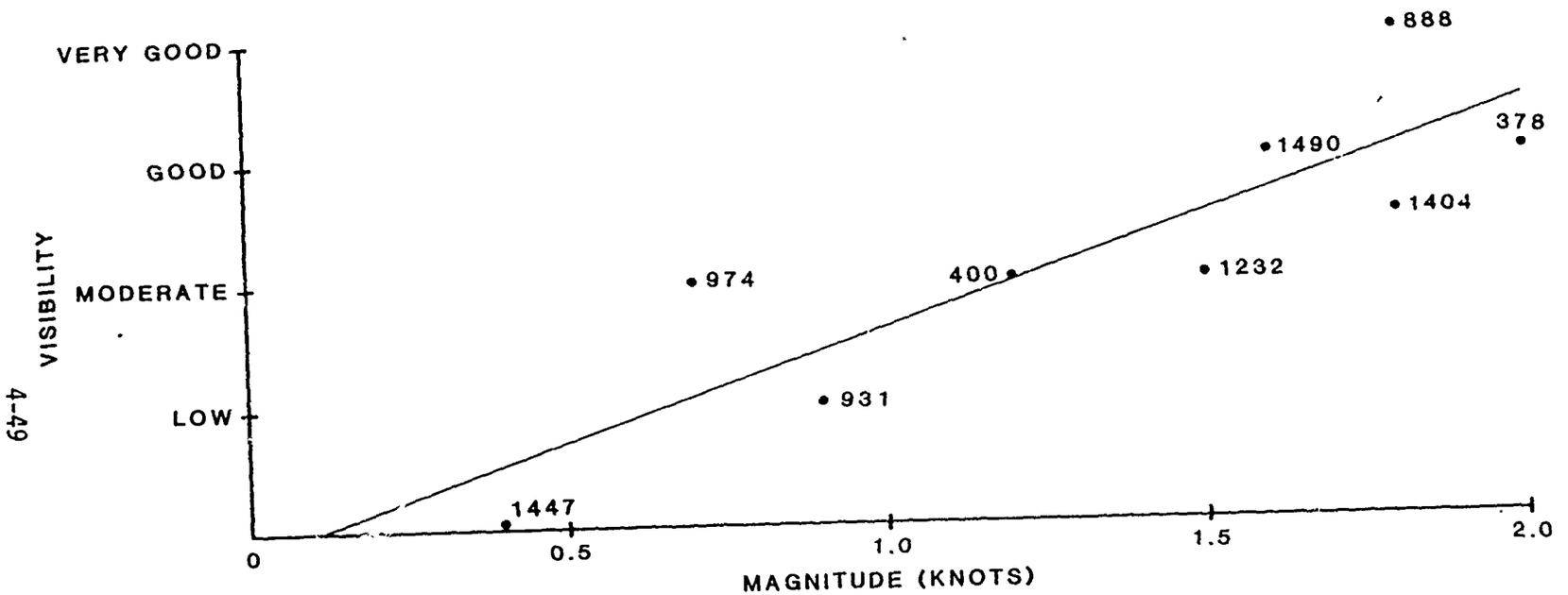

Figure 4-9. Visibility of Diamond Shoals vs Magnitude of Current at Ocracoke Inlet.

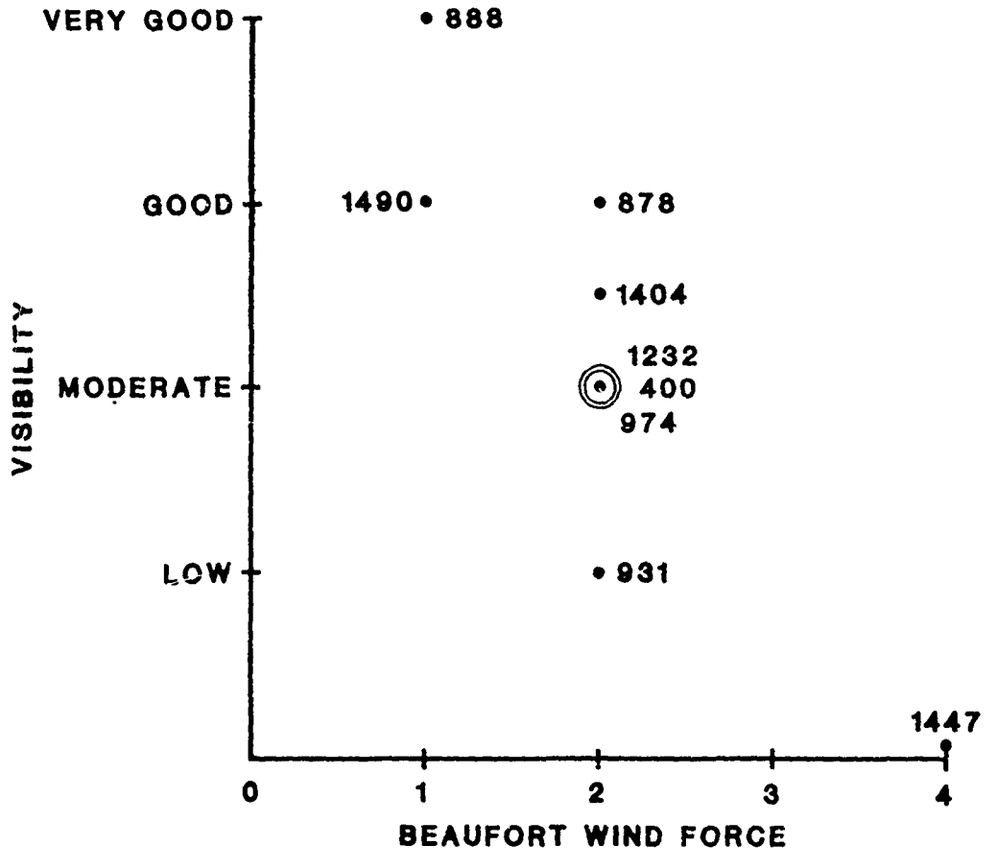

Figure 4-10. Diamond Shoals Visibility vs Wind Force.

Rev. 400 had rain, moderate winds and good currents (1.2 to 1.6 kt) and had moderate visibility so the rain may have no affect at all.

The SIR-A pass has not been included in these graphs because weather and tidal data have not been obtained. It does illustrate, however, that a sizeable variation in incidence angle, from 20° for SEASAT to 47° for SIR-A, does not affect bathymetry visibility significantly. The SIR-A image is as similar in appearance to the SEASAT images as they are to one another.

Finally, an illustration of the Diamond Shoals bathymetry is included. Figure 4-11 shows Hatteras Island, and in the lower right hand corner, Diamond Shoals extending outward from it. Figure 4-12 is a bathymetric chart of the Diamond Shoals area on a much larger scale. A comparison of the chart and image shows good correlation between the two.

FIGURE 4-11. CAPE HATTERAS, REV. 378

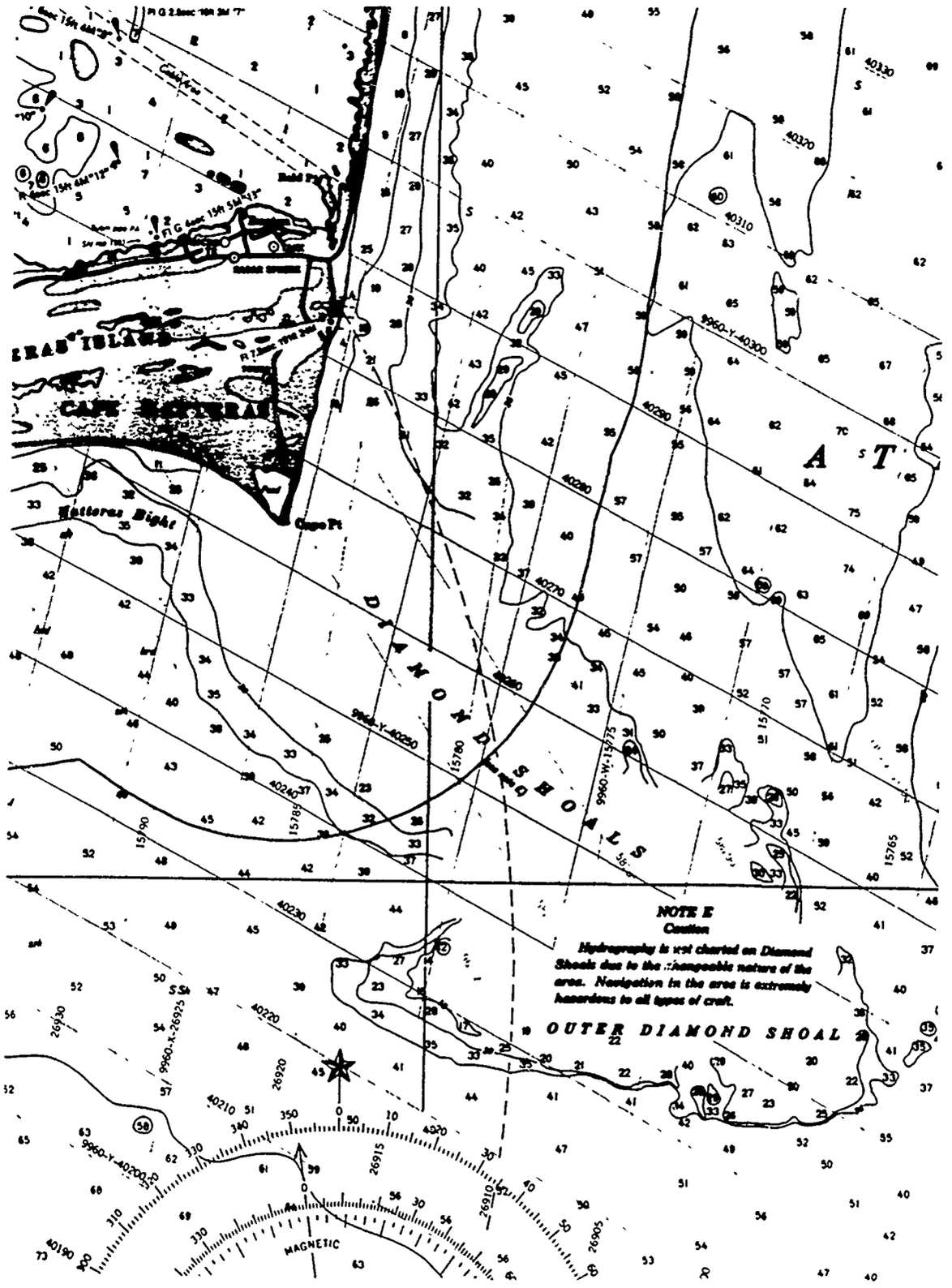

Figure 4-12. Bathymetric Map, Diamond Shoals, North Carolina.

Cape Hatteras | 7/23/78 | 10:39 GMT
Rev. 378 | 05:39 Local Time
Ascending pass

Bathymetry Visibility Evaluation

The entire Diamond Shoals is visible on this image. Detail on the shoal itself cannot be verified since no bathymetry is published for the shoal - it shifts too rapidly.

Weather

0000 GMT
Clear
Air temp. - 27°C
Dew point - 24°C
Barometer - 1020 mb
Wind, Force 2 - 4 to 7 mph
from the SW

Buoy - 35°N, 72°W
Clear
Air temp. - 27°C
Water temp. - 26°C
Barometer - 1021.4 mb
Wind, Force 2 - 4 to 7 mph
from the SW

Tides

Cape Hatteras - 35°14'N, 75°31'W

Low tide	03:16	0.4 ft
High tide	09:41	4.1 ft

Hatteras (Ocean) - 35°12'N, 75°42'W

Low tide	03:16	0.4 ft
High tide	09:33	3.9 ft

Hatteras Inlet - 35°12'N, 75°44'W

Low tide	03:42	0.4 ft
High tide	09:56	2.5 ft

Ocracoke Inlet - 35°04'N, 76°01'W

Low tide	03:40	0.4 ft
High tide	09:57	2.4 ft

Currents

Hatteras Inlet - 35°12'N, 75°45'W

Slack	Maximum		
00:56	03:35	3.0 kt ebb	150°
07:21	09:32	2.9 kt flood	305°

2.1 kt ebb current at time of image

Ocracoke Inlet (Channel Entrance) - 35°04'N, 76°01'W

Slack	Maximum		
00:41	03:25	3.3 kt ebb	145°
07:06	09:22	2.3 kt flood	000°

1.98 kt ebb current at time of image

Cape Hatteras
Rev. 400
Descending pass

7/25/78
7/24/78

00:05 GMT
19:05 Local Time

Bathymetry Visibility Evaluation

The inner Diamond Shoal is visible as dark marks against a bright, mottled background and is more outstanding than Rev. 378, whereas the outer shoal disappears here. Clam shoal (inside Hatteras Island) shows up as a dark area. There are many dark areas surrounding Hatteras Island which do not show on Revs. 378 or 931. There is no great correspondence of these areas with bathymetry so they are likely to be storm-induced effects.

Weather

0000 GMT
Completely overcast
Rain, thunderstorm
Air temp. - 28°C
Dew point - 22°C
Barometer - 1021.3 mb
Wind, Force 2 - 4 to 7 mph
from the SW

Bouy - 35°N, 72°W
Clear
Air temp. - 28°C
Water temp. - 27°C
Barometer - 1020.4 mb
Wind, Force 3 - 8 to 12 mph from the W

Tides

Cape Hatteras - 35°14'N, 75°31'W
Low tide (24th) 16:37 -0.1 ft
High tide (24th) 22:55 3.8 ft

Cape Hatteras (Ocean) - 35°12'N, 75°42'W
Low tide (24th) 16:37 -0.1 ft
High tide (24th) 22:47 3.6 ft

Hatteras Inlet - 35°12'N, 75°44'W
Low tide (24th) 17:03 -1.0 ft
High tide (24th) 23:10 2.2 ft

Ocracoke Inlet - 35°04'N, 76°01'W
Low tide (24th) 17:01 -0.1 ft
High tide (24th) 23:11 2.1 ft

Currents

Hatteras Inlet - 35°12'N, 75°45'W

Slack	Maximum		
14:13 (24th)	16:50 (24th)	2.7 kt ebb	150°
20:33 (24th)	22:46 (24th)	2.6 kt flood	305°

1.6 kt ebb current at time of image

Ocracoke Inlet - 35°04'N, 76°01'W

Slack	Maximum		
13:58 (24th)	16:40 (24th)	2.8 kt ebb	145°
20:18 (24th)	22:36 (24th)	2.2 kt flood	000°

1.26 kt ebb current at time of image

Cape Hatteras	8/26/78	02:28 GMT
Rev. 888	8/27/78	21:28 Local Time
Descending pass		

Bathymetry Visibility Evaluation

The Diamond Shoals shows distinct bright patches against a dark background. The ocean has the mottled, patchy look characteristic of storm areas. There are two bright lines extending northeastward from the tip of Diamond Shaols which very roughly follow some 50-ft banks. This is the most outstanding view of the Diamond Shoals obtained in the SEASAT data.

Weather

0000 GMT
Station - 36°50'N, 76°10'W
Completely overcast
Air temp. - 26°C
Dew point - 22°C
Barometer - 1018.3 mb
Winds, Force 1 - 1 to 3 mph from the SE

0600 GMT
35°N, 76°W
Partly cloudy
Air temp. - 24°C
Dew point - 23°C
Barometer - 1019.2 mb
Wind, Force 2 - 4 to 7 mph
from the S

0600 GMT
Buoy - 35°N, 72°W
Clear
Air temp. - 26°C
Water temp. - 28°C
Barometer - 1021.6 mb
Wind, Force 2 - 4 to 7 mph
Waves - 7 second period, 1 m height

Tides

Cape Hatteras - 35°14'N, 75°31'W

Low tide (27th)	20:56	0.6 ft
High tide	03:07	3.3 ft

Cape Hatteras (Ocean) - 35°12'N, 75°42'W

Low tide (27th)	20:56	0.6 ft
High tide	02:59	3.1 ft

Hatteras Inlet - 35°12'N, 75°44'W

Low tide (27th)	21:22	0.6 ft
High tide	03:22	1.7 ft

Ocracoke Inlet - 35°04'N, 76°01'W

Low tide (27th)	21:20	0.6 ft
High tide	03:23	1.6 ft

Currents

Hatteras Inlet - 35°12'N, 75°45'W

Slack	Maximum		
18:36 (27th)	21:35 (27th)	1.6 kt ebb	150°
00:07	03:34	1.2 kt flood	305°

1.6 kt at time of image

Ocracoke Inlet (Channel Entrance) - 35°04'N, 76°01'W

Slack	Maximum		
18:21 (27th)	21:25 (27th)	1.8 kt ebb	145°
23:52	03:24	1.0 kt flood	000°

1.8 kt at time of image

Cape Hatteras	8/31/78	02:40 GMT
Rev. 931	8/30/78	21:40 Local Time
Descending pass		

Bathymetry Visibility Evaluation

The ocean background in this image is a fairly uniform grey, neither bright nor dark, with only a little patchiness or streaking. All of the Diamond Shoals are nearly invisible, with only a few dark marks on the inner shoal. However, Clam Shoal and Gull Shoal inside Hatteras Island are distinct black areas.

Weather

0000 GMT
Station - 37°N, 76°W
Completely overcast
Air temp. - 25°C
Dew point - 23°C
Barometer - 1017.9 mb
Wind, Force 2 - 4 to 7 mph
from the SSE

0000 GMT
Buoy - 35°N, 72°W
Clear
Air temp. - 27°C
Water temp. - 28°C
Barometer - 1021.0 mb
Wind, Force 2 - 4 to 7 mph
from the SSW
Waves - 5 sec period, 1 m height

0600 GMT - weather at buoy is the same as 0000 GMT

Tides

Cape Hatteras - 35°14'N, 75°31'W

High tide (30th)	17:09	3.9 ft
Low tide (30th)	23:16	0.3 ft

Cape Hatteras (Ocean) - 35°12'N, 75°42'W

High tide (30th)	17:01	3.7 ft
Low tide (30th)	23:16	0.3 ft

Hatteras Inlet - 35°12'W, 75°44'W

High tide (30th)	17:24	2.3 ft
Low tide (30th)	23:42	0.3 ft

Ocracoke Inlet - 35°04'N, 76°01'W

High tide (30th)	17:25	2.2 ft
Low tide (30th)	23:40	0.3 ft

Currents

Hatteras Inlet - 35°14'N, 75°31'W

Slack	Maximum		
14:50 (30th)	17:22 (30th)	1.9 kt flood	305°
21:05 (30th)	23:55 (30th)	2.0 kt ebb	150°

0.7 kt ebb at time of image

Ocracoke Inlet - 35°04'N, 76°01'W

Slack	Maximum		
14:35 (30th)	17:12 (30th)	1.5 kt flood	000°
20:50 (30th)	23:45 (30th)	2.2 kt ebb	145°

0.9 kt ebb at time of image

Cape Hatteras | 9/3/78 | 02:53 GMT
Rev. 974 | 9/2/78 | 21:53 Local Time
Descending pass

Bathymetry Visibility Evaluation

The ocean is a light uniform grey and the Diamond Shoals are not highly visible. As on Rev. 931, the inner shoal is marked by a few dark lines. However, a faint line roughly follows the easternmost 50-ft bank, going northward from the tip of Diamond Shoals as on Rev. 888. Revs. 931 and 974 have similar magnitude currents (0.7 to 0.9 kt), although they are in opposite directions. These two images look very similar.

Weather

0000 GMT
Overcast
Air temp. 27°C
Dew point - 13°C
Barometer - 1016.9 mb
Wind, Force 2 - 4 to 7 mph
from the NE

Buoy - 35°N, 72°W
Partly cloudy
Air temp. - 26°C
Water temp. - 23°C
Barometer - 1017.3 mb
Wind, Force 2 - 4 to 7 mph
from the E
Waves - 8 sec period

Tides

Cape Hatteras - 35°14'N, 75°31'W

High tide (2nd)	19:42	4.0 ft
Low tide (3rd)	01:07	0.1 ft

Hatteras (Ocean) - 35°12'N, 75°42'W

High tide (2nd)	19:34	3.8 ft
Low tide (3rd)	01:07	0.1 ft

Hatteras Inlet - 35°12'N, 75°44'W

High tide (2nd)	19:57	2.4 ft
Low tide (3rd)	01:33	0.1 ft

Ocracoke Inlet - 35°04'N, 76°01'W

High tide (2nd)	19:58	2.3 ft
Low tide (3rd)	01:31	0.1 ft

Currents

Hatteras Inlet - 35°12'N, 75°45'W

Slack	Maximum		
16:49	18:59	2.42 kt flood	305°
22:54 (3rd)	01:28	2.3 kt ebb	150°

1.0 kt flood current at time of image

Ocracoke Inlet (Channel Entrance) - 35°04'N, 76°01'W

Slack	Maximum		
16:34	18:49	2.0 kt flood	000°
22:39 (3rd)	01:10	2.5 kt ebb	145°

0.7 kt flood current at time of image

Cape Hatteras | 9/21/78 | 04:08 GMT
Rev. 1232 | 9/20/78 | 23:08 Local Time
Descending pass

Bathymetry Visibility Evaluation

The inner Diamond Shoal is again dark and visible, and the outer shoal invisible as on Revs. 974 and 931. The markings are all opposite to Rev. 378 (dark instead of bright) and the Clam and Gull shoals are dark areas.

Weather

0600 GMT
Clear
Air temp. - 22°C
Dew point - 18°C
Barometer - 1018.5 mb
Wind, Force 2 - 4 to 7 mph
from the NE

Buoy - 35°N, 72°W
Clear
Air temp. - 25°C
Water temp. 27°C
Barometer - 1017.2 mb
Wind, Force 4 - 13 to 18 mph
from the NE
Waves - 6 sec period, 1.5 m height

Tides

Cape Hatteras - 35°14'N, 75°31'W

High tide (20th)	21:56	3.8 ft
Low tide	03:49	0.2 ft

Cape Hatteras (Ocean) - 35°12'N, 75°42'W

High tide (20th)	21:48	3.6 ft
Low tide	03:49	0.2 ft

Hatteras Inlet - 35°12'N, 75°44'W

High tide (20th)	22:11	2.2 ft
Low tide	04:15	0.2 ft

Ocracoke Inlet - 35°04'N, 76°01'W

High tide (20th)	22:12	2.1 ft
Low tide	04:13	0.2 ft

Currents

Hatteras Inlet - 35°12'N, 75°44'W

Slack	Maximum		
19:44 (20th)	21:46 (20th)	2.3 kt flood	305°
01:35	04:10	2.25 kt ebb	150°

1.84 kt flood current at time of image

Ocracoke Inlet - 35°04'N, 76°01'W

Slack	Maximum		
19:29 (20th)	21:36 (20th)	1.9 kt flood	000°
01:20	04:00	2.5 kt ebb	145°

1.5 kt flood current at time of image

Cape Hatteras 10/03/78 04:59 GMT
Rev. 1404 10/02/78 23:59 Local Time
Descending pass

Bathymetry Visibility Evaluation

The inner Diamond Shoal is again a distinctive dark patch while the middle and outer shoals are barely visible. The Clam Shoal is a dark thin area - this pass has the best visibility of any descending pass on the Clam and Gull shoals. The shoal directly west of Gibbs Point is also visible here as a dark area.

Weather

0600 GMT
Clear
Air temp. - 24°C
Dew point - 16°C
Barometer - 1017.0 mb
Wind, Force 2 - 4 to 7 mph
from the NNE

Buoy, 35°N, 72°W
Clear
Air temp. - 23°C
Water temp. - 26°C
Barometer - 1014.6 mb
Wind, Force 4 - 13 to 18 mph
Waves - 6 second period, 2 m height

Tides

Cape Hatteras - 35°14'N, 75°31'W

High tide (2nd)	19:12	4.0 ft
Low tide	01:07	0.0 ft

Cape Hatteras (Ocean) - 35°12'N, 75°42'W

High tide (2nd)	19:04	3.8 ft
Low tide	01:07	0.0 ft

Hatteras Inlet - 35°12'N, 75°44'W

High tide (2nd)	19:27	2.4 ft
Low tide	01:33	0.0 ft

Ocracoke Inlet - 35°04'N, 76°01'W

High tide (2nd)	19:28	2.3 ft
Low tide	01:31	0.0 ft

Currents

Hatteras Inlet - 35°12'N, 75°44'W

Slack	Maximum		
22:54 (2nd)	01:31	2.3 kt ebb current	150°
05:14	07:26	2.75 kt flood current	305°

1.7 kt ebb current at time of image

Ocracoke Inlet - 35°04'N, 76°01'W

Slack	Maximum		
22:39 (2nd)	01:21	2.6 kt ebb	145°
04:59	07:16	2.25 kt flood	000°

1.8 kt ebb current at time of image

Cape Hatteras 10/06/78 5:12 GMT
Rev. 1447 0:12 Local Time
Descending pass

Bathymetry Visibility Evaluation

It looks like a large storm over the Cape. Many areas are blacked out including much of the ocean directly adjoining Cape Hatteras. The Cape itself stands out very bright against the dark background. The inner Diamond Shoal has the barest visibility while the middle and outer Diamond and Clam Shoals are totally gone. This image had a combination of the lowest currents at the Hatteras and Ocracoke Inlets of any SEASAT pass, rain and moderately high winds so the effect of each paremeter in wiping out bathymetry is still undetermined.

Weather

Buoy - 32°N, 76°W
Partly cloudy
Light rain
Air temp. - 24°C
Dew point - 11°C
Water temp. - 28°C
Barometer - 1014.0 mb
Waves - 4 sec period,
1.5 m height
Wind, Force 4 - 13 to 18 mph from the S

Buoy - 35°N, 72°W
Clear, no rain
Air temp. - 25°C
Water temp. - 26°C
Barometer - 1014.6 mb
Waves - 6 sec period, 1.5 m height
Wind, Force 3 - 8 to 12 mph from the S

Tides

Cape Hatteras - 35°14'N, 75°31'W

High tide (5th)	21:14	3.8 ft
Low tide	03:05	0.0 ft

Cape Hatteras (Ocean) - 35°12'N, 75°42'W

High tide (5th)	21:06	3.6 ft
Low tide	03:05	0.0 ft

Hatteras Inlet - 35°12'N, 75°44'W

High tide (5th)	21:29	2.2 ft
Low tide	03:31	0.0 ft

Ocracoke Inlet - 35°04'N, 76°01'W

High tide (5th)	21:30	2.1 ft
Low tide	03:29	0.0 ft

Currents

Hatteras Inlet - 35°12'N, 75°45'W

Slack	Maximum	
19:07 (5th)	21:16 (5th)	2.5 kt flood 305°
00:45	03:33	2.3 kt ebb 150°

0.5 kt flood at time of image

Ocracoke Inlet - 35°04'N, 76°01'W

Slack	Maximum	
18:52 (5th)	21:06 (5th)	2.1 kt flood 000°
00:30	03:23	2.6 kt ebb 145°

0.4 kt flood at time of image

Cape Hatteras 10/09/78 05:25 GMT
Rev. 1490 00:25 Local Time
Descending pass

Bathymetry Visibility Evaluation

The ocean background is quite dark and fairly uniform. The Diamond Shoals are all visible but somewhat fuzzy. The Clam Shoal is a dark line against a dark background. Reprocessing this image with a different dynamic range could bring out many details in the ocean.

Weather

0600 GMT
Clear
Air temp. - 14°C
Barometer - 104.4 mb
Wind, Force 1 - 1 to 3 mph
from the N

Buoy - 35°N, 72°W
Clear
Air temp. - 18°C
Water temp. - 25°C
Barometer - 1023.0 mb
Wind, Force 3 - 8 to 12 mph
from the NNE
Waves - 5 sec period, 1.5 m height

Tides

Cape Hatteras - 35°14'N, 75°31'W

Low tide (8th)	17:49	0.4 ft
High tide	00:03	3.6 ft
Low tide	05:56	0.3 ft

Cape Hatteras (Ocean) - 35°12'N, 75°42'W

Low tide (8th)	17:49	0.4 ft
High tide (8th)	23:55	3.4 ft
Low tide	05:56	0.3 ft

Hatteras Inlet - 35°12'N, 75°44'W

Low tide (8th)	18:15	0.4 ft
High tide	00:18	1.9 ft
Low tide	06:22	0.3 ft

Ocracoke Inlet - 35°04'N, 76°01'W

High tide	00:19	1.8 ft
Low tide	06:20	0.3 ft
Low tide (8th)	18:13	0.4 ft

Currents

Hatteras Inlet - 35°12'N, 75°44'W

Slack	Maximum		
21:59 (8th)	23:56 (8th)	2.0 kt flood	305°
03:36	06:21	2.2 kt ebb	150°

2.0 kt flood current at time of image

Ocracoke Inlet

Slack	Maximum		
21:44 (8th)	23:46 (8th)	1.6 kt flood	000°
03:21	06:11	2.4 kt ebb	145°

1.6 kt flood current at time of image

Cape Hatteras 11/13/81 07:00 GMT
SIR-A Image

Bathymetric Visibility Evaluation

The inner Diamond Shoal is again more visible than the outer shoals. On this image the shoal outlines are both bright and dark on one image, unlike SEASAT which are either all bright or all dark on any one image.

No weather, tidal or current information has been obtained.

4.3.6 Summary of Straits of Juan de Fuca Images

There are only two images for this area, so not too much can be said. The line paralleling the coast from Slip Point to Pillar Point on the Rev. 1269 image may actually be caused by bathymetry or may be a chance current boundary. More images of the same area at varying current conditions would be necessary to determine this. The current at Pillar Point for Rev. 1269 was 0.2 kt, roughly parallel to the features, whereas Rev. 474 which does not show this line has essentially no current. We may then be seeing a current dependence. More images with higher current velocities and a few more with no current could give a definitive idea of the current dependence.

Straits of Juan de Fuca 7/30/78 04:07 GMT
Rev. 474 7/29/78 20:07 Local Time
Descending pass

Bathymetry Visibility Evaluation

Constance Bank and the channel inside show at 8 fathoms and Race Rocks show at 2 fathoms. This image shows the easternmost portion of the Straits of Juan de Fuca where it intersects the Straits of Georgia and the Rosario Straits.

Weather

0600 GMT
Clear
Air temp. - 12°C
Dew point - 10°C
Barometer - 1021.1 mb
Wind, Force 1 - 1 to 3 mph from the NE

Tides

Cape Flattery (Tatoosh Island) - 48°23'N, 124°44'W

Low tide (29th)	14:09	2.2 ft
High tide (29th)	20:17	7.4 ft

Twin Rivers - 48°10'N, 123°57'W

Low tide (29th)	15:04	2.0 ft
High tide (29th)	21:14	6.6 ft

Port Angeles - 48°07'N, 123°26'W

Low tide (29th)	15:49	4.9 ft
High tide (29th)	22:00	6.5 ft

Currents

Straits of Juan de Fuca (Entrance) - 48°27'N, 124°35'W

Slack	Maximum	
13:02	16:35	0.9 kt ebb 290°
---	21:52	Current weak and variable
---	04:21(30th)	1.8 kt ebb 290°

Current weak and variable at time of image

Pillar Point - 48°16'N, 124°04'W

Slack	Maximum	
13:27	17:05	1.1 kt ebb 280°
---	22:22	Current weak and variable
---	04:51 (30th)	2.2 kt ebb 280°

Current weak and variable at time of image

Race Rocks (4 Miles South) - 48°14'N, 123°32'W

Slack	Maximum	
15:00	17:50	1.0 kt ebb 271°
---	22:35	Current weak and variable
---	05:30	2.4 kt ebb 271°

Current weak and variable at time of image

Straits of Juan de Fuca 9/23/78 17:15 GMT
Rev. 1269 09:15 Local Time
Ascending pass

Bathymetry Visibility Evaluation

This image covers the Straits of Juan de Fuca at the intersection with the Pacific Ocean. In the Pacific we are seeing the Flattery Rocks off of Cape Alava, the 17 fathom line north of Cape Alava, and possibly the 30 fathom line west of Pachena Point (north of the strait). In the strait itself, there is a line paralleling the coast from Slip Point to Pillar Point which lines up with the 100 fathom contour.

Weather

Completely overcast
Air temp. - 13°C
Dew point - 12°C
Barometer - 1021.6 mb
Wind, Force 2 - 4 to 7 mph from the NE
Water temp. - 16°C
Waves - 8 sec period, 2 m height

Tides

Cape Flattery (Tatoosh Island) - 48°23'N, 124°44'W

High tide	05:16	6.1 ft
Low tide	11:06	2.6 ft

Twin Rivers - 48°10'N, 123°57'W

High tide	06:11	5.4 ft
Low tide	12:03	2.3 ft

Port Angeles - 48°07'N, 123°26'W

High tide	08:59	5.9 ft
Low tide	13:05	4.6 ft

Currents

Straits of Juan de Fuca (Entrance) - 48°27'N, 124°35'W

Slack	Maximum		
04:30	06:53	0.6 kt	flood 115°
09:22	13:13	1.0 kt	ebb 290°
	18:43	Current weak and variable	

Current is 0.06 kt at time of image

Pillar Point - 48°16'N, 124°04'W

Slack	Maximum		
04:55	07:23	0.7 kt	flood 100°
09:47	13:43	1.2 kt	ebb 280°
	19:13	Current weak and variable	

Current is 0.2 kt flood at time of image

Race Rocks (4 Miles South) - 48°14'N, 123°32'W

Slack	Maximum		
05:05	08:30	1.5 kt	flood 91°
11:55	14:20	1.3 kt	ebb 271°

Current is 1.35 kt flood at time of image

4.4 Individual SAR Passes

4.4.1 Alaska

Cook Inlet Anchorage, Alaska Rev. 289	7/17/78 7/16/78	05:47 GMT 19:47 Local Time Time Meridian 150°W 10 hrs less than GMT

Bathymetry Visibility Evaluation

A great deal of detail is visible in Cook Inlet. The mud banks east of Fire Island are black against the light water and do not entirely match the map; they are partially covered in the image. A flow pattern is visible in Knik Arm and from there on down to North Foreland, on the west side of the Inlet, the 10 fathom line is well outlined. There is a bank in mid-channel extending south from Fire Island which is fairly well outlined at the 10 fathom break. Moose Point Shoal shows as a dark area and Middle Ground Shoal is outlined further south. There are also numerous bright lines present which do not follow the bathymetry and must be due to current flow.

Weather

This data was missing from the NOAA weather map file.

In northern part of picture, we are at approximately 1 kt, ebb tide, southern part at slack from ebb to flood.

There is a tidal bore in Turnagain Arm which begins shortly after ebb and may reach 6 ft in height.

Tides

Anchorage

High tide	15:21	25.8 ft
Low tide	21:17	5.9 ft

East Foreland

High tide	13:03	17.4 ft
Low tide	18:05	4.8 ft
High tide (17th)	00:43	21.0 ft

Fire Island

High tide	14:55	24 ft
Low tide	20:18	5.5 ft

Sunrise

High tide	15:52	29.8 ft
Low tide	22:38	5.7 ft

North Foreland

High tide	14:13	17.1 ft
Low tide	19:58	5.2 ft
High tide	1:53	21.4 ft

Anchorage	38 ft maximum tidal difference	13 ft minimum tidal difference
Seldovia	28 ft maximum tidal difference	5 ft minimum tidal difference

Currents

Anchorage, 1 mile offshore (close inshore at Anchorage an eddy current flows up Knik Arm during the ebb)

Slack	Maximum		Direction
16:18	17:18	2.0 kt ebb	220°
22:04	01:09	2.64 kt flood	50°

3 miles NW of Moose Point - 60°59'N, 150°47'W

Slack	Maximum		Direction
14:29	16:53	2 kt ebb	245°
20:15	22:54	2.64 kt flood	65°

West Foreland, mid-channel - 60°45'N, 151°32'W

Slack	Maximum		Direction
14:13	17:03	2.75 kt ebb	205°
19:59	23:04	3.3 kt flood	25°

Controller Bay, Alaska 9/13/78 17:46 GMT
Rev. 1126 08:46 Local Time
Ascending pass

Bathymetry Visibility Evaluation

On the southeast side of Kayak Island, a line of breakers shows at approximately the 5 fathom line. It curves off toward the mainland on the northeast end but does not reach the mainland.

Off the south tip of Kayak Island, the underwater double point shows and the 5 fathom line. A 9 fathom bank is faintly visible out to southeast Rock, then what is probably a current line curves north and west of the island.

Further north and west, a line at about 18 fathoms shows parallel to the coast and many mud flats show.

The bathymetric measurements are sparse in some spots on the map and the islands at the mouth of the Copper River are different on the map than on the photograph.

We may be seeing the Okalee Channel.

Weather

18:00 GMT
Station, 59°30'N, 139°W
Overcast, continuous rain
Air temp. - 11°C
Dew point - 11°C
No pressure reading
Wind, Force 6 - 25 to 31 mph
from the ESE

18:00 GMT
Station, 62°30'N, 145°W
Partly cloudy, no rain
Air temp. - 11°C
Dew point - 1°C
Barometer - 999.2 mb
Wind, Force 2 - 4 to 7 mph
from the SSE

Tides

Wingham Island (Controller Bay) - 60°03'N, 144°24'W

Low tide	04:03	-0.3 ft
High tide	10:25	8.5 ft

Currents

Wingham Island (Off NE Corner) - 60°03'N, 144°23'W

Slack	Maximum		
04:34	08:17	1.6 kt	flood 70°
11:01	14:36	1.4 kt	ebb 290°

1.6 kt flood at time of pass

Kanak Island (Southeast) - 60°05'N, 144°18'W (in Okalee Channel)

Slack	Maximum		
04:39	07:52	1.95 kt	flood 65°
11:06	14:11	1.75 kt	ebb 255°

1.8 kt flood at time of pass

4.4.2 Algeria

Bejaia, Algeria
Rev. 791 8/21/78 07:17 GMT
Ascending pass

Bathymetry Visibility Evaluation

There are sediment patterns or river outflow patterns in the ocean, but no bathymetry.

Weather

0600 GMT
Clear
Air temp. - 20°C
Dew point - 17°C
Barometer - 1018.5 mb
Wind, Force 1 - 1 to 3 mph from the SW

4.4.3 Bermuda

Bermuda
Rev. 1267
Ascending pass

9/23/78

14:24 GMT
10:24 Local Time

Bathymetry Visibility Evaluation

The entire island is surrounded by dark parallel lines which run in roughly the same direction. There is no current information available, but it is likely that these lines are in the direction of current flow. The dark lines cover the shallower areas of the reef surrounding the island. These are at 1, 2 and 3 fathoms on the north side of the island, 10 fathoms on the south side and 15 fathoms on the east side.

Weather

1200 GMT
Partly cloudy
Air temp. - 27°C
Dew point - 23°C
Barometer - 1023.1 mb
Wind, Force 1 - 1 to 3 mph
from the NW

Buoy 4° due south
Partly cloudy
Air temp. - 27°C
Dew point - 23°C
Water temp. - 30°C
Barometer - 1021.7 mb
Wind, Force 1 - 1 to 3 mph
from the E
Waves - 4 sec period, 0.5 m height
Swell - from the East
5 sec period, 1.5 m height

Tides

Ireland Island - 32°19'N, 64°50'W

Low tide	06:59	1.3 ft
High tide	13:30	3.6 ft

Ferry Reach (Biological Station)

Low tide	06:50	1.5 ft
High tide	13:18	3.6 ft

Currents

No information available

4.4.4 California

Point Loma, CA
Rev. 107 7/4/78 12:11 GMT
Ascending pass 04:11 Local Time

Bathymetry Visibility Evaluation

There is no bathymetry evident in this image, although the ocean shows much detail due to storms or wind.

Weather

1200 GMT
Completely overcast
Air temp. - 17°C
Dew point - 15°C
Barometer, 1011.4 mb
Light fog
Wind, Force 1 - 1 to 3 mph from the SE
However, approximately 250 miles SSW out to sea, there are
Force 4 - 13 to 18 mph from the NW

Tides

Point Loma - 32°40'N, 117°14'W

Low tide	02:50	-0.55 ft
High tide	09:20	3.8 ft

Ensenada (Todos Santos Bay) - 31°51'N, 116°38'W

Low tide	02:45	-0.5 ft
High tide	09:07	3.7 ft

Currents

San Diego Bay (Entrance) - 32°41'N, 117°14'W

Slack	Maximum		
03:37	06:37	1.4 kt	flood 355°
09:39	12:02	1.0 kt	ebb 175°

San Nicolas Island, CA
Rev. 308 7/18/78 13:16 GMT
Ascending pass 05:16 Local Time

Bathymetry Visibility Evaluation

Northwest of San Nicolas Island, the 3 and 7 fathom shoals appear as black areas. The chart indicates this is a seaweed bed. The dark patches around Santa Barbara Island are shoals and also seaweed beds. This image has a unique bathymetry visibility mechanism: seaweed. No where else does bathymetry appear as a darkened area - it is usually an outlined area where the perimeter contrasts with the interior. The seaweed here seems to dampen the waves, creating solid dark areas.

Weather

1200 GMT
Light fog, overcast
Air temp. - 17°C
Dew point - 16°C
Barometer - 1010.7 mb
No wind

Tides

Los Angeles - 33°43'N, 118°16'W

Low tide	01:55	-1.0 ft
High tide	08:18	4.2 ft

San Nicolas Island - 33°16'N, 119°30'W

Low tide	02:14	-0.9 ft
High tide	08:27	3.8 ft

Currents

San Pedro Channel - 33°36'N, 118°16'W

San Pedro Channel is 7 miles south of Los Angeles Harbor Breakwater. There are two periodic currents here, both of which are rotary, turning

clockwise and rather weak. The tidal current has a velocity at strength of about 0.2 kt. The other current, due apparently to daily land and sea breezes, has a period of 24 hours and an average velocity of about 0.2 kt. The greatest velocity during 5 months of observations was 1.5 kt. Currents greater than 1 kt occur infrequently.

4.4.5 Chesapeake Bay

Chesapeake Bay
Rev. 1468 10/7/78 15:59 GMT
75° Time Meridian
10:59 Local time

Bathymetry Visibility Evaluation

Nothing shows in the Atlantic off of the Eastern Shore. In the bay there are many lines, some of which correspond to bathymetry. These include the 4 to 6 ft bank and 20 ft banks west of Savage Neck and Cherrystone Inlet and the bank west of Old Town Neck. A 60 ft line east and south of Cape Henry is visible and the Thimble Shoal channel is faintly visible from the tunnel all the way to Old Point Comfort.

Weather

1200 GMT

3/4 overcast
Air temp. - 11°
Dew point - 8°C
Barometer - 1013.5 mb
Winds, Force 1 - 1 to 3 mph
from the NW

Buoy, 35°N, 72°W

Clear
Air temp. - 26°C
Water temp. - 26°C
Barometer - 1008.8 mb
Winds, Force 2 - 4 to 7 mph
from the WSW
Waves - 6 sec period,
1.5 m height

1800 GMT

Complete overcast
Air temp. - 8°C
Dew point - 3°C
Barometer - 1013.8 mb
Winds, Force 2 - 4 to 7 mph
from the WNW

Buoy, 35°N, 72°W
Clear
Air temp. - 23°C
Water temp. - 26°C
Barometer - 1009.1 mb
Winds, Force 4 - 13 to 18 mph
Waves - 5 sec period,
1.5 m height

Tides

Virginia Beach - 36°51'N, 75°58'W

Low tide	04:30	0.2 ft
High tide	11:03	4.0 ft

Cape Henry - 36°56'N, 76°00'W

Low tide	04:50	0.2 ft
High tide	11:41	3.4 ft

Old Point Comfort - 37°00'N, 76°18'W

Low tide	5:30	0.2 ft
High tide	12:22	3.1 ft

Fisherman's Island - 37°06'N, 75°59'W

Low tide	5:05	0.2 ft
High tide	11:46	3.6 ft

Cape Charles Harbor - 37°16'N, 76°01'W

Low tide	6:02	0.2 ft
High tide	12:15	3.0 ft

Pungoteague Creek - 37°40'N, 75°50'W

Low tide	8:43	0.2 ft
High tide	14:55	2.3 ft

New Point Comfort, Mobjack Bay - 37°18'N, 76°17'W

Low tide	6:01	0.2 ft
High tide	12:22	2.9 ft

Very close (within minutes at Virginia Beach) to high tide.

Currents

Chesapeake Bay (Entrance) - 36°59'N, 76°00'W

Slack	Maximum	
09:27	12:13	1.2 kt flood 305°
15:19	18:52	1.3 kt flood 125°

Cape Charles Light (9.5 Miles WSW) - 37°04'N, 76°05'W

Slack	Maximum	
09:37	12:13	1.8 kt flood 320°
15:29	18:52	1.2 kt ebb 125°

Old Point Comfort (0.4 Miles E) - 37°00'N, 76°18'W

Slack	Maximum	
07:12	10:08	1.6 kt flood 235°
14:04	16:47	1.0 kt ebb 045°

New Point Comfort (1.5 Miles W) - 37°18'N, 76°18'W

Slack	Maximum		
06:57	09:48	0.7 kt flood	320°
12:49	16:17	0.4 kt ebb	130°

Pocomoke Sound Approach - 37°38'N, 75°58'W

Slack	Maximum		
Unknown	13:33	0.8 kt flood	10°
Unknown	20:12	0.7 kt ebb	195°

4.4.6 Cuba

Nicaro Mountains, Cuba
Rev. 371 7/22/78 23:36 GMT
Descending pass 18:36 Local Time

Bathymetry Visibility Evaluation

The 10 m line shows spectacularly all along the coast as a narrow dark line. The map indicates breakers along much of this coast at about 10 m depth, so we may be seeing that. North of Punta Sotavento there is a double line.

Weather

0000 GMT, 23rd
Clear, dense fog
Air temp. - 28°C
Dew point - 25°C
Barometer - 1015.5 mb
Wind, Force 1 - 1 to 3 mph from the WNW

Tides

Bahia de Nipe (entrance), 20°47'N, 75°34'W

Low tide	15:48	-0.4 ft
High tide	22:10	2.6 ft

Currents

No information available

4.4.7 Dominican Republic, Haiti

Dominican Republic
Rev. 335
Ascending pass

7/20/78

10:31 GMT
05:31 Local Time

Bathymetry Visibility Evaluation

The image is blurred and nothing shows but a few outflow lines perpendicular to the shore.

Weather

Partly cloudy
Air temp. - 27°C
Dew point - 24°C
Water temp. - 22°C
Barometer - 1015.2 mb
Light rain
Waves - 3 sec period, 1.5 m high; swell from the E, 6 sec period, 2 m height
Wind, Force 2 - 4 to 7 mph from the ESE

Tides

Santo Domingo - 18°27'N, 69°53'W

Low tide (19th)	23:56	0.6 ft
Hight ide	08:31	0.68 ft

Currents

No information available

Port a Piment, Haiti
Rev. 450 7/28/78 11:21 GMT
Ascending pass 06:21 Local Time

Bathymetry Visibility Evaluation

Just south of the Monts de la Hotte, there are lines parallel to shore which follow the 20 fathom contour.

Weather

1200 GMT
Partly cloudy
Air temp. - 28°C
Dew point - 27°C
Barometer - 1016.4 mb
Wind, Force 1 - 1 to 3 mph from the ENE

Tides

Jacmel - 18°13'N, 72°34'W

High tide (27th)	23:19	1.7 ft
Low tide	08:00	-0.1 ft

Currents

No information available

Haiti
Rev. 737 9/17/78 12:42 GMT
Ascending pass 07:42 Local TIme

Bathymetry Visibility Evaluation

There are three digital images over Haiti that were processed for this revolution. Each of these will be evaluated here.

St. Nicolas - 19°40'N, 73°08'W

There is a line west of St. Nicolas, east of the Windward Passages which is most likely a current line. The chart indicates a strong current setting to the north around this end of the island, the line does not follow the bathymetric contour well and the water depth here is 500 to 800 fathoms.

Isle de la Gonave - 18°55'N, 72°48'W

Sediment patterns are visible, but no bathymetry.

Port au Prince - 18°15'N, 72°30'W

Again, sediment patterns, but nothing which follows bathymetric contours.

Weather

1200 GMT
Partly cloudy
Air temp. - 28°C
Water temp. - 28°C
Barometer - 1012.2 mb
Waves - 5 sec period, 1 m height
Wind, Force 2 - 4 to 7 mph from the ESE

Tides

Port au Prince - 18°33'N, 72°21'W

Low tide	02:23	0.2 ft
High tide	08:40	1.8 ft

Currents

No information available

4.4.8 Jamaica

Jamaica
Rev. 608 8/8/78 12:20 GMT
Ascending pass

Bathymetry Visibility Evaluation

Some 3.5 fathom shoals show off of Portland Point.

Weather

Clear
Air temp. - 25°C
Dew point - 22°C
Barometer - 1014.0 mb
Wind, Force 3 - less than 8 mph, direction unknown

Jamaica
Rev. 809 8/22/78 13:22 GMT
Ascending pass

Bathymetry Visibility Evaluation

There are two digital images which were processed for this pass.

Montego Bay, 18°21'N, 77°50'W

No bathymetry is visible.

Jamaica, 18°08'N, 77°50'W

No bathymetry is visible.

Weather

1200 GMT
Partly cloudy
Air temp. - 24°C
Dew Point - 21°C
Water temp. - 24°C
Barometer - 1013.1 mb
Wind, Force 1 - 1 to 3 mph from the SE

4.4.9 Mississippi Delta

Mississippi Delta
Rev. 393 7/24/78 11:48 GMT
Ascending pass Time meridian 90°W
05:48 Local Time
6 hrs less than GMT

Bathymetry Visibility Evaluation

There are two curved lines in the westernmost V of the delta which follow bathymetry lines and the Grand Gosier and Breton Island banks appear as dark areas. There are many more lines present which do not correspond to any kind of bathymetry which are likely due to currents or boundaries between water masses.

Weather

3/4 Overcast
Air temp. - 24°C
Dew point - 23°C
Light fog
Barometer - 1019.6 mb
Wind, Force 1 - 1 to 3 mph from the east

Sea station to east:

Partly cloudy
Air temp. - 28°C
Dew point - 27°C
Water temp. - 27°C (81°F)
Barometer - 1018.0
Waves - 2 sec period, 1 m height
Wind, Force 3 - 8 to 12 mph from the ESE

Currents weak (less than 1.5 kt maximum) and no information given in Missisippi Delta region.

Tides

Pass a Loutre (entrance)

High tide	21:19	0.5 ft
Low tide	11:37	0.9 ft
(23rd)		

Southwest Pass

High tide	19:48	0.5 ft
Low tide	10:51	1.0 ft
(23rd)		

Mississippi Delta
Rev. 637 8/10/78 13:01 GMT
Ascending pass 07:01 Local Time

Bathymetry Visibility Evaluation

A few good current or water mass boundary lines are present but no bathymetry is visible.

Weather

12:00 GMT
Partly cloudy
Air temp. - 24°C
Dew point - 22°C
Barometer - 1016.9 mb
Wind, Force 1 - 1 to 3 mph from the E

Tides

Pass a Loutre (Entrance)

High tide	02:16	1.0 ft
Low tide	13:36	0.6 ft

Southwest Pass

High tide	01:30	1.1 ft
Low tide	12:05	0.6 ft

Mississippi Delta
Rev. 838 8/27/78 14:02 GMT
Ascending pass 08:02 Local Time

Bathymetry Visibility Evaluation

The bathymetry curves visible on Rev. 393 do not appear here and the frame stops short of the underwater Gosier and Breton banks. There are many lines but no bathymetry is visible.

Weather

Partly cloudy
Air temp. - 26°C
Dew point - 23°C
Barometer - 1014.6 mb
Wind, Force 2 - 4 to 7 mph from the SE

Sea station to southeast:

Slight overcast
Air temp. - 28°C
Water temp - 28°C
Barometer - 1016.8 mb
Waves - 5 sec period, 1.5 m height
Wind, Force 2 - 4 to 7 mph from the east

Diurnal Tides

Pass a Loutre (Entrance)

04:15	1.5 ft
16:25	0.4 ft

Southwest Pass

03:29	1.6 ft
14:54	0.4 ft

4.4.10 Nantucket Island

Nantucket Island — 8/27/78 — 12:34 GMT
Rev. 880 — 07:34 Local Time
Ascending pass

Bathymetry Visibility Evaluation

This image has been extensively investigated by several researchers including Kasischke, Schuchman and Lyden (1980) at ERIM. Strong, clear lines delineate many of the banks surrounding Nantucket Island.

Weather

12:00 GMT
Partly cloudy
Air temp. - 17°C
Dew Point - 13°C
Barometer - 1018.9 mb
Wind, Force 2 - 4 to 7 mph from the N

Tides

Siasconset - 41°16'N, 69°58'W

High tide	06:28	1.1 ft
Low tide	12:34	0.2 ft

Great Point - 41°23'N, 70°03'W

High tide	06:54	2.7 ft
Low tide	12:41	0.5 ft

Muskeget Island (North Side) - 41°20'N, 70°18'W

High tide	06:36	1.7 ft
Low tide	12:28	0.3 ft

Currents

Nantucket Harbor (Entrance Channel) - 41°18'N, 70°06'W

Slack	Maximum	
00:57	04:29	1.14 kt flood 170°
07:37	10:21	1.26 kt ebb 350°

Cotuit Bay Entrance (Bluff Point) - 41°37'N, 70°26'W

Slack	Maximum	
00:37	04:39	0.6 kt flood 35°
07:17	10:31	0.6 kt ebb 220°

4.3.11 New York (Niagara Falls)

Hamilton, Buffalo, NY
Rev. 874 8/27/78 02:56 GMT
Descending pass, 43°08'N, 79°18'W

Bathymetry Visibility Evaluation

One channel shows in Lake Erie. There are a lot of markings including spiral patterns which are storm or wind effects, but no other bathymetry in Lake Erie or Ontario.

Weather

0000 GMT, Station 42.5°N, 78°W
Overcast
Air temp. - 21°C
Dew point - 15°C
Barometer - 1017.3 mb
Wind, Force 1 - 1 to 3 mph from the NNW

Station 43°N, 81°W, wind is Force 1 from the south. Possible convergence of conflicting wind directions over this area.

4.4.12 Columbia River, Oregon

Columbia River, Oregon	8/19/78	05:27 GMT
Rev. 761	8/18/78	21:27 Local Time
Descending pass		Time Meridian 120°W
		8 hrs less than GMT

Bathymetry Visibility Evaluation

In the Columbia River itself, the channel and mud bank just south of Grays Point are visible. Also, the channel from Tansy Point to Astoria is evident and at least part of Desdemona Sands. South of Columbia River in the Pacific, the 10 fathom line shows west of Clatsop Plains. To the north there is a great deal of detail in Willapa Bay such as the mud banks to the east of Stanley Channel.

Weather

Overcast
Air temp. - 17°C
Dew point - 14°C
Barometer - 1017.8 mb
Wind force unknown, probably less than 2 (7 mph)

Columbia River is subject to annual freshets. Short range predictions are available at local river forecast centers.

Columbia River (Entrance N. Jetty) - 46°16'N, 124° 04'W

Low tide	18:25	0.8 ft
High tide	00:40	8.1 ft
(19th)		

Baker Bay (Ilwaco, Washington) - 46°18'N, 124°, 04'W

Low tide	19:26	0.6 ft
High tide	01:13	8.3 ft
(19th)		

Brighton (Just South of Image) - 45°40', 123°56'

Low tide	17:17	1.7 ft
High tide	00:05	8.7 ft
(19th)		

Long Beach (Washington) - 46°21'N, 124°03'W

Low tide	18:24	0.6 ft
High tide	00:10	8.6 ft
(19th)		

Tarlatt Slough - 46°22'N, 124°00'W

Low tide	20:17	0.3 ft
High tide	01:36	9.8 ft
(19th)		

Nahcotta - 46°30'N, 124°01'W

Low tide	19:39	0.6 ft
High tide	01:35	10.8 ft
(19th)		

Willapa Bay (Entrance) - 46°43'N, 124°,04'W

Low tide	18:46	0.6 ft
High tide	00:47	8.6 ft
(19th)		

Currents

Columbia River Lightship - 46°11'N, 124°11'W.

The tidal current here is rotary, turning clockwise, but rather weak; the velocity of the current at strength being about 0.3 kt setting 20° (true) on the flood and 200° on the ebb.

The current from the Columbia River completely masks the flood current at the lightship, with observations showing that there is a nontidal current at the lightship with an average velocity of 0.4 kt setting 235° from February to October and 295° from October to February. When there is considerable run off from the river, the combined tidal and nontidal current at the lightship frequently attains a velocity of 2 kt or more in a southwesterly direction. The greatest observed velocity at Columbia River Lightship is 3.5 kt.

Tillamook Bay (Entrance) - 45°34'N 123°56'W

Slack	Maximum		
13:22	16:04	4.1 kt ebb	305°
19:20	22:05	4.3 kt flood	140°
01:25 (19th)	04:15	4.7 kt ebb	305°

Clatsop Spit (0.5 Mile NE) - 46°14'N, 124°00'W

Slack	Maximum		
13:45	16:36	4.0 kt ebb	300°
19:43	22:35	2.4 kt flood	120°
01:39 (19th)	04:54	5.2 kt ebb	300°

The image is about halfway between low and high tides. It is almost at maximum flood current which sets south east.

4.4.13 Ormonde Seamount

Ormonde Seamount
Rev. 785
Descending pass

8/20/78

21:44 GMT

Bathymetry Visibility Evaluation

There are markings in the area of the seamount but the registration is too poor (with no land bearings) to ascertain whether these marks are over the seamount itself.

4.4.14 Shetland Islands

Shetland Islands
Rev. 1149 9/15/78 08:22 GMT
Ascending pass

Bathymetry Visibility Evaluation

East of the south corner of Foula Island, the 1.5 to 8 fathom Hoevdi Rocks show and the 12 fathom Foula Bank, but the 16 fathom bank further east is invisible. There is also a shadow pattern south of these banks which is probably current induced. The lines around Fair Isle do not match the bathymetry and are probably also current lines.

Weather

0600 GMT
Completely overcast
Air temp. - 8°C
Dew point - 7°C
Barometer - 989.6 mb
Low pressure center over area
Wind, Force 3 - 8 to 12 mph from the NE
More northerly sea buoys

NW wave period, 2 sec, 0.5 m wave height
swell from 220° (from SSW)
period 7 sec, height 3 m

NE wave period, 1 sec, 0.5 m wave height from NE
swell direction undetermined
10 sec period, height 2 m

Weather

1200 GMT
Half overcast
Air temp. - 11°C
Dew point - 6°C
Barometer - 1001.7 mb
Wind, Force 4 - 13 to 18 mph from the WNW
The low pressure center is moving eastward

To NE, buoy data

Air temp. - 10°C
Water temp. - 8°C
1 or 2 sec wave period
1 m wave height from the east

Tides

Scalloway (West Side of Main Island) - 60°08'N, 1°16'W

Low tide	01:33	1.4 ft
High tide	07:55	4.8 ft
Low tide	13:53	1.6 ft

Currents

No information available

CHAPTER 5

AUTOMATIC EXTRACTION OF SUBSURFACE SIGNATURES

5.1 Introduction

A previous Underwater Systems, Inc. (USI) study of ocean surface features produced by surface ships resulted in the development of techniques that could be used to automatically detect and extract the surface ship signature. In summary, satellite collected Synthetic Aperture Radar (SAR) raw data (doppler phase histories in a non-image form) could be rapidly processed to detect and segregate surface ships and subsequently be further processed to yield added information about ship heading, size, shape and speed. These operations can be performed quickly and the techniques used can lead to real-time processing of space collected synthetic aperture images.

A simplified description of how the knowledge gained during the referenced study overcomes prior limitations is shown in Figure 5-1. The process is based on:

- Use of a simplified real-time process to detect ship targets and filter them from the data set.
- Continued processing of a sharply reduced data volume with automatic information extraction processes that key on the bright ship to provide classification data.

The techniques for reducing SAR data for this application are based on the use of unfocused azimuth (radar along-track) processing techniques for ship detection and segregation to limit the data field and reduce the data volume. The remaining data can be processed using full focusing

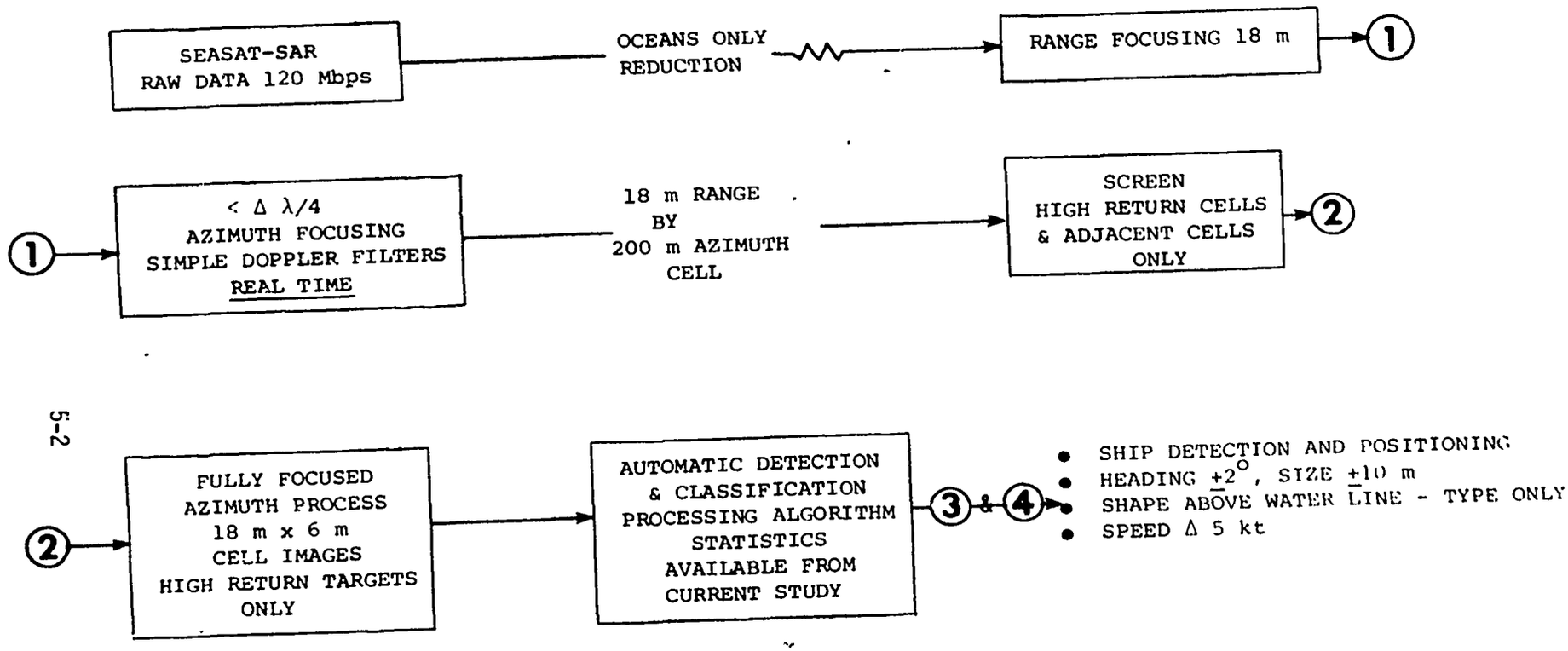

Figure 5-1. A Real Time Technique for Reducing Synthetic Aperture Radar Data.

Based on the use of unfocused azimuth processing techniques to reduce the data field.

techniques and existing systems already processing space based SAR data. This part of the process searches for the existence of a wake signature to eliminate non-ships and furthermore to determine ship heading, position, orientation, size, shape and possibly speed.

Automation of a surface ship detection and classification processor is directly related to and is feasible because of the singular large backscatter return from the surface ship. Automatic wake pattern extraction and other ship classification algorithms stem from this a priori condition. Alas, no salient feature like this is present in the ocean subsurface signature. Automatic extraction of these signatures will have to proceed from images produced with nearly fully focused azimuth processing (i.e. to ≃ 5 looks). From this departure point, pattern recognition techniques can be tested to determine if automatic extraction is feasible.

5.2 Automatic Extraction Possibilities

Figure 5-2 provides hope that the signatures are strong enough and perhaps unique in the shape of contour perimeters to support automatic extraction. A computer compatible digital tape of the Nantucket Shoals image was processed using an adaptation of one of the image enhancement techniques developed by USI for surface ship analyses. The technique exaggerates the signals associated with the bottom topographic contour as long as certain population size and density rules are obeyed (e.g. neighboring pixels fall into a certain backscatter intensity tolerance range and successively connect to build up to an adequate lineal dimension and area). Conversely, signatures of limited areal extent such as ocean waves or signatures with less distinct perimeters such as wind stress will be

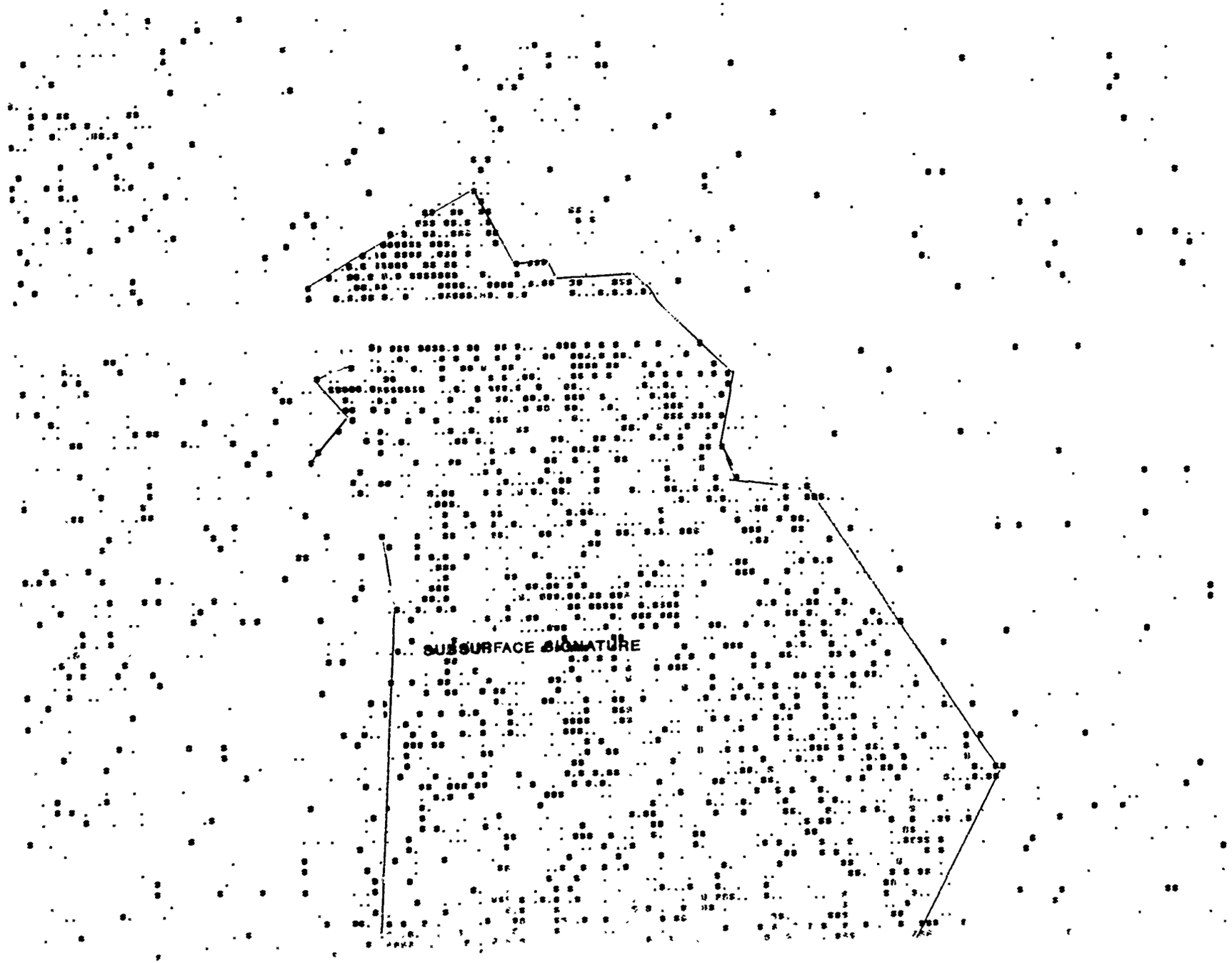

Figure 5-2. Subsurface Signature, Nantucket Shoals, Rev 880.

suppressed. The result is an enhancement such as that shown in Figure 5-2. The weaker signals associated with the subsurface signature are represented by the dark region and the surrounding region of deeper water has been reduced to an absence of symbols.

This simple demonstration of the obvious nature of these signatures, while not conclusive, gives hope that similar or even more sophisticated pattern enhancement techniques can be coupled with pattern recognition techniques to find and identify subsurface signatures. There are a considerable number of algorithms that have been developed as a results of machine-aided image analyses of Landsat and other spaced based imagers (Andrews, 1978). A more detailed evaluation and adaptation of some of these techniques is in order to determine if automatic extraction is possible and, if successful, to find out how quickly an extraction could be accomplished using state of the art processors.

REFERENCES

1. Alpers, W. R., Ross, D. B. and Rufenach, C. L., "On the Detectability of Ocean Surface Waves by Real and Synthetic Aperture Radar," J. Geophys. Res., Vol. 86, 1981, pp. 6481-6498.

2. Andrews, Harry C., Digital Image Processing, IEEE Computer Society, New York, 1978.

3. Barnett, T. P. and Kenyon, K. E., "Recent Advances in the Study of Wind Waves," Rep. Prog. Phys., Vol. 38, 1975, pp. 667-729.

4. Bascom, Willard, Waves and Beaches, Anchor Books, Garden City, New York, 1980.

5. Bowditch, N., "American Practical Navigator," Defense Mapping Agency, Hydrographic Center, 1977, p. 792.

6. De Loor, G. P., "The Observation of Tidal Patterns, Currents and Bathymetry with SLAR Imagery of the Sea," IEEE Journal of Oceanic Engineering, Vol. OE-6, October 1982, p. 124.

7. Hasselmann, K., Ross, D. B., Muller, P. and Sell, W., "A Parametrical Wave Prediction Model," unpublished manuscript from JONSWAP.

8. Hughes, B. A., "The Effect of Internal Waves on Surface Wind Waves: 2. Theoretical Analysis," J. Geophys. Res., Vol. 83, 1978, pp. 455-465.

9. Hughes, B. A. and Grant, H. L., "The Effect of Internal Waves on Surface Wind Waves: 1. Experimental Measurements," J. Geophys. Res., Vol. 83, 1978, pp. 443-454.

10. Kasishke, E. S., Shuchman, R. A. and Lyden, J. D., "Detection of Bathymetric Features Using SEASAT Synthetic Aperture Radar - A Feasibility Study," Environmental Research Institute of Michigan, Internal Technical Report, April 1980.

11. Ko, D. R. S. and Kubota, T., "A Review of Existing Ocean Surface Wave Interaction Models," Dynamics Technology Technical Report No. DT-7601-7, 1977.

12. Lewis, J. E., Lake, B. M. and Ko, D. R. S., "On the Interaction of Internal Waves and Surface Gravity Waves," J. Fluid Mech., Vol. 10, 1974, pp. 529-549.

13. Liu, A. K. and Benney, D. J., "The Spectral Transport Equation for the Description of Long-Short Wave Interaction," Dynamics Technology Technical Report No. DTN-8001-36, 1980.

REFERENCES

1. Alpers, W. R., Ross, D. B. and Rufenach, C. L., "On the Detectability of Ocean Surface Waves by Real and Synthetic Aperture Radar," J. Geophys. Res., Vol. 86, 1981, pp. 6481-6498.

2. Andrews, Harry C., Digital Image Processing, IEEE Computer Society, New York, 1978.

3. Barnett, T. P. and Kenyon, K. E., "Recent Advances in the Study of Wind Waves," Rep. Prog. Phys., Vol. 38, 1975, pp. 667-729.

4. Bascom, Willard, Waves and Beaches, Anchor Books, Garden City, New York, 1980.

5. Bowditch, N., "American Practical Navigator," Defense Mapping Agency, Hydrographic Center, 1977, p. 792.

6. De Loor, G. P., "The Observation of Tidal Patterns, Currents and Bathymetry with SLAR Imagery of the Sea," IEEE Journal of Oceanic Engineering, Vol. OE-6, October 1982, p. 124.

7. Hasselmann, K., Ross, D. B., Muller, P. and Sell, W., "A Parametrical Wave Prediction Model," unpublished manuscript from JONSWAP.

8. Hughes, B. A., "The Effect of Internal Waves on Surface Wind Waves: 2. Theoretical Analysis," J. Geophys. Res., Vol. 83, 1978, pp. 455-465.

9. Hughes, B. A. and Grant, H. L., "The Effect of Internal Waves on Surface Wind Waves: 1. Experimental Measurements," J. Geophys. Res., Vol. 83, 1978, pp. 443-454.

10. Kasishke, E. S., Shuchman, R. A. and Lyden, J. D., "Detection of Bathymetric Features Using SEASAT Synthetic Aperture Radar - A Feasibility Study," Environmental Research Institute of Michigan, Internal Technical Report, April 1980.

11. Ko, D. R. S. and Kubota, T., "A Review of Existing Ocean Surface Wave Interaction Models," Dynamics Technology Technical Report No. DT-7601-7, 1977.

12. Lewis, J. E., Lake, B. M. and Ko, D. R. S., "On the Interaction of Internal Waves and Surface Gravity Waves," J. Fluid Mech., Vol. 10, 1974, pp. 529-549.

13. Liu, A. K. and Benney, D. J., "The Spectral Transport Equation for the Description of Long-Short Wave Interaction," Dynamics Technology Technical Report No. DTN-8001-36, 1980.

14. McLeish, W., Swift, D. J. P., Long, R. B., Ross, D. and Merrill, G., "Ocean Surface Patterns Above Sea-Floor Bedforms as Recorded by Radar, Southern Bight of North Sea," Marine Geology, Vol. 43, 1981, pp. 25-32.

15. Phillips, O. M., "The Dispersion of Short Wavelets in the Presence of a Dominant Long Wave," J. Fluid Mech., Vol. 107, 1981, pp. 465-485.

16. Phillips, O. M., The Dynamics of the Upper Ocean, 2nd ed., Cambridge University Press, New York, 1977.

17. Ruck, G. T., Barrick, D. E., Stuart, W. D. and Krichbaum, C. K., Radar Cross Section Handbook, Plenum Press, New York, 1970.

18. Sabins, F. F. Jr., Remote Sensing Principles and Interpretation, W. H. Freeman, San Fransciso, 1978.

19. Shemdin, O. H., Hsiao, S. V., Carlson, H. J. E., Hasselmann, K. and Schulze, K., "Mechanisms of Wave Transformation in Finite-Depth Water," J. Geophys. Res., Vol. 85, 1980, pp. 5012-5018.

20. Shuchman, R. A. and Polcyn, F. C., "Satellite Bathymetry Technology Assessment for the 1980-1990 Time Frame," Environmental Research Institute of Michigan, Internal Technical Report, December 1978.

21. Valenzuela, G. R., "An Asymptotic Formulation for SAR Images of the Dynamical Ocean Surface," Radio Sci., Vol. 15, 1980, pp. 105-114.

22. Valenzuela, G. R. and Wright, J. W., "Modulation of Short Gravity-Capillary Waves by Long-Scale Periodic Flows--A Higher-order Theory," Radio Sci., Vol. 14, 1979, pp. 1099-1110.

23. Ven Te Chow, Ed., Advances in Hydroscience, Vol. 9, Academic Press, New York, 1973, pp. 49-83.

24. Wright, J. W., "Detection of Ocean Waves by Microwave Radar: the Modulation of Short Gravity - Capillary Waves," Boundary-Layer Meteorology, Vol. 13, 1978, pp. 87-105.